

UNCLASSIFIED

AD 4 2 0 8 3 8

DEFENSE DOCUMENTATION CENTER

FOR

SCIENTIFIC AND TECHNICAL INFORMATION

CAMERON STATION, ALEXANDRIA, VIRGINIA



UNCLASSIFIED

NOTICE: When government or other drawings, specifications or other data are used for any purpose other than in connection with a definitely related government procurement operation, the U. S. Government thereby incurs no responsibility, nor any obligation whatsoever; and the fact that the Government may have formulated, furnished, or in any way supplied the said drawings, specifications, or other data is not to be regarded by implication or otherwise as in any manner licensing the holder or any other person or corporation, or conveying any rights or permission to manufacture, use or sell any patented invention that may in any way be related thereto.

420838

U. S. A R M Y
TRANSPORTATION RESEARCH COMMAND
FORT EUSTIS, VIRGINIA

TRECOM TECHNICAL REPORT 63-38

INVESTIGATION
OF
VENTILATED CLINGING FLOW PHENOMENON

Task 1D021701A04812
(Formerly Task 9R99-01-005-12)
Contract DA 44-177-TC-848

August 1963

prepared by:

HILLER AIRCRAFT COMPANY
Palo Alto, California



DISCLAIMER NOTICE

When Government drawings, specifications, or other data are used for any purpose other than in connection with a definitely related Government procurement operation, the United States Government thereby incurs no responsibility nor any obligation whatsoever; and the fact that the Government may have formulated, furnished, or in any way supplied the said drawings, specifications, or other data is not to be regarded by application or otherwise as in any manner licensing the holder or any other person or corporation, or conveying any rights or permission, to manufacture, use, or sell any patented invention that may in any way be related thereto.

* * *

DDC AVAILABILITY NOTICE

Qualified requesters may obtain copies of this report from
Defense Documentation Center
Cameron Station
Alexandria, Virginia 22314

* * *

This report has been released to the Office of Technical Services, U. S. Department of Commerce, Washington 25, D. C., for sale to the general public.

* * *

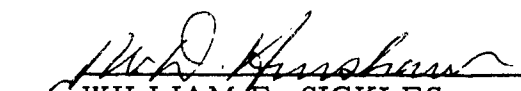
The findings and recommendations contained in this report are those of the contractor and do not necessarily reflect the views of the U. S. Army Mobility Command, the U. S. Army Materiel Command, or the Department of the Army.

HEADQUARTERS
U S ARMY TRANSPORTATION RESEARCH COMMAND
FORT EUSTIS, VIRGINIA

This report presents the results of an investigation of a variation of the flow phenomenon known as Coanda effect. This phenomenon, wherein a series of flat surfaces set at increasing angles is placed immediately adjacent to the orifice of a jet sheet, has been shown by many investigators to result in efficient turning of the jet sheet. The results of the present investigation indicate that ventilation, that is, a discrete distance between the jet exit and the turning surface, results in increased efficiency and, in some cases, a modest thrust augmentation.

Other related investigations have shown that a step discontinuity at the jet achieves substantially the same results as ventilated flows. However, none of the investigations have indicated that a high thrust augmentation could be achieved. Therefore, it is concluded that the primary area of application of these phenomena will be to redirect a jet flow with high efficiency.


WILLIAM D. HINSHAW
Project Engineer


WILLIAM E. SICKLES
Group Leader
Ground Effect Research Group

APPROVED.

FOR THE COMMANDER:


LARRY M. HEWIN
Technical Director

Task 1D021701A04812
(Formerly Task 9R99-01-005-12)
Contract DA 44-177-TC-848
TRECOM Technical Report 63-38
August 1963

INVESTIGATION
OF
VENTILATED CLINGING FLOW
PHENOMENON
ARD-311

Prepared By
Advanced Research
Hiller Aircraft Company
Division of ELTRA Corporation
Palo Alto, California

For
U. S. Army Transportation Research Command
Fort Eustis, Virginia

PREPARED BY:

L. A. Burdick, Jr. -- Research Assistant
M. F. Gates -- Principal Investigator

APPROVED BY:

E. R. Sargent -- Manager, Propulsion
Research Department
E. P. Schuld -- Manager, Advanced
Research Division

TRECOM Personnel:

Mr. W. D. Hinshaw -- Contracting Officer's
Representative

FOREWORD

This report fulfills the requirements of Contract DA 44-177-TC-848. The program was conducted by Mr. L. A. Burdick, Jr., under the direction of Mr. M. F. Gates, Principal Investigator, and Mr. E. R. Sargent, Manager, Propulsion Research Department.

Substantial contributions to the program were made by Prof. Irmgard Flugge-Lotz, Stanford University, Mr. D. A. Graber, Head Propulsion Lab Technician, and Mr. E. P. Schuld, Manager, Advanced Research Division.

The support of the Transportation Research Command Ground Effects Research Group is gratefully acknowledged.

The program was initiated in July 1962 and culminated in February 1963.

TABLE OF CONTENTS

	<u>Page No.</u>
FOREWORD	iii
LIST OF ILLUSTRATIONS	vi
LIST OF SYMBOLS	x
SUMMARY	1
CONCLUSION	2
INTRODUCTION	3
MATHEMATICAL DESCRIPTION	5
TEST PROGRAM	8
CORRELATION OF DATA	15
REFERENCES	17
APPENDIX I - ILLUSTRATIONS - (Figures 1 through 51)	19
APPENDIX II - MATHEMATICAL ANALYSES	71
APPENDIX III - TEST FACILITY, EXPERIMENTAL PROCEDURES AND DATA REDUCTION	89
DISTRIBUTION	95

LIST OF ILLUSTRATIONS

<u>FIGURE NO.</u>		<u>Page No.</u>
1	DEFLECTION SURFACE PARAMETERS	20
2	DEFLECTION SURFACE CONFIGURATIONS	21
3	PRIMARY NOZZLE INSTALLED ON TEST STAND	22
4	NOZZLE EFFICIENCY VS. PRESSURE RATIO	23
5	TOTAL PRESSURE DISTRIBUTION ACROSS PRIMARY NOZZLE SPAN	24
6	NOZZLE WITH SIDE PLATES FOR DETERMINATION OF SIDE PLATE LOSSES	25
7	SIDE PLATE-JET BOUNDARY LAYER TRACE (NOZZLE WITH SIDE PLATES)	26
8	CONFIGURATION A INSTALLED ON TEST STAND	27
9	EFFECT OF VERTICAL DISPLACEMENT ON RESULTANT FORCE (CONFIGURATION A)	28
10	EFFECT OF VERTICAL DISPLACEMENT ON LIFT FORCE (CONFIGURATION A)	29
11	EFFECT OF VERTICAL DISPLACEMENT ON DEFLECTION ANGLE (CONFIGURATION A)	30
12	PRESSURE PROFILE AROUND DEFLECTION SURFACE (AT JET CENTERLINE OF CONFIGURATION A, $h = .25$, $l = .5$)	31
13	PRESSURE PROFILE AROUND DEFLECTION SURFACE (3.00 INCHES OFF CENTERLINE OF CONFIGURATION A, $h = .25$, $l = .5$)	32
14	PRESSURE PROFILE AROUND DEFLECTION SURFACE (AT JET EDGE OF CONFIGURATION A, $h = .25$, $l = .5$)	33
15	PRESSURE PROFILE AROUND DEFLECTION SURFACE (AT JET CENTERLINE OF CONFIGURATION A, $h = .75$, $l = 1.5$)	34
16	PRESSURE PROFILE AROUND DEFLECTION SURFACE (3.00 INCHES OFF CENTERLINE OF CONFIGURATION A, $h = .75$, $l = 1.5$)	35
17	PRESSURE PROFILE AROUND DEFLECTION SURFACE (AT JET EDGE OF CONFIGURATION A, $h = .75$, $l = 1.5$)	36

LIST OF ILLUSTRATIONS

<u>FIGURE NO.</u>		<u>Page No.</u>
18	SURFACE STATIC PRESSURE DISTRIBUTION (CONFIGURATION A, $h = .25$, $l = .50$)	37
19	SURFACE STATIC PRESSURE DISTRIBUTION (CONFIGURATION A, $h = .75$, $l = 1.50$)	38
20	FLOW VISUALIZATION AT JET EDGE (CONFIGURATION A) $h = .50$, $l = .25$, $P_r = 1.1$	39
21	FLOW VISUALIZATION BETWEEN JET SHEET AND DEFLECTION SURFACE AT CENTER SPAN (CONFIGURATION A) $h = .50$, $l = .25$, $P_r = 1.1$	40
22	FLOW VISUALIZATION OF EXTERNALLY ENTRAINED AIR AT CENTER SPAN (CONFIGURATION A) $h = .50$, $l = .25$, $P_r = 1.1$	41
23	FLOW VISUALIZATION OF EXTERNALLY ENTRAINED AIR AT CENTER SPAN (CONFIGURATION A) $h = .50$, $l = .25$, $P_r = 1.1$	42
24	CONFIGURATION B INSTALLED ON TEST STAND	43
25	EFFECT OF VERTICAL DISPLACEMENT ON RESULTANT FORCE (CONFIGURATION B)	44
26	EFFECT OF VERTICAL DISPLACEMENT ON LIFT FORCE (CONFIGURATION B)	45
27	EFFECT OF VERTICAL DISPLACEMENT ON DEFLECTION ANGLE (CONFIGURATION B)	46
28	PRESSURE PROFILE AROUND DEFLECTION SURFACE (AT JET CENTERLINE OF CONFIGURATION B, $h = 1.00$, $l = 1.00$)	47
29	PRESSURE PROFILE AROUND DEFLECTION SURFACE (3.00 INCHES OFF CENTERLINE OF CONFIGURATION B, $h = 1.00$, $l = 1.00$)	48
30	PRESSURE PROFILE AROUND DEFLECTION SURFACE (AT JET EDGE OF CONFIGURATION B, $h = 1.00$, $l = 1.00$)	49
31	SURFACE STATIC PRESSURE DISTRIBUTION (CONFIGURATION B, $h = 1.00$, $l = 1.00$)	50

LIST OF ILLUSTRATIONS

<u>FIGURE NO.</u>		<u>Page No.</u>
32	FLOW VISUALIZATION OF ENTRAINMENT FROM SIDE OF NOZZLE (CONFIGURATION B) $h = 1.00$, $l = 1.00$, $P_r = 1.4$	51
33	FLOW VISUALIZATION BETWEEN JET SHEET AND DEFLECTION SURFACE AT CENTER SPAN (CONFIGURATION B) $h = 1.00$, $l = 1.00$, $P_r = 1.4$	52
34	FLOW VISUALIZATION OF EXTERNALLY ENTRAINED AIR AT CENTER SPAN (CONFIGURATION B) $h = 1.00$, $l = 1.00$, $P_r = 1.4$	53
35	FLOW VISUALIZATION OF EXTERNALLY ENTRAINED AIR AT CENTER SPAN (CONFIGURATION B) $h = 1.00$, $l = 1.00$, $P_r = 1.4$	54
36	CONFIGURATION C INSTALLED ON TEST STAND	55
37	EFFECT OF VERTICAL DISPLACEMENT ON RESULTANT FORCE (CONFIGURATION C)	56
38	EFFECT OF VERTICAL DISPLACEMENT ON LIFT FORCE (CONFIGURATION C)	57
39	EFFECT OF VERTICAL DISPLACEMENT ON DEFLECTION ANGLE (CONFIGURATION C)	58
40	PRESSURE PROFILE AROUND DEFLECTION SURFACE (AT JET CENTERLINE OF CONFIGURATION C, $h = 1.25$, $l = 1.00$)	59
41	PRESSURE PROFILE AROUND DEFLECTION SURFACE (3.00 INCHES OFF CENTERLINE OF CONFIGURATION C, $h = 1.25$, $l = 1.00$)	60
42	PRESSURE PROFILE AROUND DEFLECTION SURFACE (AT JET EDGE OF CONFIGURATION C, $h = 1.25$, $l = 1.00$)	61
43	SURFACE STATIC PRESSURE DISTRIBUTION (CONFIGURATION C, $h = 1.25$, $l = 1.00$)	62
44	EFFECT OF PRESSURE RATIO ON RESULTANT FORCE (CONFIGURATION C)	63

LIST OF ILLUSTRATIONS

<u>FIGURE NO.</u>		<u>Page No.</u>
45	FLOW VISUALIZATION BETWEEN JET SHEET AND DEFLECTION SURFACE AT CENTER SPAN (CONFIGURATION C) $h = 1.25$, $l = 1.00$, $P_r = 1.4$	64
46	FLOW VISUALIZATION OF ENTRAINMENT AT CENTER SPAN (CONFIGURATION C) $h = 1.25$, $l = 1.00$, $P_r = 1.4$	65
47	FLOW VISUALIZATION OF ENTRAINED AIR AT CENTER SPAN (CONFIGURATION C) $h = 1.25$, $l = 1.00$, $P_r = 1.4$	66
48	FLOW VISUALIZATION OF SECONDARY AIR SHOWN WITH SMOKE GENERATOR (CONFIGURATION C) $h = 1.25$, $l = 1.00$, $P_r = 1.4$	67
49	SIDE PLATE-JET BOUNDARY LAYER TRACE (CONFIGURATION B) $h = 1.00$, $l = .75$, $P_r = 1.4$	68
50	SIDE PLATE-JET BOUNDARY LAYER TRACE (CONFIGURATION C) $h = .80$, $l = .5$, $P_r = 1.4$	69
51	CONFIGURATION C WITH SPLITTER	70
52	MATHEMATICAL MODEL IN PHYSICAL PLANE (Z) - POTENTIAL FLOW ANALYSIS	73
53	MATHEMATICAL MODEL IN HODOGRAPH PLANE (ζ and Ω) - POTENTIAL FLOW ANALYSIS	75
54	MATHEMATICAL MODEL - THICK JET ANALYSIS	79
55	PERFORMANCE ENVELOPE - THICK JET ANALYSIS	87
56	PRESSURE RAKE DETAILS	92

SYMBOL LIST

All Pressures Gage Unless Otherwise Noted

All Dimensions are in Compatible Units Unless Otherwise Noted

GENERAL

C_p	Specific heat at constant pressure
F	Force
g	Gravitational constant
h	Secondary inlet height or vertical displacement of nozzle centerline from station 0 on surface (ref. Figure 1)
J	778 ft lb/BTU
k	Ratio of specific heat
l	Horizontal displacement of nozzle exit from station 0 on surface (ref. Figure 1)
p	Static pressure
P	Total pressure
P_r	Pressure ratio
r	Radius
s	Distance along surface
t	Thickness of jet
T	Total temperature
V	Velocity
\dot{w}	Weight flow rate
γ	Wake deflection angle
θ	Temperature ratio $\frac{T}{T_{osl}}$
η	Efficiency
ρ	Density
ϕ	Normalized thrust force (refer to Appendix II, Data reduction)

GENERAL SUBSCRIPTS

e	Nozzle exit
j	Jet
m	Measured

SYMBOL LIST

GENERAL SUBSCRIPTS (Con't)

n	Nozzle
o	Ambient
osl	Sea level standard
r	Resultant
s	Surface
x	Horizontal or drag direction (ref. Figure 1)
z	Vertical or lift direction (ref. Figure 1)

SUPERSCRIPT

Prime indicates "per unit surface span"

MISCELLANEOUS SPECIFIC SYMBOLS ARE DEFINED WHERE USED

I. SUMMARY

This report describes the contractor's studies of the ventilated clinging flow phenomenon conducted under Contract DA 44-177-TC-848. This phenomenon is the result of a jet sheet following a curved surface located close to, but separated from, the jet by an induced stream of ambient air. When the jet sheet is not separated from the surface by an induced stream, the phenomenon is commonly referred to as the Coanda effect. A thick jet analysis of the phenomenon was derived that assesses the thrust augmentation possibilities of the concept. The report discusses the test program, which utilized three deflection surfaces in a test series, directed towards obtaining basic flow field data and determining the feasibility of augmenting the thrust while deflecting the jet.

Thrust augmentation was found definitely possible by the ventilated clinging flow deflection principle. One of the surfaces, tested at the optimum ventilation, produced a thrust augmentation of 6% (based on the primary jet thrust) while deflecting the jet 58° from its original direction. Without ventilation (jet adjacent to surface), the jet was deflected 60° with loss in thrust of 20%.

The experimental data obtained in this program describe the deflection surface operation in terms of resultant force, ϕ , lift force, ϕ_z , and jet deflection angle, γ . A qualitative description of the flow field of the three deflection surface configurations is presented in terms of the deflection surface static surface pressures, and wake pressure profiles. Flow visualization studies were also conducted to aid in the understanding of the phenomenon.

II. CONCLUSION

- A. The analytical and experimental work conducted in this program has proven that flow deflection with thrust augmentation is possible by means of the ventilated clinging flow concept.
- B. In all tests, the thrust increased as the ventilating gap was increased within the limits of flow attachment.
- C. An augmentation in thrust of 6% was obtained with a surface that deflected the jet 58° . (This can be compared to a loss of about 10% for an optimum Coanda effect deflection system.)
- D. Side plates were required for best performance of the configurations tested, which all had a primary nozzle aspect ratio of 100.
- E. Side plate frictional effects caused a thrust loss of approximately 2%; thus an augmentation approaching 8% can be expected with larger aspect ratios.
- F. Thin jet ventilated clinging flow theory is adequate for the prediction of the surface pressures, but does not permit assessment of thrust augmentation possibilities.
- G. The thick jet analysis indicated that the tested configurations may not be optimum; however, the effects of stream mixing need more rigorous inclusion in the analysis.

III. INTRODUCTION

The clinging phenomenon of a two-dimensional jet flowing over a curved or deflected surface is commonly known as the Coanda effect (ref. 1). This effect has been studied as a thrust-augmenting device and as a means of air deflection by many investigators. Foa's (ref. 2) investigations of a two-dimensional air jet tangent to a curved surface indicated rather high thrust augmentation. However, a study by Gates (ref. 3) of Hiller Aircraft under ONR contract did not confirm Foa's results, although clinging flow did prove to be a surprisingly efficient jet turning device. von Glahn's (ref. 4) work at NASA agreed, in general, with Gates' study. From these various works, it is interesting to note that the surface to which the ejected fluid attaches need not be curved, but can be a flat plate set at an angle to the jet axis. In fact, Boyer (ref. 5) found that in certain cases with large plate deflections, the flow actually detached locally yet was still turned by the influence of the surface. The locally detached but deflected flow obtained with flat surfaces was also experienced by Gates and von Glahn.

The study of ventilated clinging flow is relatively recent. Ventilated clinging flow is a flow system which incorporates clinging flow over a surface where the surface is separated from the jet by an induced stream of ambient air. von Glahn had indicated in his early work (ref. 4) that small leakage between jet and surface had no apparent ill effect on the clinging phenomenon. Hiller studies which began in 1961 considered, in particular, the way the secondary flow was induced and mixed with the primary stream. The process appeared to be very similar to the flow conditions in an ejector type thrust augmentor. Thus it was thought that it might be possible to produce a flow deflection device with a turning efficiency greater than 100%. Preliminary tests were then made which indicated efficiencies as high as 98%.

More recently, Korbacher (ref. 6), at the University of Toronto, reported high turning efficiencies for detached deflection surfaces, i.e., in the ventilated clinging flow regime. Korbacher has not used a configuration conducive to thrust augmentation in his tests, as his interests, apparently, were only in turning the jet. The sharp leading edge of the deflection surface tends to cause losses that can appreciably reduce the amount of secondary flow that can be induced. Korbacher offers a non-viscous, thin jet theory not unlike that proposed by Chaplin (ref. 7) for a jet sheet in ground effect. This theory adequately predicts and correlates the deflection surface pressures as related to the radius of the deflection surface and thrust of the primary jet.

In the current investigation, supported by the U. S. Army Transportation Research Command, the operation and flow field characteristics have been documented in greater detail with special emphasis on the thrust augmentation. An attempt has also been made to formulate a mathematical description of the phenomenon.

The basic purpose of this program is to determine and develop a more efficient, easier applied, thrust augmentation and deflection device for use in future Army transportation systems than is currently available.

IV. MATHEMATICAL DESCRIPTION

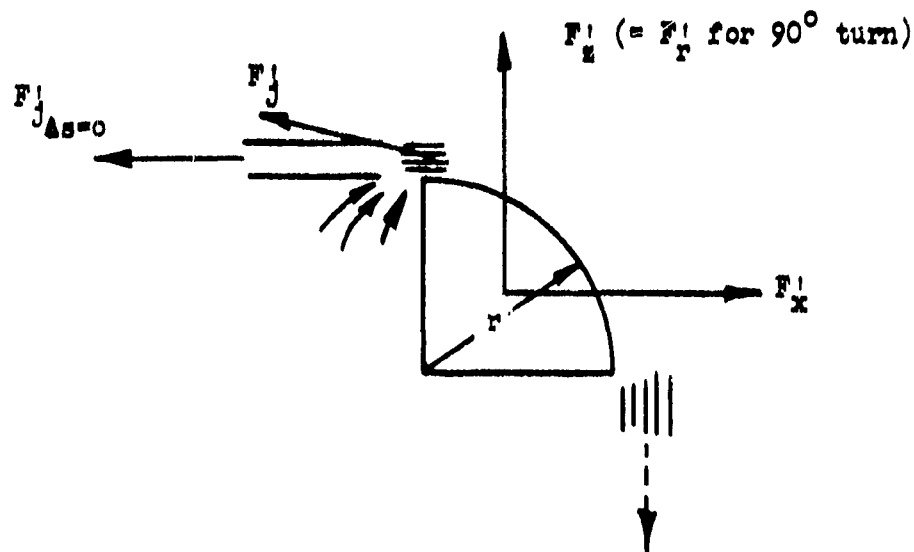
The mathematical description of the ventilated clinging flow phenomenon has been considered from the standpoint of a problem in potential flow and from the standpoint of an assumed flow distribution which was thought reasonable under certain restricted conditions. In the latter work, both thick and thin jets have been considered.

A. POTENTIAL FLOW ANALYSIS

Yen and Bursik in reference 8 suggest a possible analysis of the blown slotted flap, which is, in essence, the ventilated clinging flow concept. Their analysis assumes inviscid, incompressible flow and is patterned after an earlier analysis of clinging flow by Lighthill (ref. 9). The prime interest of Yen's was the location of the separation points between the induced stream and physical surface. Their solution would, however, give a good description of the potential inlet flow and the transition of the uniform jet flow into the vortex flow around the surface. The solution would also permit prediction of the surface pressures. The solution entails a hodograph transformation and the description of the streamline separating the jet and ambient flow, which is predicated on conditions of continuous pressure and velocity sense across the separating streamline. In order to describe the flow system in the hodograph plane, it is necessary to define the ambient or induced flow as a jet at infinity (i.e., velocity of ambient air at infinity, V_{amb} , is finite rather than zero). Consequently, this makes the analysis of the static ($V_{amb} = 0$) impossible to achieve by this technique. However, it can be simulated by assuming a high velocity ratio between the jet and ambient stream. Yen does not complete the solution of this flow system in reference 8 due to admitted mathematical difficulties. He does indicate the possibility of solution through use of electrical analog plot. This was the course of analysis initially pursued by the writers. The details of the solution are outlined in Appendix II. This technique was not carried through to completion, as the effort required to achieve a solution was not deemed commensurate with the benefit obtainable from a non-mixing (inviscid) solution at this stage of development. In the analog solution, the time-consuming manipulation is the trial and error analog-numerical integration required to match an assumed jet ambient stream interface with an assumed deflection surface. The test program and simplified analyses have better defined the input conditions and the importance of the information the potential analysis can provide. It can now be an effective part of future research.

B. THIN JET ANALYSIS

The measured force produced by the system is the result of the primary nozzle jet reaction, the summation of the external surface pressures, and the fluid-model surface shear force. For the purpose of the analysis, the shear force can be ignored and all the external pressure will be assumed to act on a 90° circular deflection surface.



Assuming an equal pressure distribution over the surface, it can be shown that

$$F'_r = p_s r$$

Now by the thin jet theory (ref. 6),

$$p_s = \frac{F'_j}{r}$$

which is the suction pressure developed by the flow to overcome the centrifugal force caused by turning the thrust, F'_j . Combining these expressions gives

$$\phi = \frac{F'_r}{F'_{j\Delta s=0}} = \frac{F'_j}{F'_{j\Delta s=0}} \text{ or } = \frac{p_s}{p_{s\Delta s=0}}$$

It is apparent that the thrust of the turned jet, F'_j , must be greater than the thrust of the primary jet, $F'_{j\Delta s=0}$, in order for thrust augmentation (ϕ) to occur; or the observed surface pressure must be greater than that predicted on the basis of the primary jet thrust. In summation, flow augmentation must take place upstream of the turn. In a way of speaking, it is seen in this system that the curved deflection surface strengthens the sink inducing the secondary flow in a manner similar to the diffuser of a conventional ejector.

While stream mixing has been ignored in drawing this parallel, it is actually this effect that energizes the secondary flow so that it can leave the surface at ambient pressure or, in other words, so that an exit sink does not exist as well.

C. THICK JET ANALYSIS

The difficulties of the potential flow analysis have been circumnavigated by making several rather arbitrary assumptions and then only considering the flow condition at specific areas which tend to be relatable to the physical configuration. In this way it has been possible to obtain an expression which shows that the augmentation ratio,

$$\phi = f \left(\frac{t_s}{t_p}, \eta \right)$$

where

$\frac{t_s}{t_p}$ is the ratio of the initial thickness of primary stream and secondary stream.

η is an assumed efficiency of energy transfer between the streams.

The analysis defines the radius of the deflection surface only for the zone where the flows are unmixed and flowing with a free vortex distribution in curved paths with coincident radii centers. For these conditions to be satisfied,

$$\frac{r_d}{t_p} = f \left(\frac{t_s}{t_p}, \eta \right) \text{ also,}$$

where

$\frac{r_d}{t_p}$ is the ratio of the radius of the deflection plate to the primary jet thickness.

The thrust augmentation, ϕ , is plotted as a function of these and other parameters in Figure 55. A detailed derivation is in Appendix II. The implications of the assumptions are discussed and conclusions drawn relative to experimental results also in Appendix II.

V. TEST PROGRAM

The test facility, experimental procedures, and the data reduction are discussed in Appendix II. Figures 1 and 2 provide a general description of the deflection surface configurations (and primary nozzle) evaluated in this program. Except as otherwise noted, the tests were conducted at primary jet pressure ratio (P_r) of 1.4.

A. PRIMARY NOZZLE

1. Description

Figure 1 shows the primary, jet sheet, nozzle used through the test program. The nozzle exit is 0.085 inch high and 8.78 inches wide (aspect ratio approximately 103). The nozzle is made of .25-inch steel plate to maintain a constant exit cross-section. The inner sides of the nozzle exit edges are machined to a feather edge so that the jet exit width is essentially equal to the overall width. A pressure tap is located in the rear of the nozzle plenum opposite the supply duct connection (see Figure 3). The reservoir pressure measured at this tap is the reference primary jet supply pressure (P_j) and is used to establish the operating pressure ratio (P_r).

2. Calibration

The nozzle thrust efficiency was determined for various pressure ratios (see Figure 4) by operating the nozzle in both the horizontal and the vertical positions. A nozzle thrust efficiency of 0.942 was obtained for the normal operating pressure ratio of 1.4. The nozzle thrust efficiency is defined by the equation

$$\eta_h = \frac{F_m}{F_{\Delta s=c}}$$

where

$$F_{\Delta s=0} = \frac{\dot{w}_m V_{thec}}{g}$$

This is completely defined in Appendix II.

3. Velocity Distribution

A jet survey was conducted to calibrate the reference pressure tap and to obtain the total pressure profile across the nozzle span, 0.10 inch downstream of the nozzle exit horizontal centerline. The calibrated total pressure tube had an outside diameter of 0.050 inch. The data obtained (see Figure 5) indicate no significant abnormalities in the nozzle which would adversely affect the performance of the nozzle and deflection surface system. The data also validate the P_j tap. The nozzle pressure survey did not reflect the loss

indicated by the thrust measurements because the survey was made only at the horizontal centerline, i.e., the peak velocity point. The thinness of the jet made determination of the vertical pressure gradient of the jet impractical due to the size of the probe in relation to jet thickness.

4. Side Plate Evaluation

The nozzle was tested with parallel side plates to determine the losses inherent in such a system for comparison with subsequent model data. The setup is shown in Figure 6. Data indicated a nozzle thrust efficiency of .918 with the side plates, while previous data gave a nozzle efficiency of .942 for the nozzle without side plates. This amounts to an indicated side plate loss of 2.6% for this flow system. An indication of the "scrubbing" between the jet and side plate is illustrated by Figure 7.

B. CONFIGURATION A DEFLECTION SURFACE

The basic dimensions of Configuration A are shown in Figures 1 and 2. The deflection surface had a 6.00-inch radius over a 135° arc. The leading or inlet edge had a radius of 1.25 inches. The span of Configuration A was 20 inches as shown in Figure 2, or approximately 2.3 times the nozzle span. Side plates were not used. Figures 9 through 23 present the data which describe the operation and performance of this deflection surface.

1. Performance

Figure 9, which describes the effect of h and l on the resultant deflected thrust, is very interesting. This curve shows that ϕ is slightly greater than the actual primary jet thrust after the jet has apparently separated from the deflection surface. Figure 10 helps explain this point. Figure 10 shows that after separation has occurred, for all practical purposes, sufficient ambient air is still entrained to produce a small lift force, ϕ_z . This lift force, when combined with the measured thrust force, is sufficient to produce a resultant force, ϕ , in excess of the initial jet thrust.

Study of Figures 10 and 11 shows that the maximum lift force (73.7% of the ideal jet thrust) occurred while turning the jet 67° at a value of $h = 0.25$ inch. Figure 9 reveals that the jet was turned with a 78% thrust efficiency at this condition.

The region of flow separation and hysteresis, which is indicated on the curves, was noted to be unusually narrow and not nearly as sharply defined as compared to previous experience with clinging flow phenomena with side plates (ref. 3). The value of h , which resulted in separation or reattachment for a specific value of l , was found to vary widely

within the zone of separation. This zone of separation was independent of l , as can be seen from the figures.

This "soft" separation characteristic is believed to result from the fact that the jet sheet is never completely attached to the surface over the entire span of the jet sheet; i.e., portions (edges) of the jet sheet are turned only slightly from the original jet direction. This is caused by the large entrainment of ambient fluid at the jet edge and consequent loss of turning suction. The separation appears to begin at the edges and to progress toward the center of the jet span, which is the only portion of the jet effectively attached to the surface. The zone of separation corresponds to the separation of this central portion of the jet.

2. Wake Survey

Figures 12 through 17 present wake survey data (static pressure, total pressure, and velocity head) which describe the jet as it proceeds around the deflection surface. The figures support the analysis of the "soft" separation characteristic described above. With the jet located close to the surface ($h = 0.25$), Figure 12 reveals that the only portion of the jet effectively attached to the surface is in the vicinity of the jet span centerline. Comparison of Figures 12 and 13 shows that separation occurs further upstream as the observation plane moves toward the jet edge. Figure 14 shows that as the flow proceeds around the deflection surface from the nozzle in the plane of the jet edge, the flow separates from the surface between the 30° and 60° stations. Figures 15, 16, and 17 show similar wake data when the nozzle is 0.75 inch above the surface. It will be noted from this latter data that jet attachment is even more limited than in the previous case.

3. Surface Pressures

The surface static pressures are shown in Figures 18 and 19 for the same test conditions as the previous data. Strong pressure gradients are indicated by these data transverse to the jet path. The data support the "soft" separation characteristic of this model as described above. Figure 18, with the jet located close to surface, indicates that the flow in the plane of the jet edge starts separating from the surface at approximately the 45° station and is essentially separated at the 60° station. This figure also shows that flow separation in the plane of the jet centerline starts at approximately the 60° station and is essentially separated at the 105° station. Similar data shown in Figure 19 reveal that when the nozzle-to-surface distance is increased, the jet attachment is even more limited. Figure 18 shows that when $h = 0.25$ and $l = .5$ inch, unusually high suction pressures are obtained at the crest of the deflection surface. These high pressures are followed by relatively high surface pressures, approximately 1 inch downstream. This is believed to be due to the jet's turning very sharply

into the surface, thus creating the high suction pressure with the low radius turn and the relatively high static pressures downstream by stagnation against the surface.

4. Flow Visualization

The flow field of Configuration A is shown in Figures 20 through 23. Figure 20 illustrates the entrainment of secondary fluid at the jet edge and its consequent de-energization. The effective ejector action occurring between the jet and deflection surface is illustrated clearly by Figure 21. Only this secondary air, drawn over the surface beneath the primary jet sheet, is effective towards producing force augmentation. Figures 22 and 23 illustrate the free jet entrainment which is probably ineffective in producing force augmentation.

C. CONFIGURATION B DEFLECTION SURFACE

Configuration B is dimensionally identical to Configuration A except that the span of the surface was decreased to a value equal to the nozzle width and parallel side plates were added. The general geometry is shown in Figures 1 and 2. The surface is shown installed on the test stand in Figure 24. The test results of this configuration are presented in Figures 25 through 35.

1. Performance

Comparison of Figures 25 and 9 indicates a reduction in ϕ ; however, as seen from a comparison of Figures 26 and 27 with 10 and 11, the jet deflection is considerably greater with side plates. The advantages of separating the jet from the deflecting surface can be clearly seen in Figures 25 and 27 by noting the slope of the curves in the region of h between zero and .7. The value of ϕ increases almost linearly with h while γ remains relatively constant, thus indicating an improvement in turning efficiency. Study of Figures 26 and 27 shows that the maximum lift force (85.9% of the ideal jet thrust) occurred while turning the jet 84.8° at $h = 1.05$ and $l = 1.00$. Figure 25 reveals that the deflected jet was 86.4% of the ideal jet thrust. In Figure 25, only the data representing the attached flow regime are presented for simplicity, as there was much overlapping between the two cases.

The region of flow separation and hysteresis is broader and more sharply defined than Configuration A, as may be seen by comparing Figures 26 and 27 with Figures 10 and 11. This behavior is similar to that found in clinging flow phenomenon where the jet is in intimate contact with the surface (refs. 3 and 4). These tests have shown that it is necessary to seal the edges or sides of the effective ejector mixing zone (between curved jet and deflection surface) in order to obtain good jet turning. However, side plates introduce additional friction losses. These losses can be reduced by increasing the jet aspect ratio (decreasing jet thickness) or possibly by altering the basic jet nozzle outlet

shape so that it forms its own aerodynamic seal.

2. Wake Survey and Surface Pressure

Figures 28 through 30 present the wake survey data (static pressure, total pressure, and velocity head). These data show that sealing the edges of the effective ejector mixing zone, as described above, is necessary to obtain good jet turning. Study of the plots reveals that the side plates, while necessary, do introduce losses. The dynamic pressure is seen to diminish across the deflection surface from the jet centerline to the jet edge.

The wake surveys indicate that the turning radius varies. The wake centerline is seen to deflect sharply toward the surface between station 0 and 30° and then to remain a relatively constant height above the surface to the 60° station. At the 60° station and midspan, the jet is deflected away from the surface and at the edge is deflected toward the surface. These changes in effective jet radius are reflected quite well by the surface pressure shown in Figure 36.

3. Flow Visualization

The flow visualization results are shown in Figures 32 through 35. Figure 32 demonstrates the relative strengths of two sinks (outer jet surface and inner jet surface) in the flow field. In this figure, the smoke source is located outside and upstream of the side plates and level with the upper surface of the nozzle. Notice that the strength of the sink formed between the jet and deflection surface causes the smoke to flow into it even though the path to the outer surface of the jet is more direct.

D. CONFIGURATION C DEFLECTION SURFACE

As with other clinging flow systems, maximum performance was found to occur with the ventilated clinging flow system when separation was imminent. From this observation, it seemed reasonable to expect greater performance if separation could be delayed.

It was then reasoned that the addition of a flat plate, which requires no pressure differential across the fluid to sustain clinging flow downstream of the curved section, would permit a more orderly transition of the boundary layer than that which existed under influence of the "turning" pressure gradient (negative surface pressure). The flat plate can also be thought of as a diffuser permitting gradual transition from the negative surface pressure (curved surface) to ambient pressure at the downstream end of the surface.

As the first step in evaluating this hypothesis, Configuration B was modified by the addition of an adjustable, flat, tangent plate which was tested qualitatively at approximately the 45° , 60° , and 90° stations around the deflection surface. The length of the plate was also

varied. The qualitative data revealed that an 8-inch long plate attached at approximately the 60° station produced maximum augmentation:

$$\phi = 1.0, \phi_z = .86 \text{ at } \gamma = 64^\circ.$$

Subsequently, Configuration B was rebuilt to Configuration C for a more detailed investigation. Figure 36 shows this configuration installed on the test stand. Figures 37 through 48 describe the operation and performance of this configuration.

1. Performance

Figure 37, which describes the effect of h and l on resultant force, ϕ , reveals that the resultant thrust with $h = 1.32$ and $l = 1.00$ was 99.8% of the ideal primary jet thrust, which is in good agreement with the previous qualitative tests. Figures 38 and 39 show that lift force reached a maximum (of 85.1% of the ideal jet thrust) while the jet was turned 58.55° . When these data are adjusted for nozzle efficiency by data from Figure 4, a resultant augmentation ratio of 1.059% is realized.

The flow separation and hysteresis for this configuration differ from those of Configurations B and A. It is of interest to note that re-attachment occurs at roughly the same h and l as for Configuration B; but separation occurs at considerably higher values of h for comparable l values in the case of Configuration C, i.e., the hysteresis loop is larger. It is believed that the delayed separation is due to the improved boundary layer as conjectured previously.

2. Wake Survey

The wake survey data for Configuration C are presented in Figures 40, 41, and 42. These data, in general, indicate that the flow field of Configuration C is very much similar to that observed for Configuration B with the exception that the general velocity level is somewhat lower for Configuration C. It is believed that this reduction in velocity is largely due to the fact that Configuration C permitted a value of h approximately 50% greater than that which is possible with Configuration B. This increase in h results in greater entrainment of secondary air, or more rapid mixing, and, consequently, reduced wake velocities. The lower surface velocities also reduce the shear stresses at the wall and, consequently, improve the performance of the system. The net result is an increase in overall performance.

3. Surface Pressures

The surface pressure distribution shown in Figure 43 is considerably different from that found for Configuration B (Figure 31), but it still follows that trend expected from the effective jet radius given by the wake pressure profiles. In the case of Configuration C, the maximum

suction pressure obtained on the surface is slightly greater than that for Configuration B, but the steady-state suction pressure occurring around the curvature of the surface falls off more rapidly along the surface than it does in the case of Configuration B. It is also seen that the addition of the flat plate has resulted in a gradual transition to ambient pressure.

4. Effect of Pressure Ratio

The effect of pressure ratio on the resultant force was investigated and is shown in Figure 44. The resultant thrust was found to increase with pressure ratio over the range tested. It is significant to note that the curves follow the general trend of nozzle thrust efficiency presented for comparison. This increase in resultant thrust is believed to be due to Reynolds number effects.

5. Flow Visualization

Flow visualization studies shown in Figures 45 through 48 reveal the nature of the flow field of Configuration C. Figure 48 shows the secondary flow field using a smoke generator that was not available for the previous photographs. This smoke generator is described in Appendix II.

E. EVALUATION OF SIDE PLATE THRUST LOSS

The work conducted so far has indicated that side plates are necessary to obtain effective operation. While these side plates are necessary, they also introduce energy losses into the system. Figures 49 and 50 show the side plate boundary layer traces for Configurations B and C, respectively, which were made to aid the understanding of the loss. Several tests were conducted to define the magnitude of the side plate loss. As discussed in paragraph VI A, when plates were attached to the sides of the primary nozzle alone, the thrust was reduced 2.6%. Since these tests did not duplicate the flow conditions very closely, another method was tried. A splitter plate of .070 aluminum of the same dimensions as the side plates was fitted to the contour of the deflection surface for both Configurations B and C. The leading and trailing edges of this plate were rounded and feathered, respectively, to prevent additional turbulent losses. Figure 51 shows the splitter installed on the Configuration C deflection surface in the plane of the jet mid-span. The tests with Configuration B indicated a side plate thrust loss equal to 2.8%. Tests with Configuration C indicated a 2% thrust loss. While the magnitude of the side plate loss as determined by these tests is not great, it does represent a thrust loss that would otherwise appear as thrust augmentation. For example, if the span of Configuration C were increased to a value typical of jet-flap wing, a $\delta \approx 1.08$ can be expected.

VI. CORRELATION OF DATA

A. SURFACE PRESSURES COMPARED WITH THIN JET THEORY

On the basis of the thin jet theory presented by Korbacher (ref. 7), the expected surface pressure for these configurations would be 4.6 inches of water using the surface radius as the jet turning radius. The surface pressure obtained in this program equalled (or exceeded) this value only locally at the crest of the surface (station zero). This tends to indicate that the effective jet turning radius is greater than the surface radius. The optimum jet radius ($r+h$) for Configuration C was 7.34 inches. The predicted surface pressure on the basis of this radius is 3.8 inches of water, which more closely approximates the pressures obtained for this configuration.

B. VELOCITY PROFILE COMPARED WITH THICK JET THEORY

Thick jet theory as presented in paragraph IV C states that a vortex velocity distribution will exist in the flow field. Examination of the dynamic pressure profile around the deflection surface (Figures 12 through 17, 28 through 30, and 40 through 42) shows that a vortex velocity distribution exists in the secondary flow at station 0 in all cases except for Configuration A, when $h = 0.25$. The dynamic pressure distribution at downstream stations (30° , 60° , etc.) is primarily due to mixing which the theory does not include. Therefore, the dimensional relation obtained from the theory has significance only for a short distance downstream of station zero.

C. INTEGRATED SURFACE PRESSURE COMPARED WITH MEASURED FORCES

The measured surface pressures of Configurations B and C were integrated over the deflection surface. The results are tabulated below with the measured forces.

Configuration	ϕ_z	ϕ
B		
(Surface pressure)	1.09	1.11
(Measured force)	.839	.842
C		
(Surface pressure)	1.01	1.21
(Measured force)	.845	.997

The discrepancies in these figures are significant. The normal pressure surveys monitored only the deflection surface and not the upper and lower surfaces of the primary nozzle manifold or the base of the

deflection surface. Additional pressure measurements on these surfaces of Configuration C indicated pressures of significant magnitude. Ambient pressure existed on the upper surface of the nozzle, but suction pressures were measured on the lower surface as high as 4 inches of water. The deflection surface base pressure was found to be approximately .05 inch of water. When these pressures are included in the integration, the difference between the force measurement data and integrated pressure force is reduced to a value understandable in terms of the normal error involved in pressure integrations.

An important result of this finding is the warning it provides of the error that can be introduced into data by not measuring all system forces, as is apparently the case of the data of reference 7, Figure 10. These data are based on measurements made of the deflection surface forces only. The primary nozzle is isolated from the system. Analysis of these data leads to results that are incompatible with the data reported herein. It is believed that the referenced data are in error by the magnitude of the external pressure forces on the primary nozzle, which are, in general, unavoidable.

REFERENCES

1. Coanda, Henri: "Final Report of Contract No. AF 61(514) 1409 between A.R.D.C. Brussels and 'SFERI-Coanda'", Parts I, II and III, Clichy (France).
2. Foa, J. V., and Markstein, G.H.: "Theoretical Analysis of Flow Phenomena in a Pulsejet". Cornell Aeronautical Laboratory, Project SQUID Semi-Annual Progress Report, Jet Propulsion Engines (1952) pp. 195-199.
3. Gates, M. F.: "Static Lift Characteristics of Jet Slots - A Clarifying Study of the External Ejector - Final Report - Contract No. Nonr 2428(00)", Hiller Aircraft Corp., Advanced Research Division Report No. ARD-213, 15 October 1958.
4. von Glahn, U. H., and Povolny, J. H.: "Jet Deflection Devices", SAE Journal, January (1958). (Based on SAE Paper No. 219.)

von Glahn, U. H.: "Use of the Coanda Effect for Obtaining Jet Deflection and Lift with a Single Flat Plate Deflection Surface". NACA TN 4272, Lewis Flight Propulsion Laboratory, Cleveland, Ohio, June (1958).
5. Boyer, L. J.: "Preliminary Investigation and Evaluation of the Coanda Effect". Technical Intelligence Division, Air Material Command, Wright Field, Dayton, Ohio, Technical Report No. F-TR-2207-ND (1948) ATI No. 26895.
6. Korbacher, G. R.: "The Coanda Effect at Deflection Surfaces Detached from the Jet Nozzle", Canadian Aeronautics and Space Journal, January 1962, pp 1-6.
7. Chaplin, Harvey R.: "Theory of the Annular Nozzle in Proximity to the Ground", Washington, D. C., July 1957, David Taylor Model Basin. Aero Report 923.
8. Yen, K. T., and Bursik, J. W.: "On the Action of Blowing Air over a Slotted Flap", Report No. TRAE5605, Dept. of Aeronautical Engineering, Rensselaer Polytechnic Inst., Dec. 1956.
9. Lighthill, M.J.: "Notes on the Deflection of Jets by Insertion of Curved Surfaces, and on the Design of Bends in Wind Tunnels", Rand M No. 2105, Aerodynamics Division, N.P.L., Ministry of Supply, Aeronautical Research Council, September 1945.
10. Pinnes, R. W.: "A Power Plant Man's Look at the Ground Effect Machines", U. S. Navy Department, Bureau of Aeronautics, Research Division Report No. DR-1958, April 1959.

APPENDIX I
ILLUSTRATIONS
Figures 1 through 51

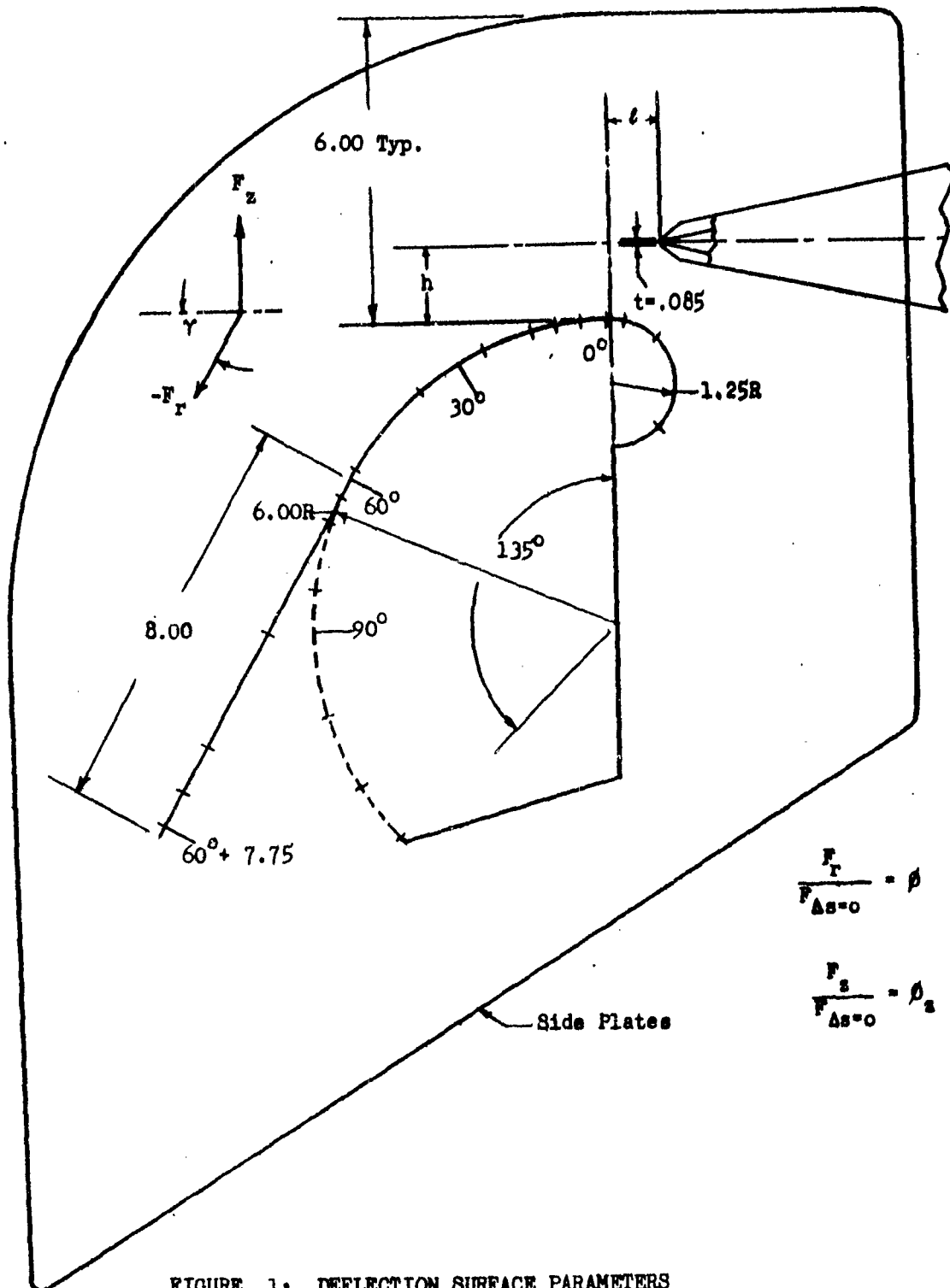
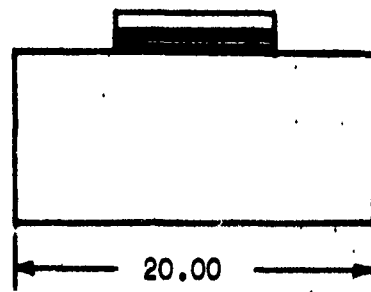
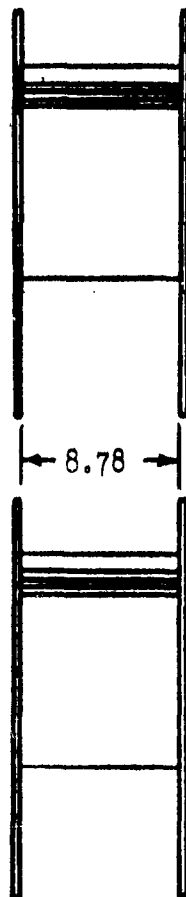
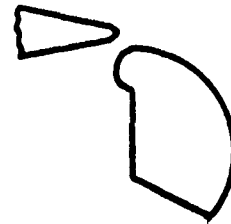


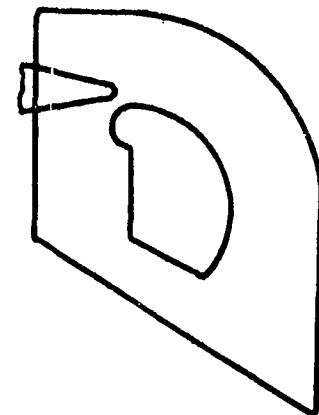
FIGURE 1: DEFLECTION SURFACE PARAMETERS



A



B



C

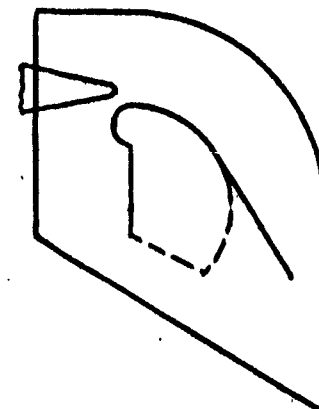


FIGURE 2: DEFLECTION SURFACE CONFIGURATIONS

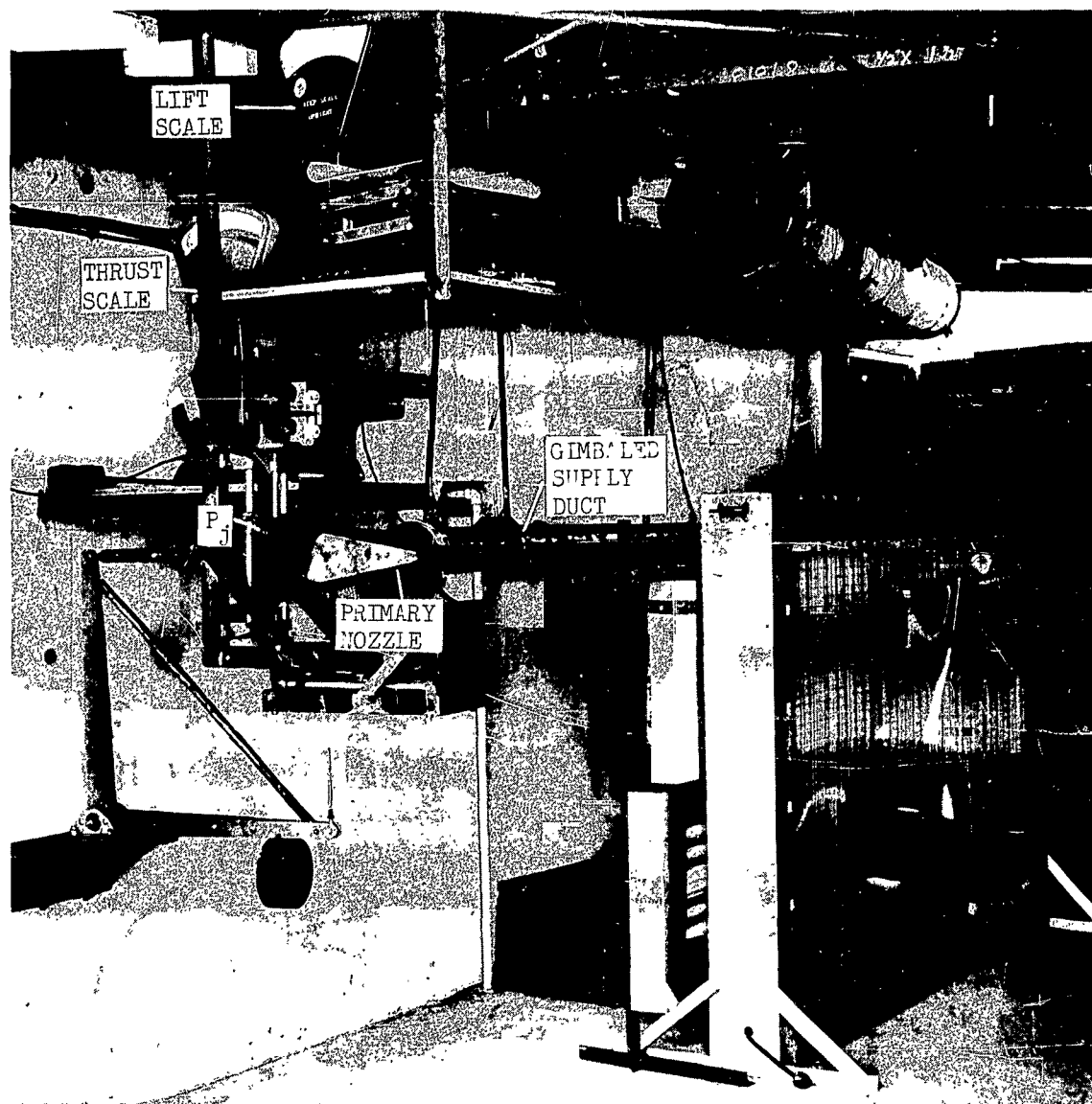


FIGURE 3: PRIMARY NOZZLE INSTALLED ON TEST STAND

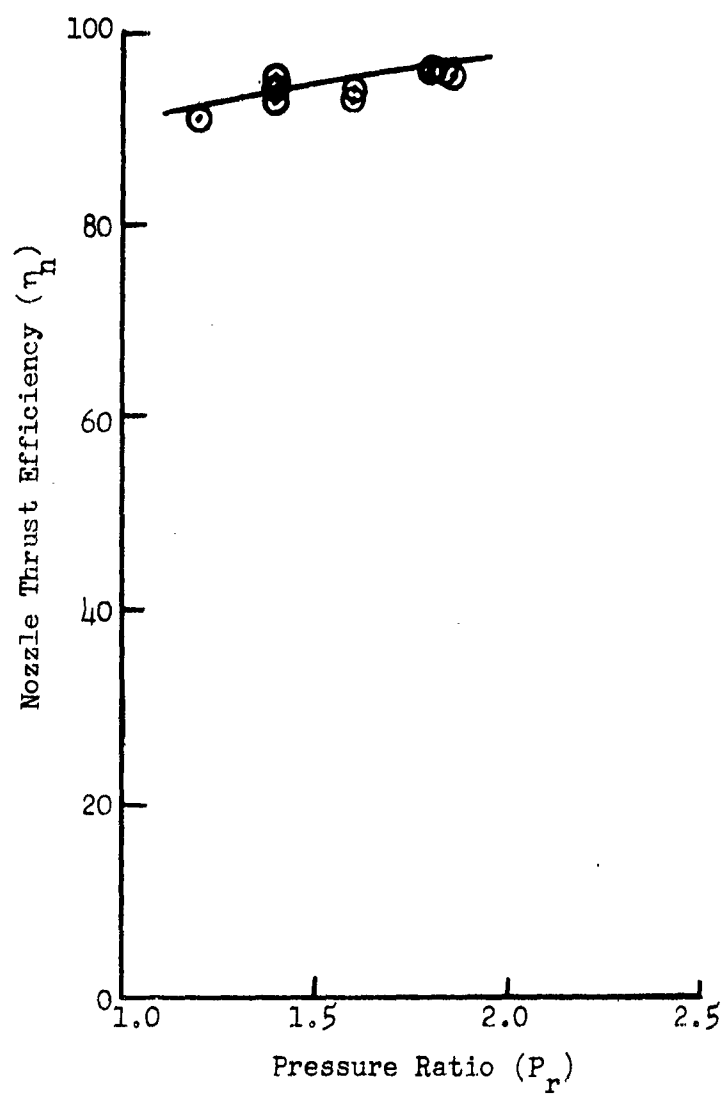


FIGURE 4: PRIMARY NOZZLE EFFICIENCY VS. PRESSURE RATIO

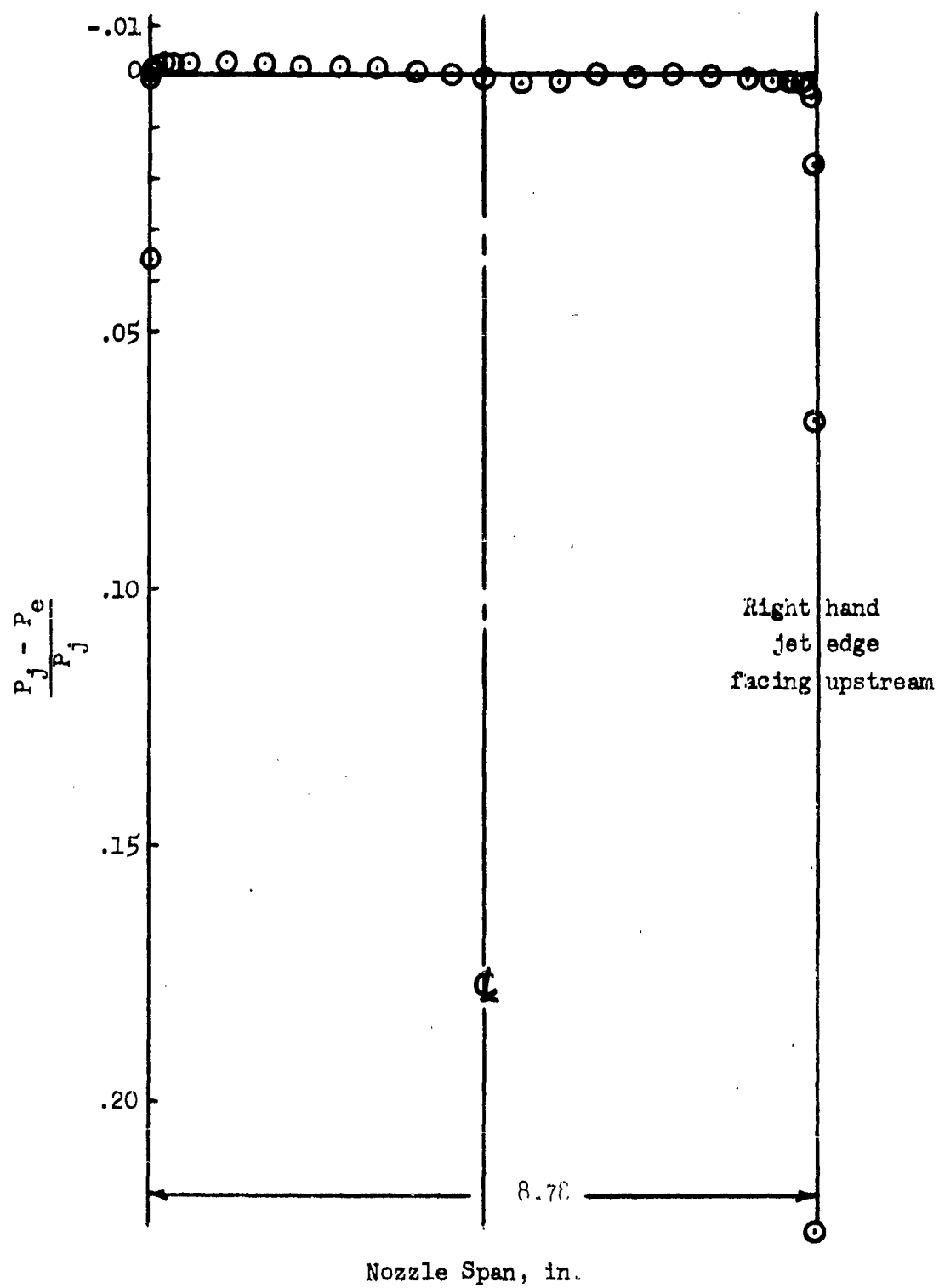


FIGURE 5: TOTAL PRESSURE DISTRIBUTION ACROSS PRIMARY NOZZLE SPAN

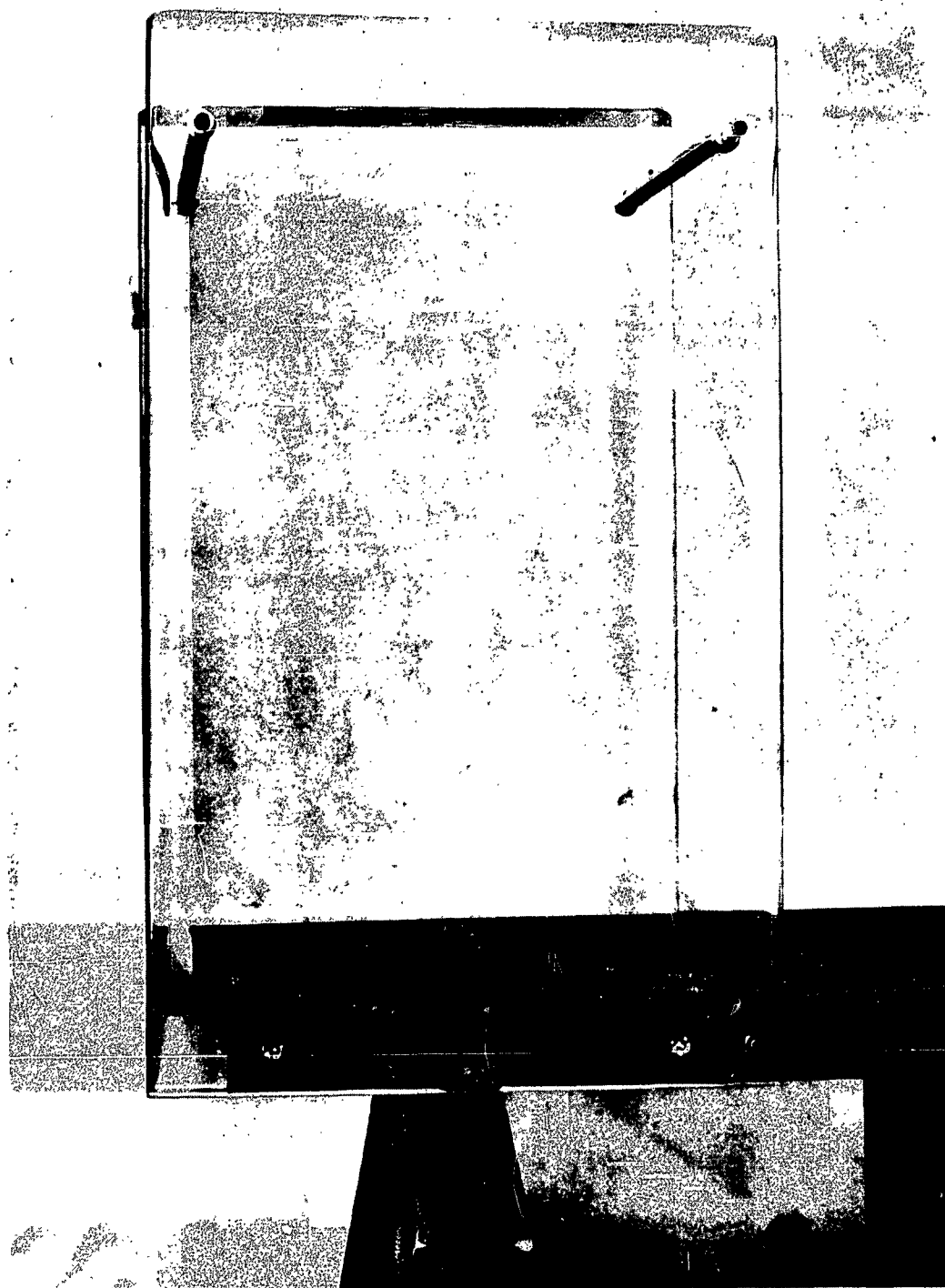


FIGURE 6: NOZZLE WITH SIDE PLATES FOR DETERMINATION OF SIDE PLATE LOSSES

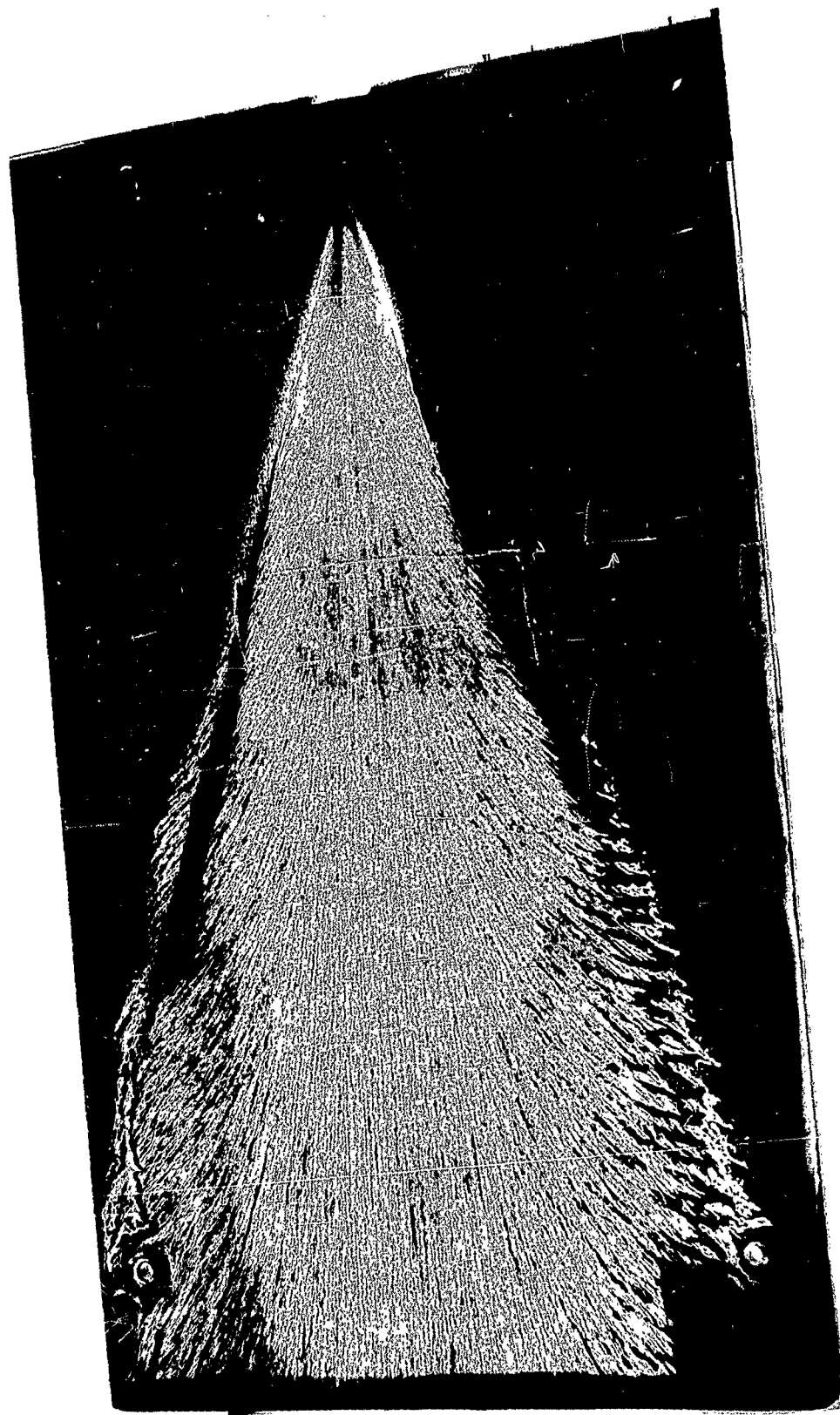


FIGURE 7: SIDE PLATE-JET BOUNDARY LAYER TRACE

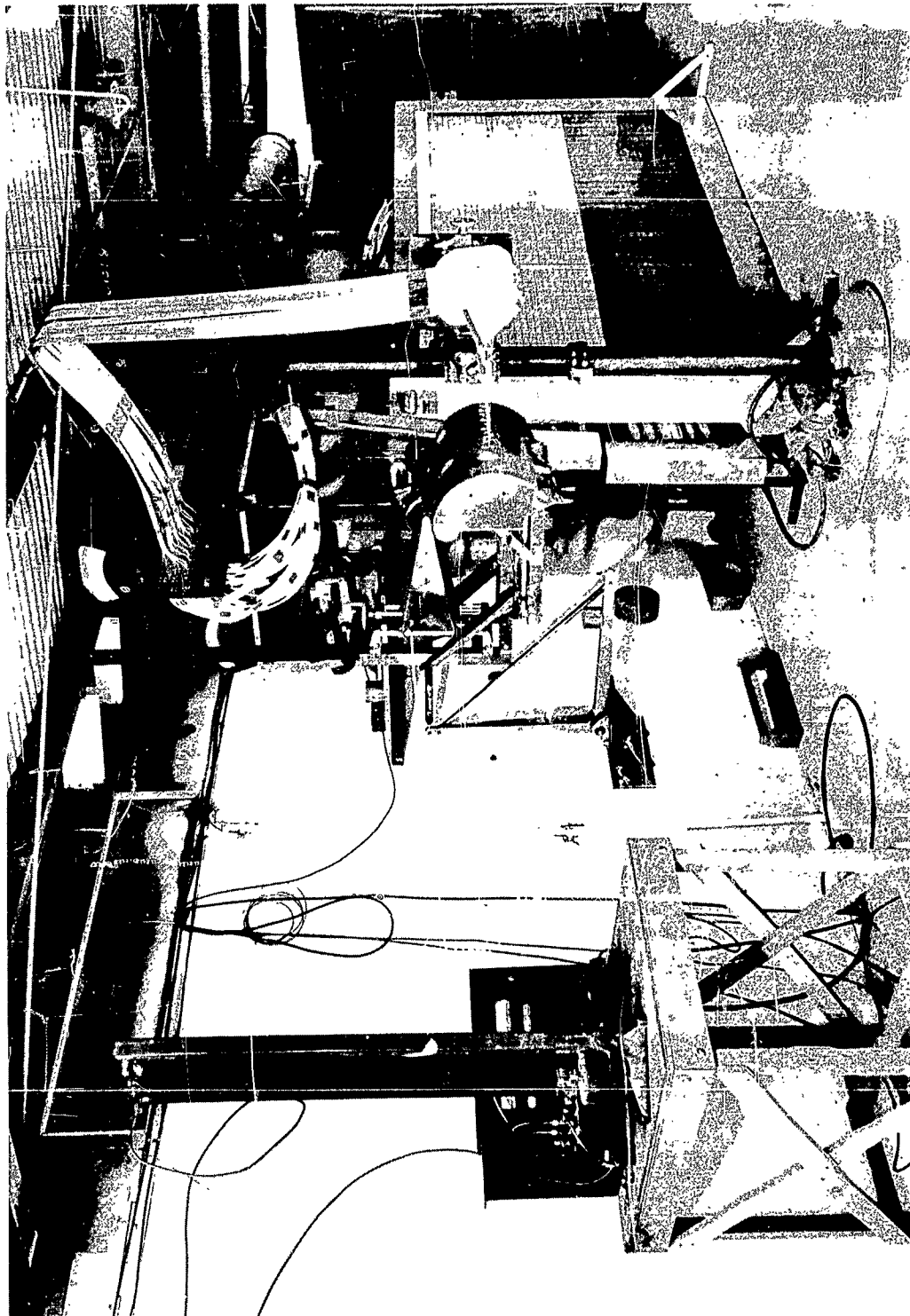


FIGURE 8: CONFIGURATION A INSTALLED ON TEST STAND

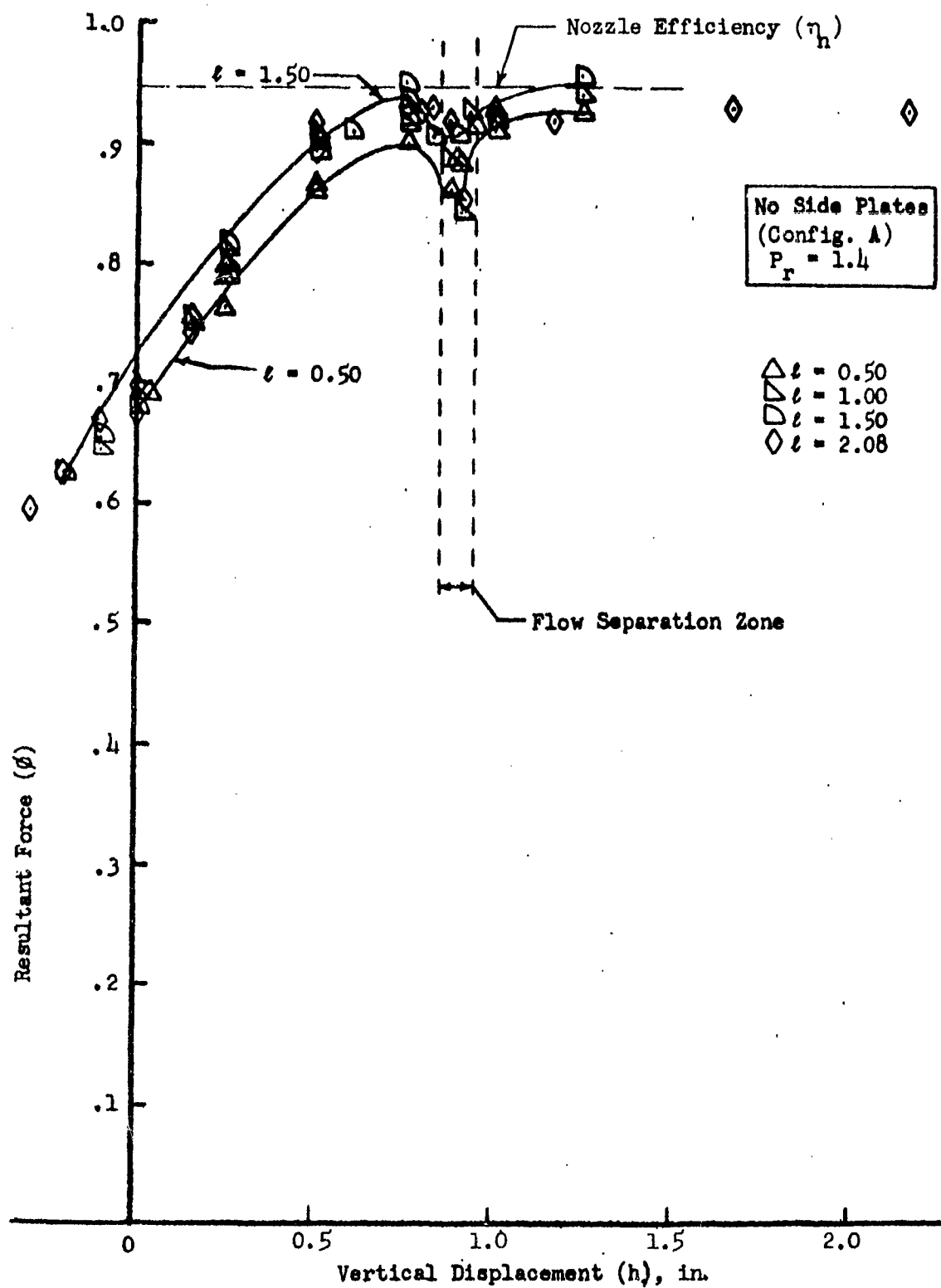


FIGURE 9: EFFECT OF VERTICAL DISPLACEMENT ON RESULTANT FORCE

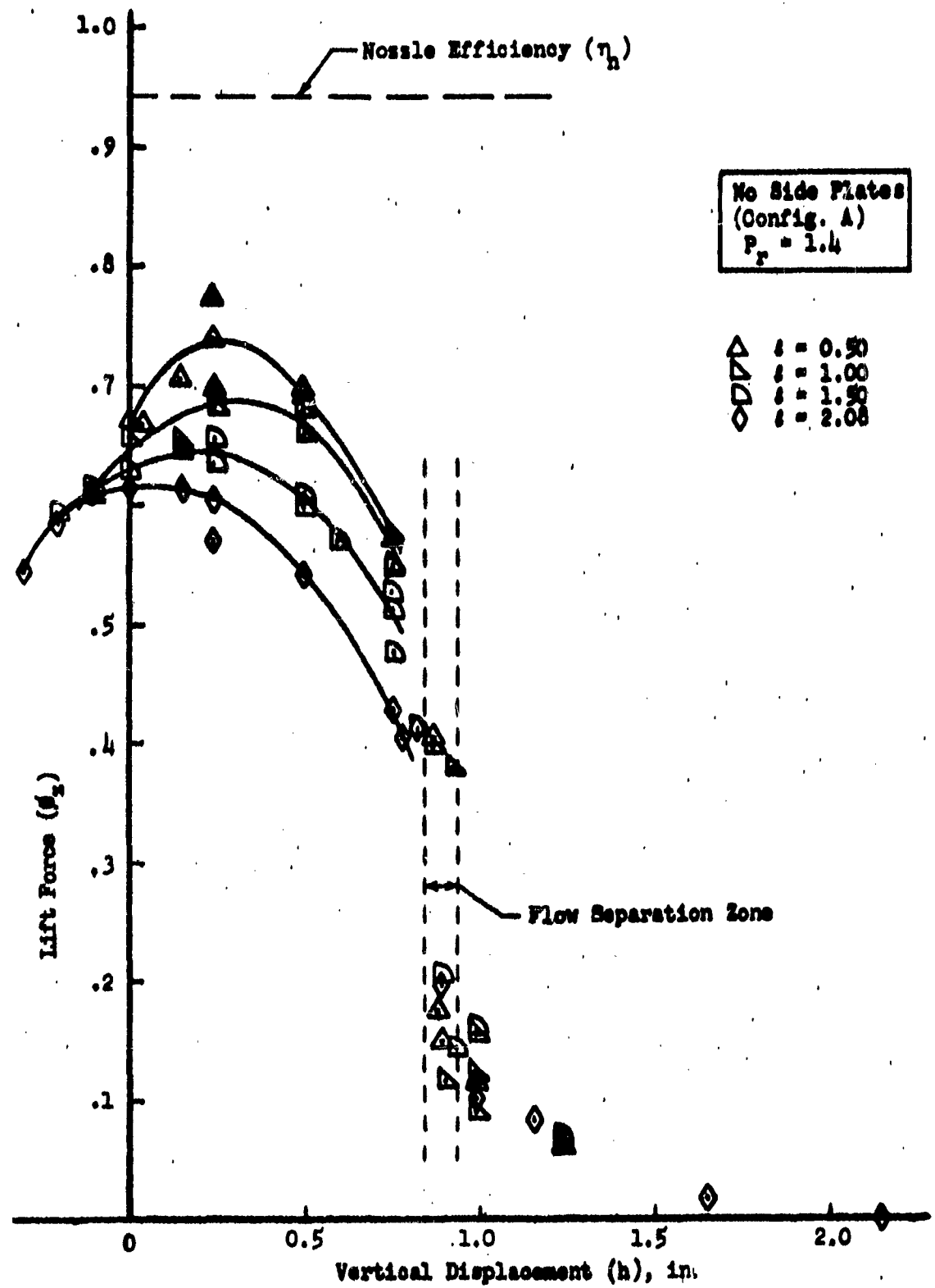


FIGURE 10: EFFECT OF VERTICAL DISPLACEMENT ON LIFT FORCE

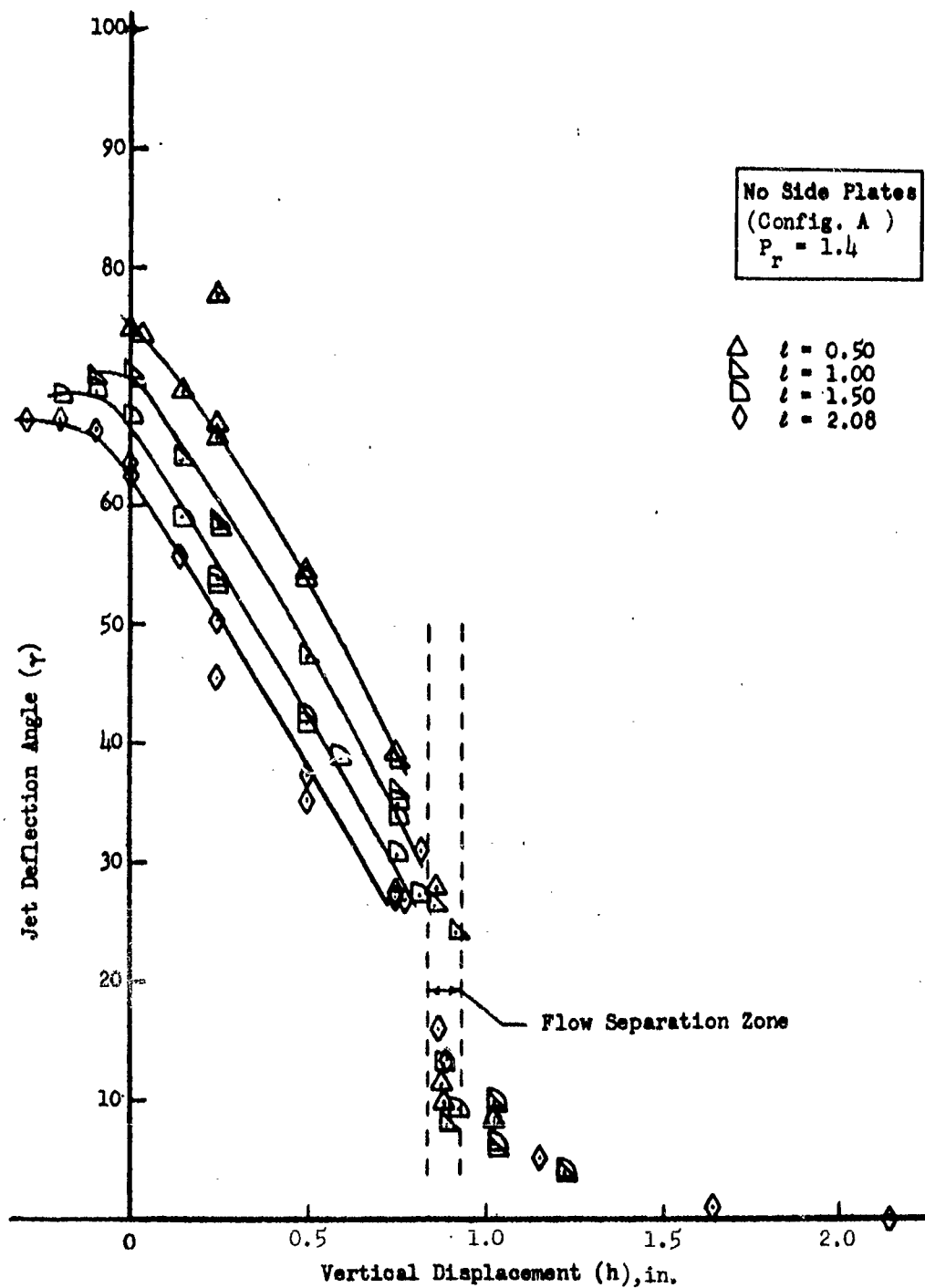


FIGURE 11: EFFECT OF VERTICAL DISPLACEMENT ON DEFLECTION ANGLE

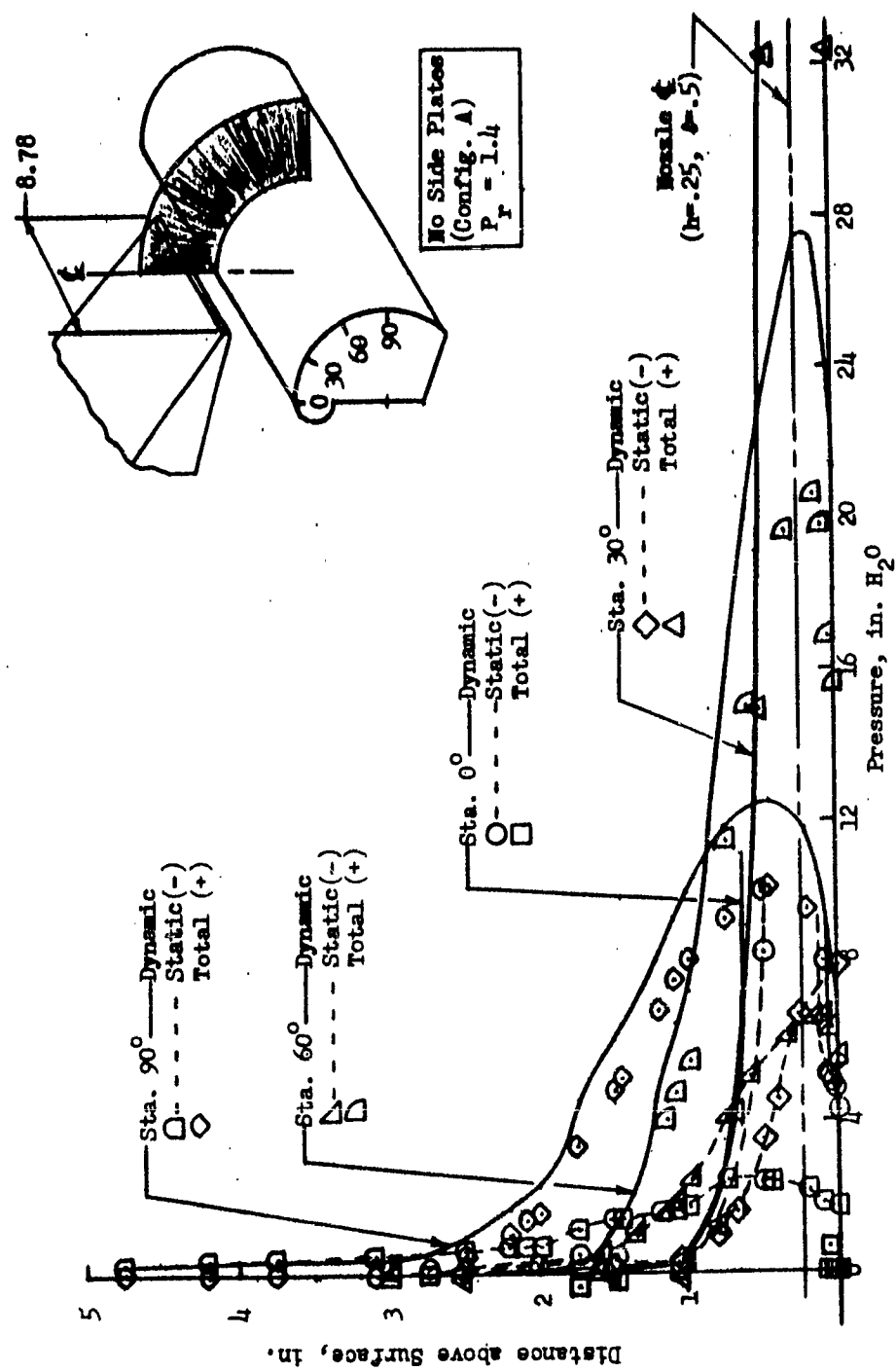


FIGURE 12: PRESSURE PROFILE AROUND DEFLECTION SURFACE

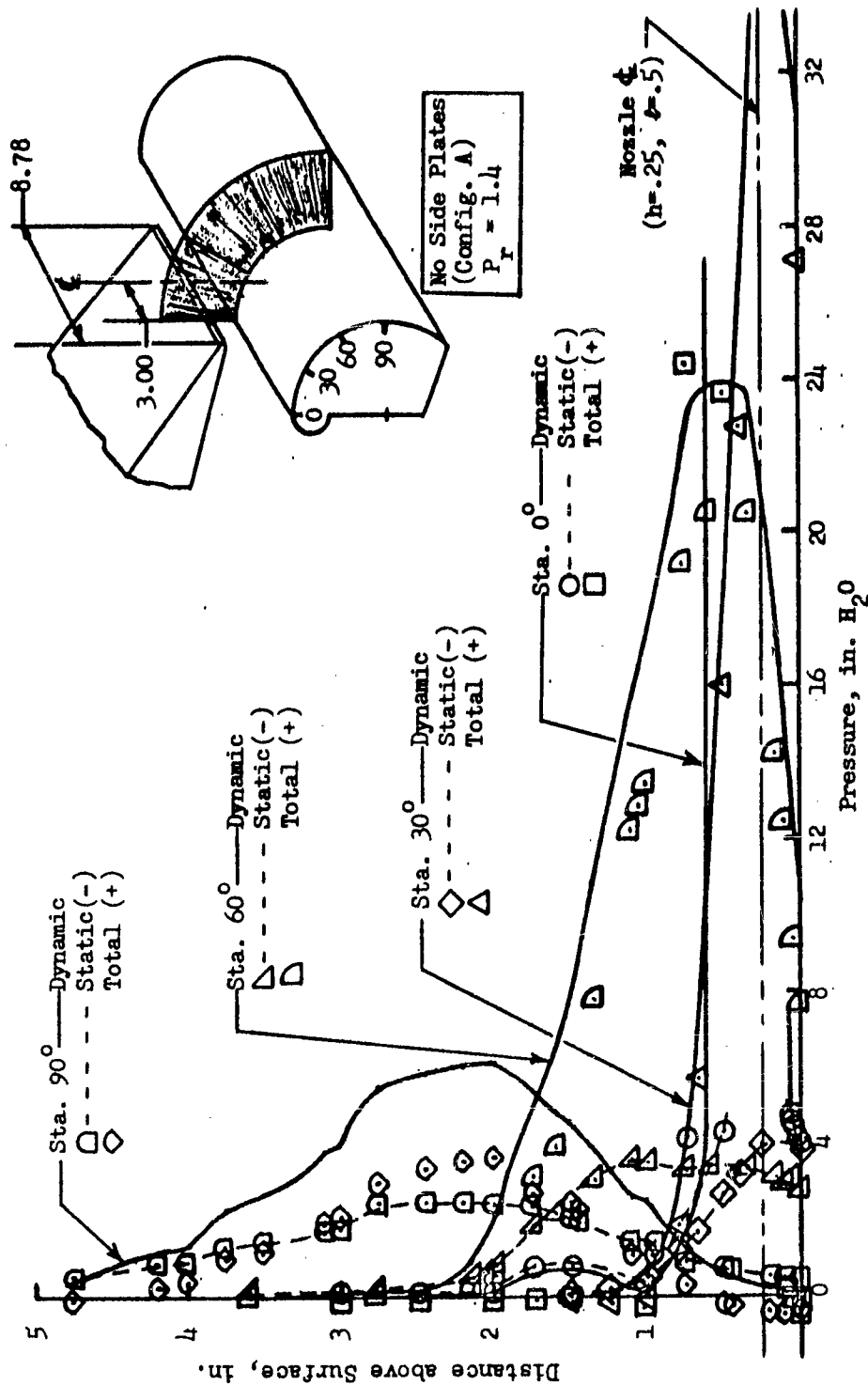


FIGURE 13: PRESSURE PROFILE AROUND DEFLECTION SURFACE

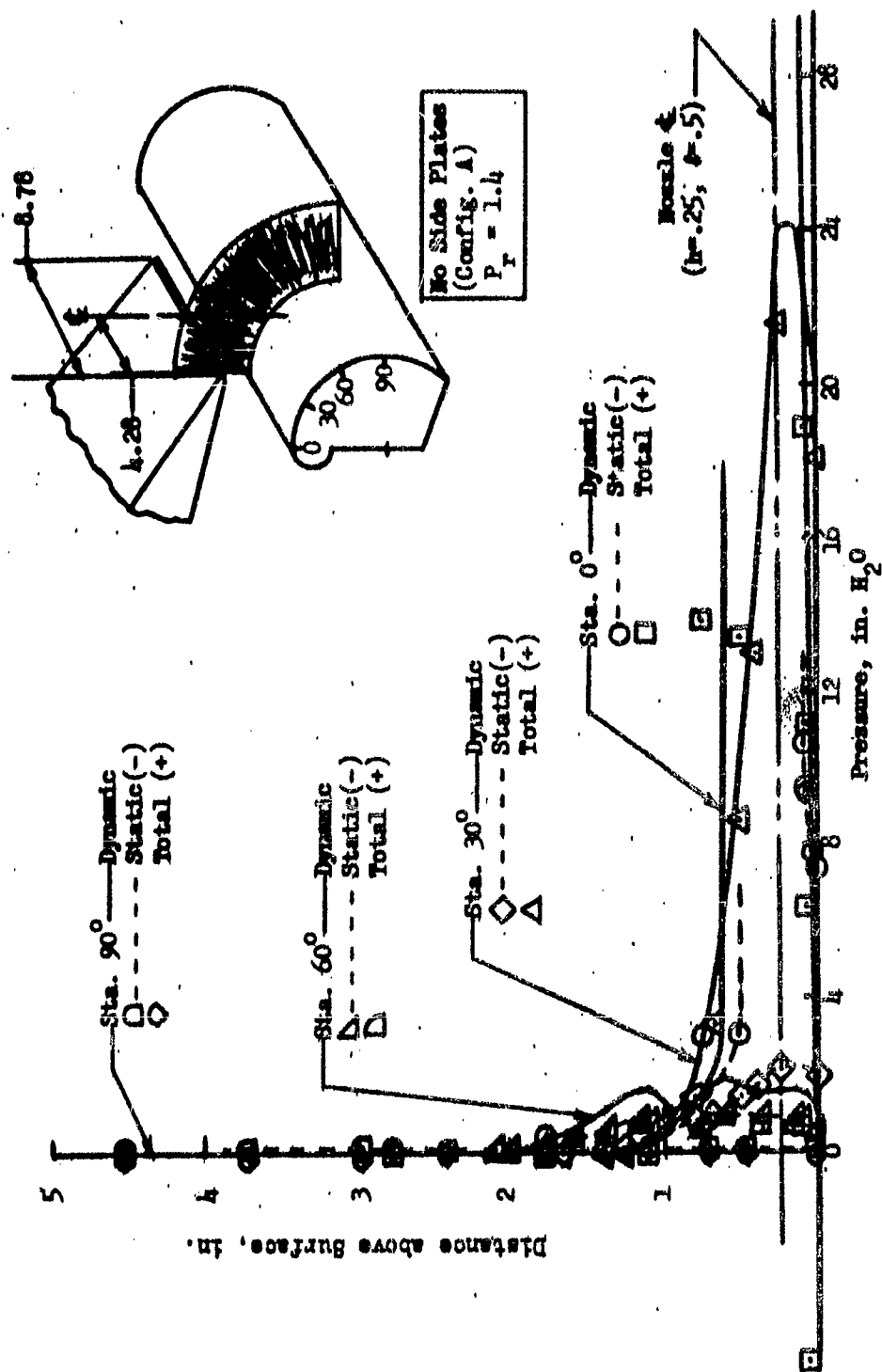


FIGURE 14: PRESSURE PROFILE AROUND DEFLECTION SURFACE

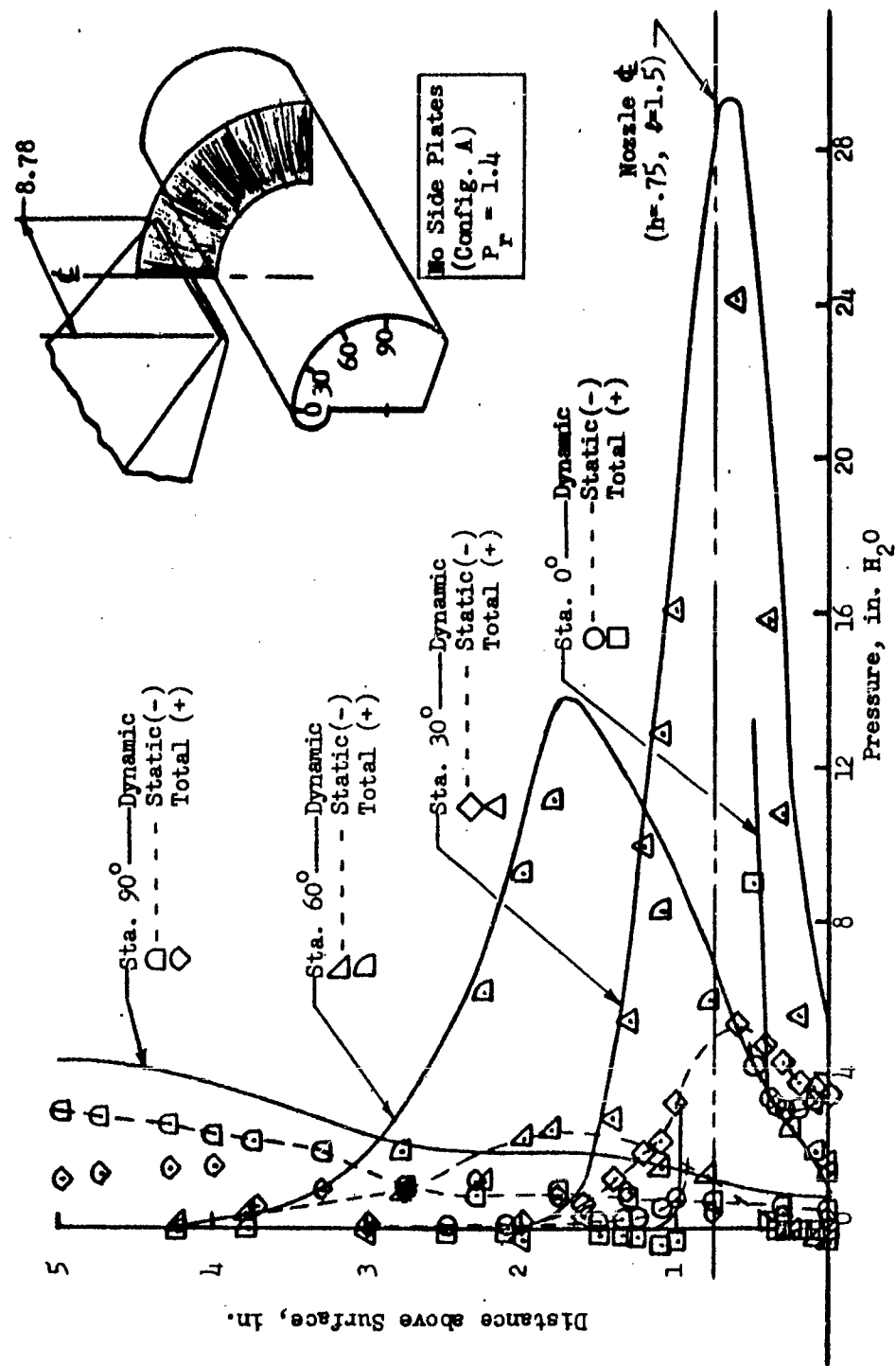


FIGURE 15: PRESSURE PROFILE AROUND DEFLECTION SURFACE

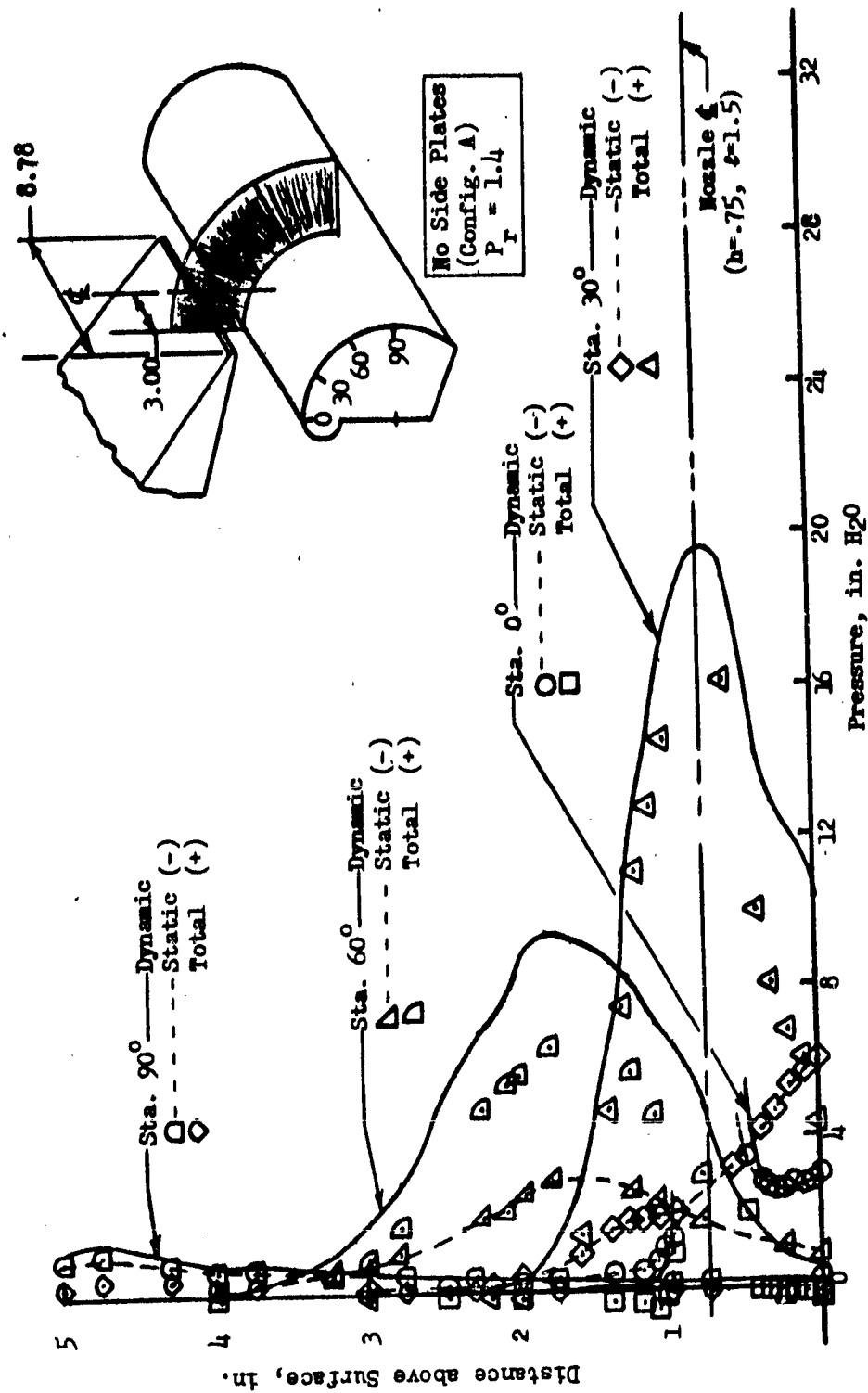


FIGURE 16: PRESSURE PROFILE AROUND DEFLECTION SURFACE

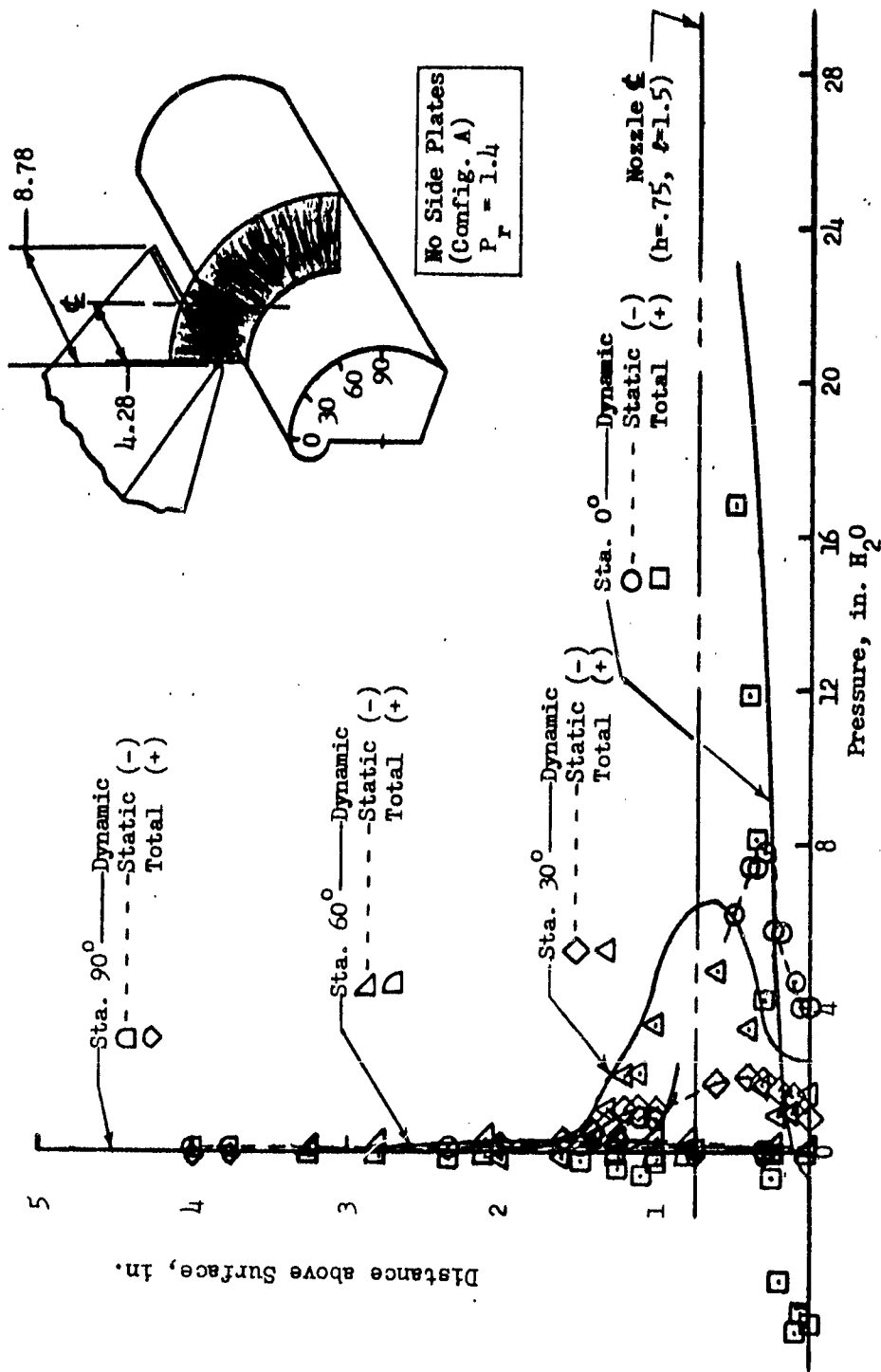


FIGURE 17: PRESSURE PROFILE AROUND DEFLECTION SURFACE

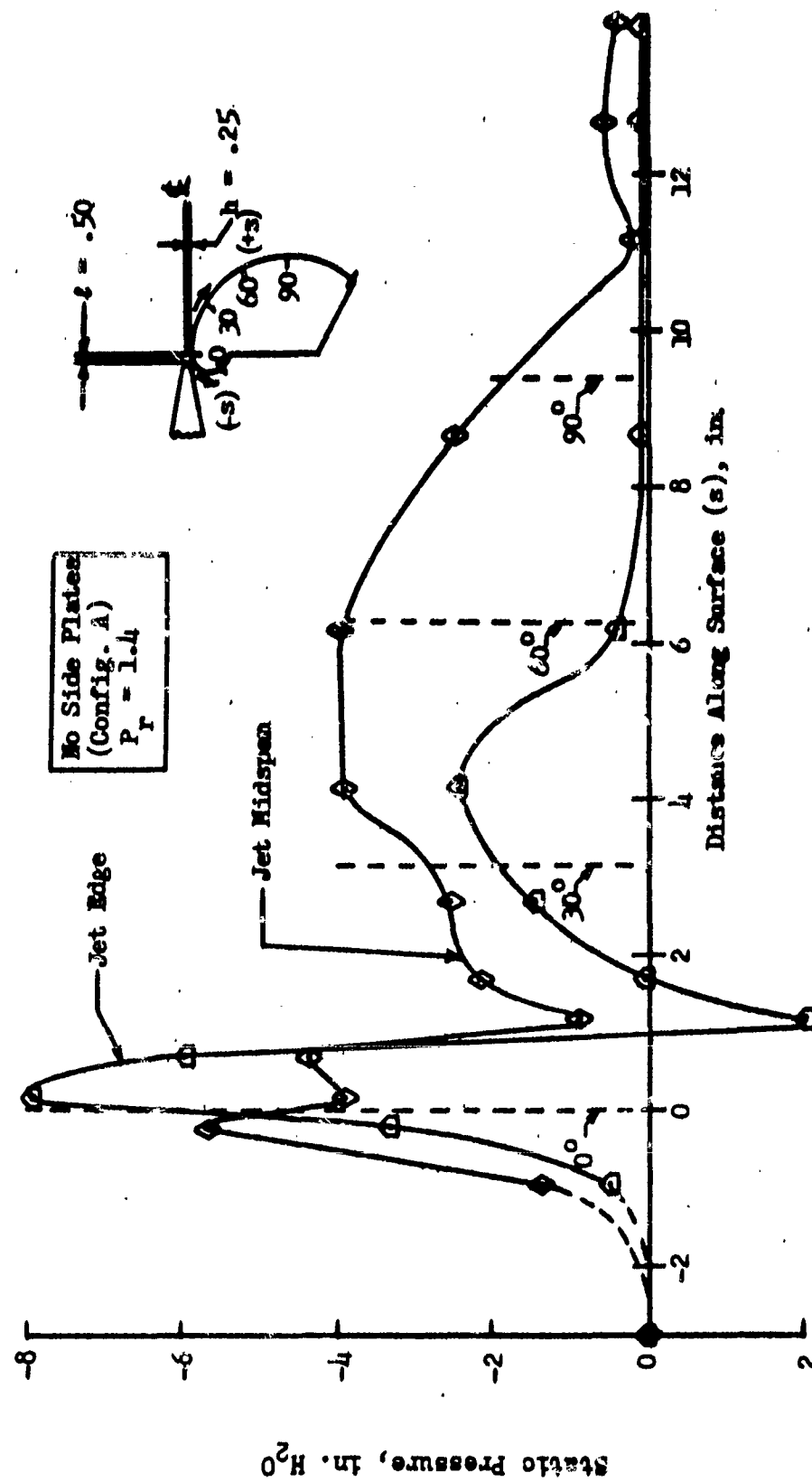


FIGURE 18: SURFACE STATIC PRESSURE DISTRIBUTION

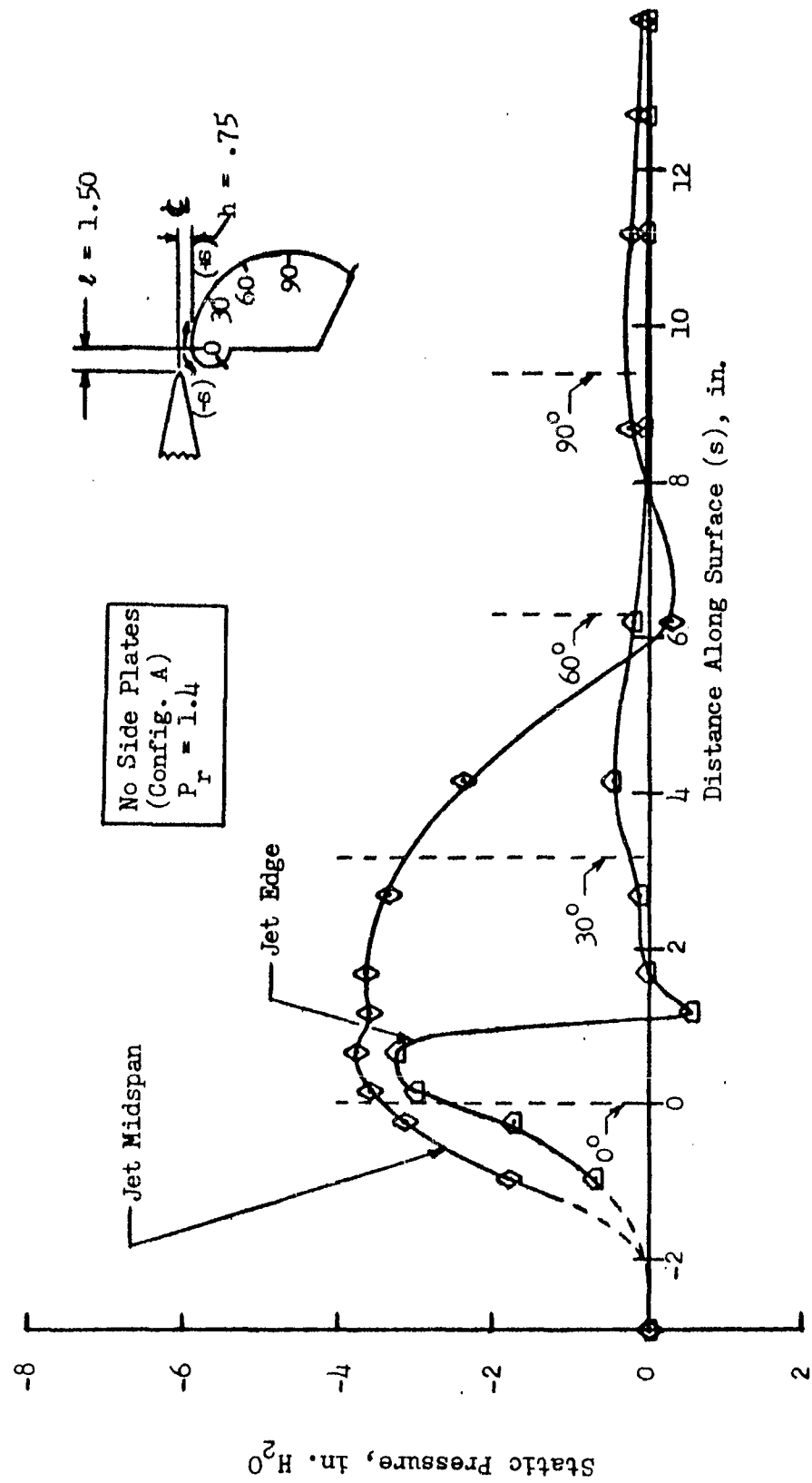


FIGURE 19: SURFACE STATIC PRESSURE DISTRIBUTION

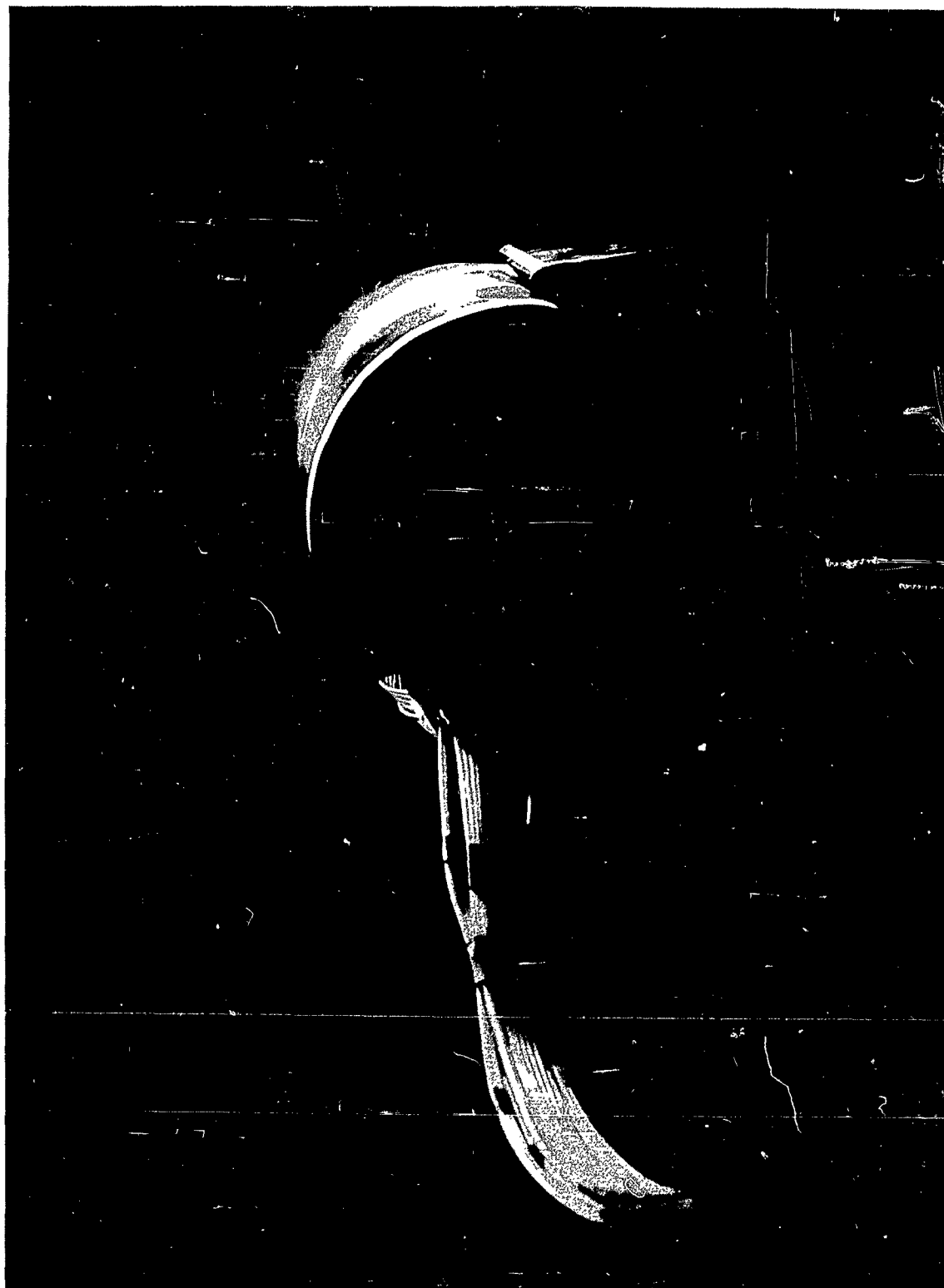


FIGURE 20: FLOW VISUALIZATION AT JET EDGE, (CONFIGURATION A)
 $h = .50$, $t = .25$, $P_r = 1.1$



FIGURE 21: FLOW VISUALIZATION BETWEEN JET SHEET AND DEFLECTION SURFACE AT CENTER SPAN (CONFIGURATION A) $h = .50$, $l = .25$, $P_r = 1.1$

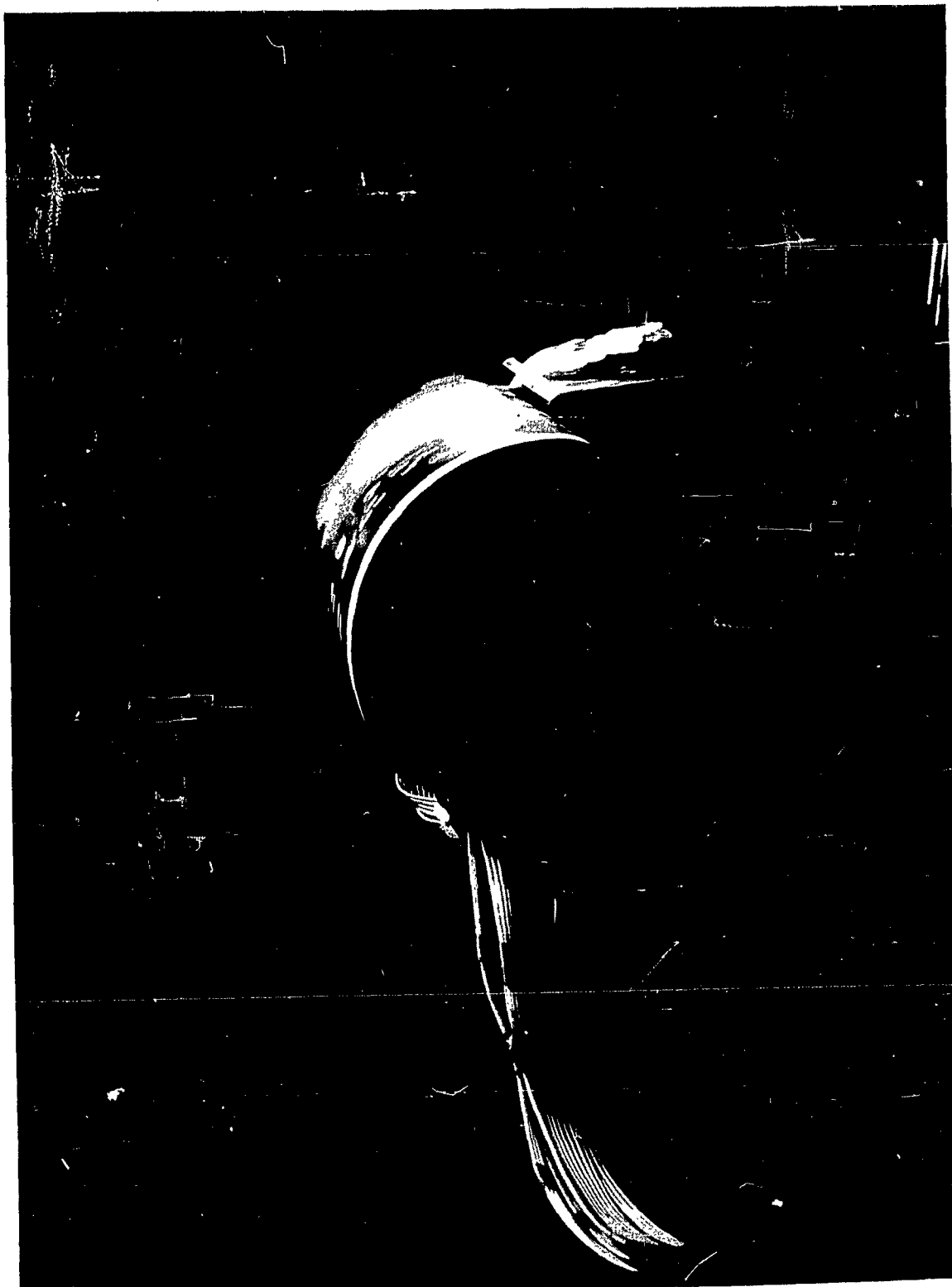


FIGURE 22: FLOW VISUALIZATION OF EXTERNALLY ENTRAINED AIR AT CENTER SPAN
(CONFIGURATION A) $h = .50$, $l = .25$, $P_r = 1.1$



FIGURE 23: FLOW VISUALIZATION OF EXTERNALLY ENTRAINED AIR AT CENTER SPAN
(CONFIGURATION A) $h = .50$, $l = .25$, $P_r = 1.1$

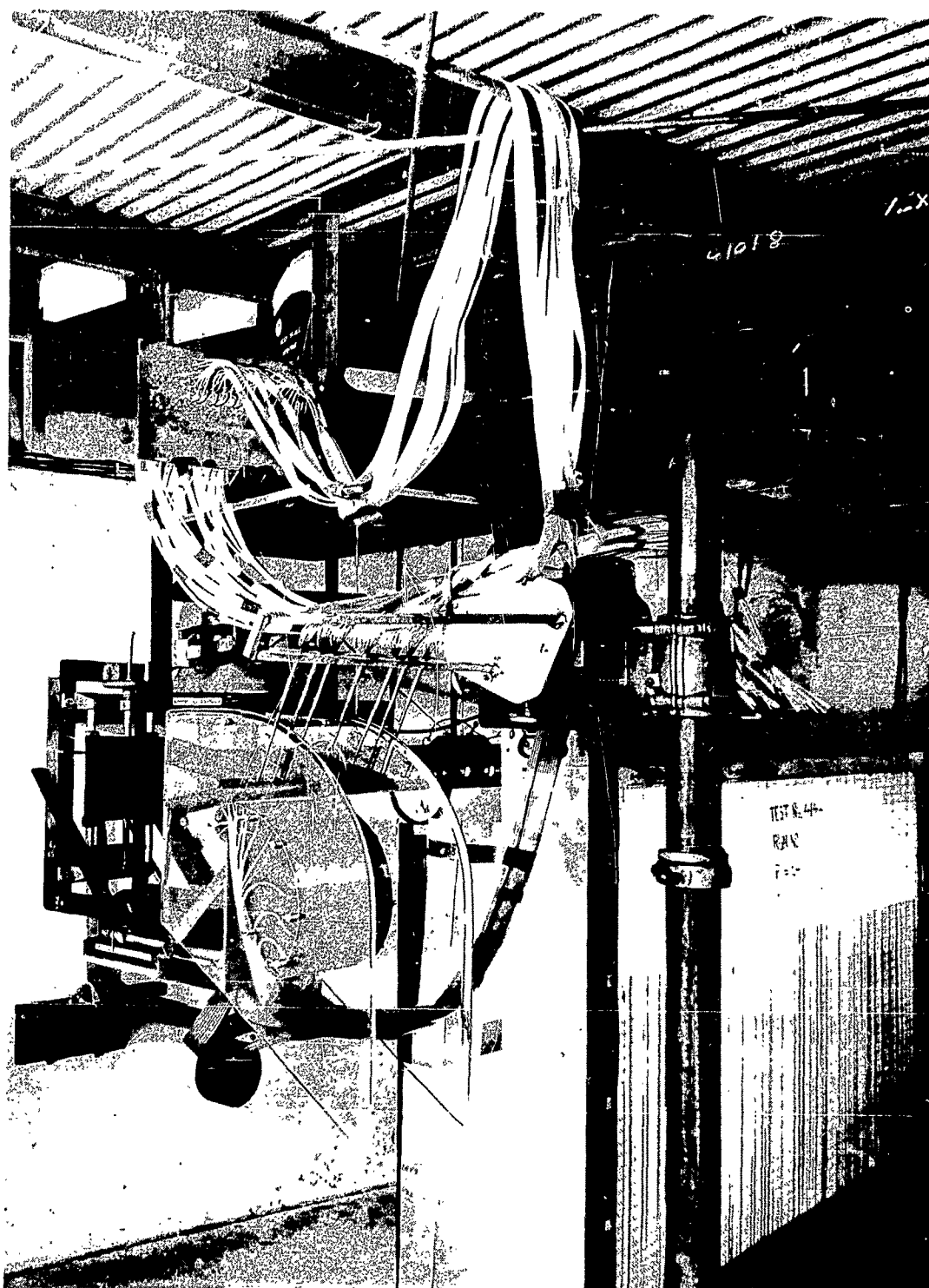


FIGURE 24: CONFIGURATION B INSTALLED ON TEST STAND

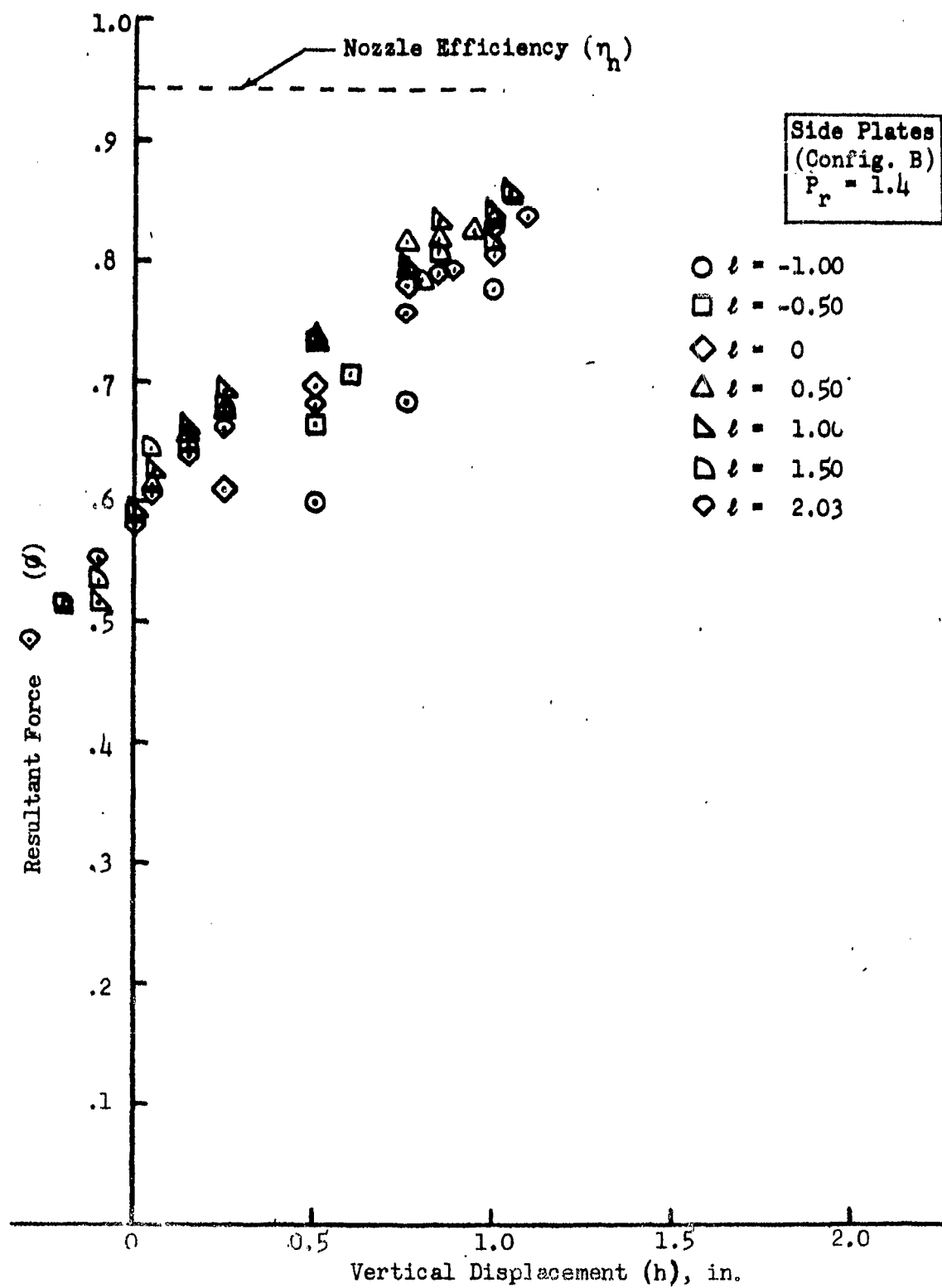


FIGURE 25: EFFECT OF VERTICAL DISPLACEMENT ON RESULTANT FORCE

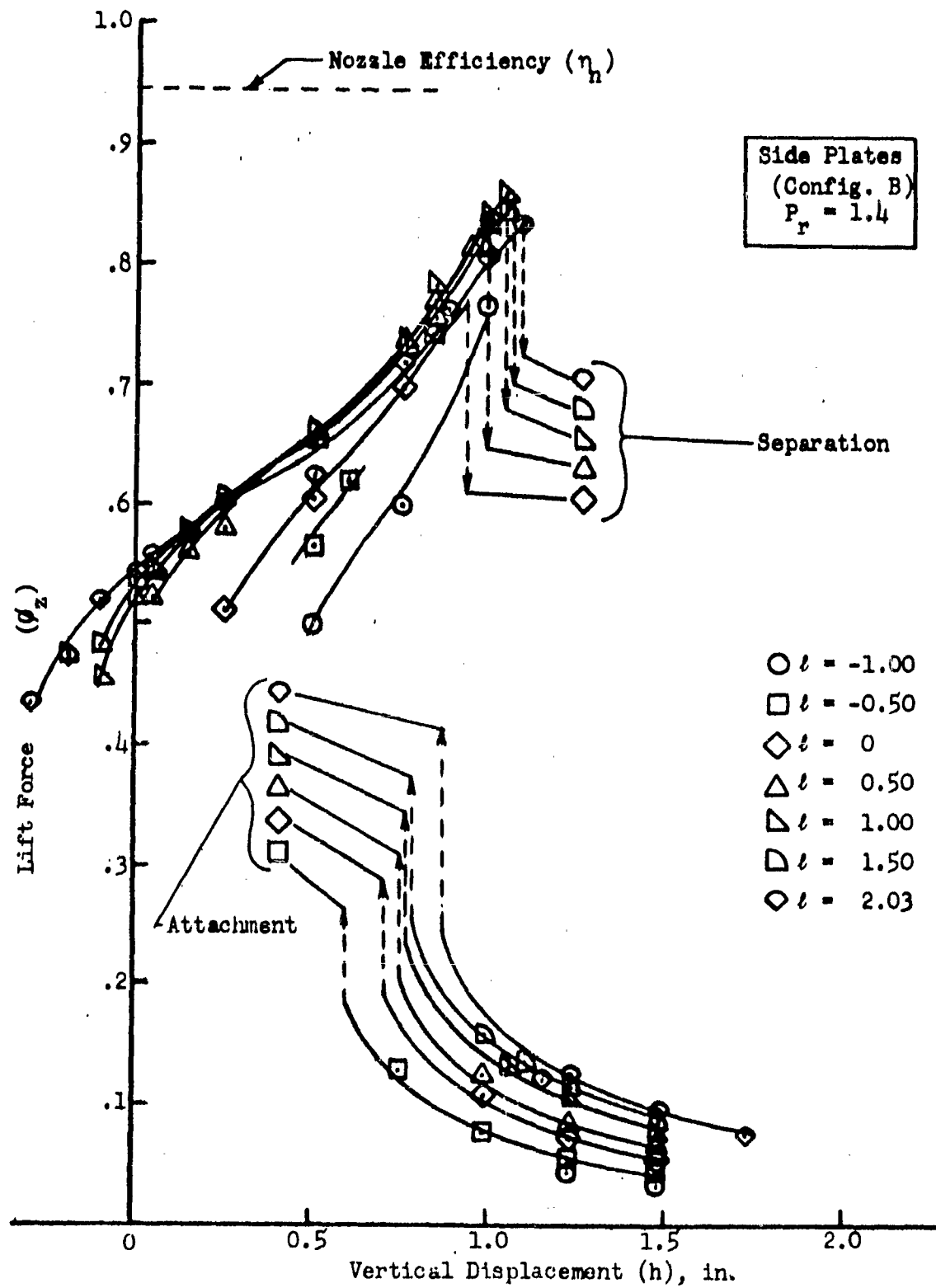


FIGURE 26: EFFECT OF VERTICAL DISPLACEMENT ON LIFT FORCE

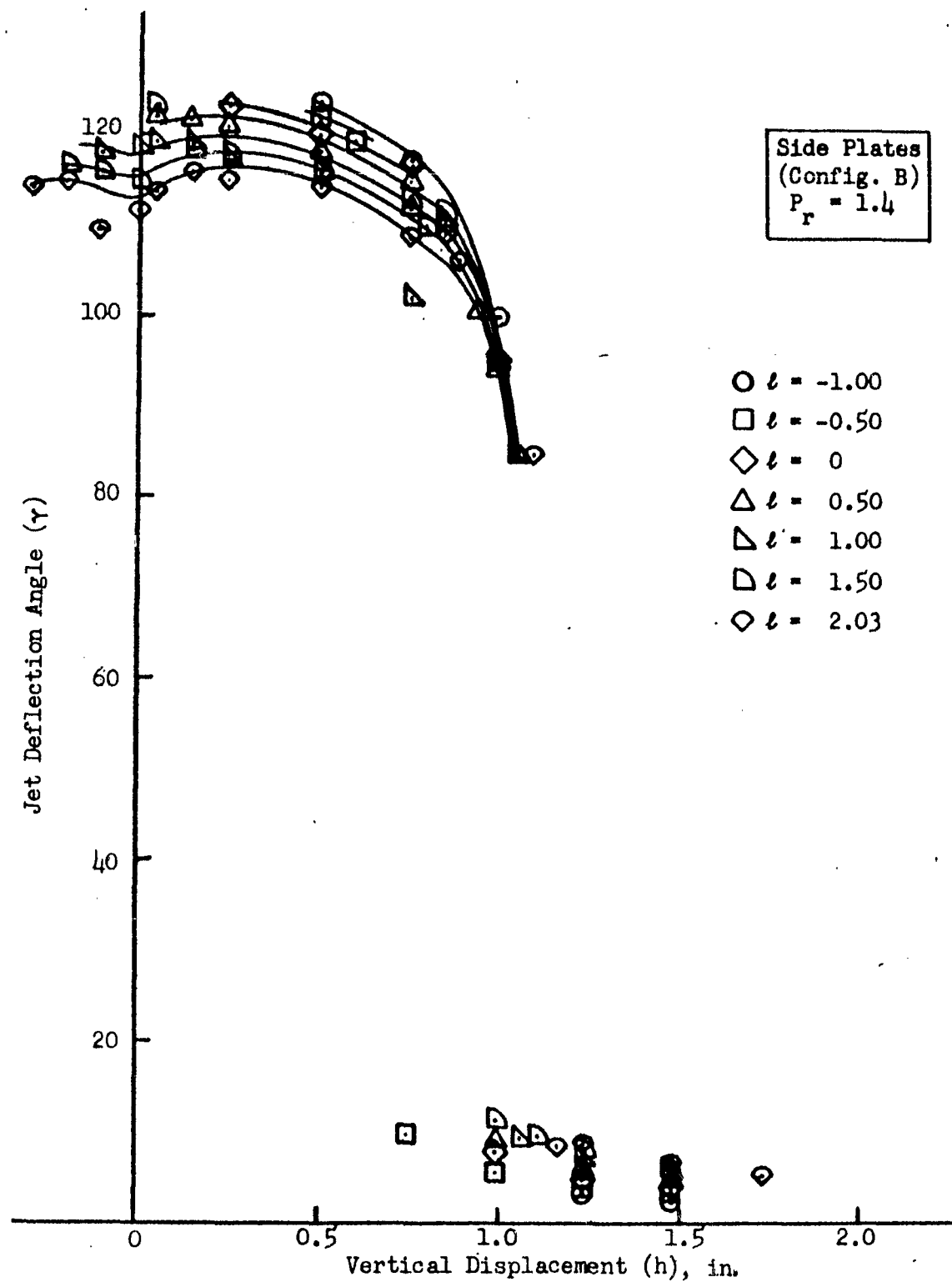


FIGURE 27: EFFECT OF VERTICAL DISPLACEMENT ON DEFLECTION ANGLE

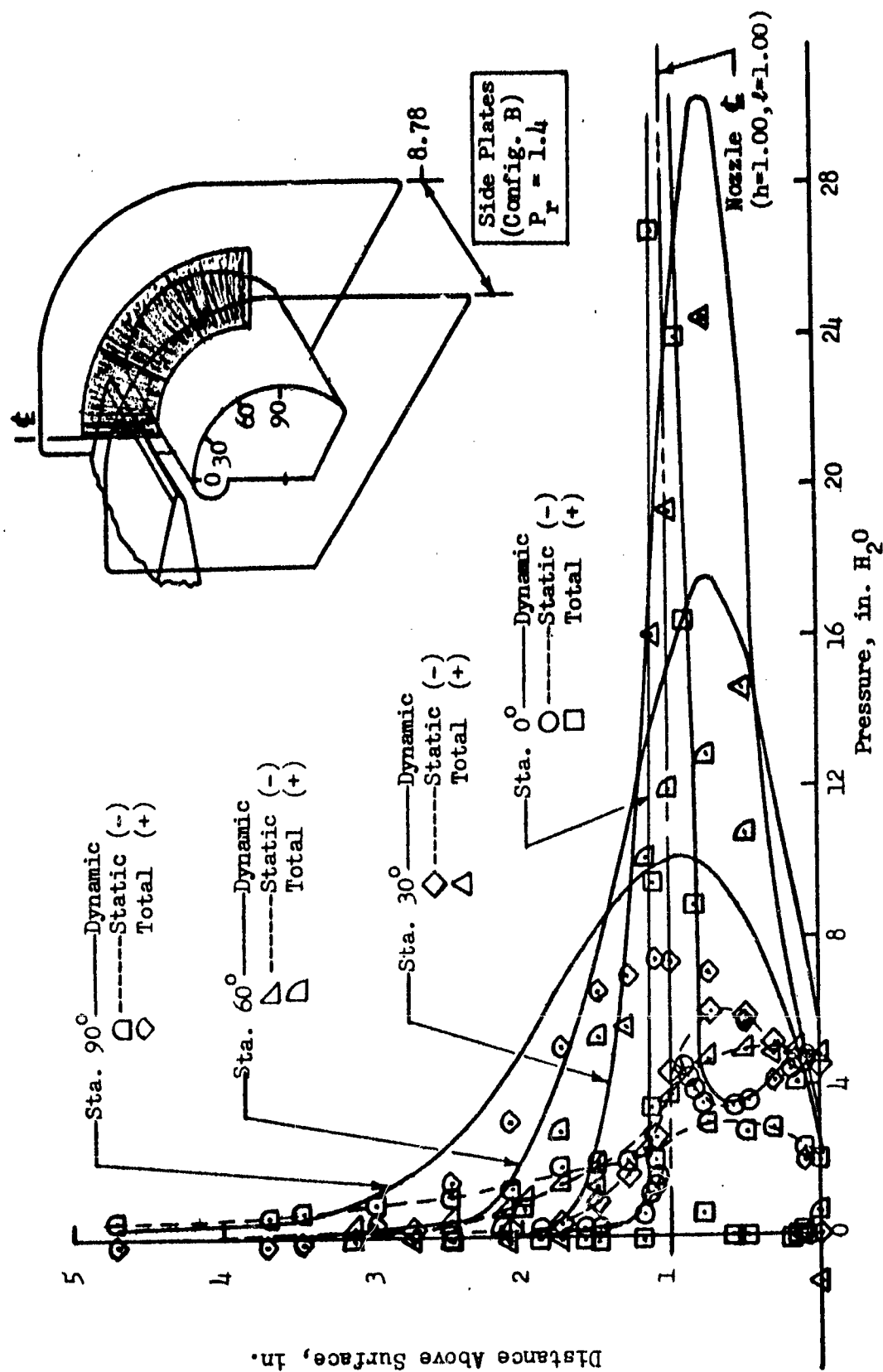


FIGURE 28: PRESSURE PROFILE AROUND DEFLECTION SURFACE

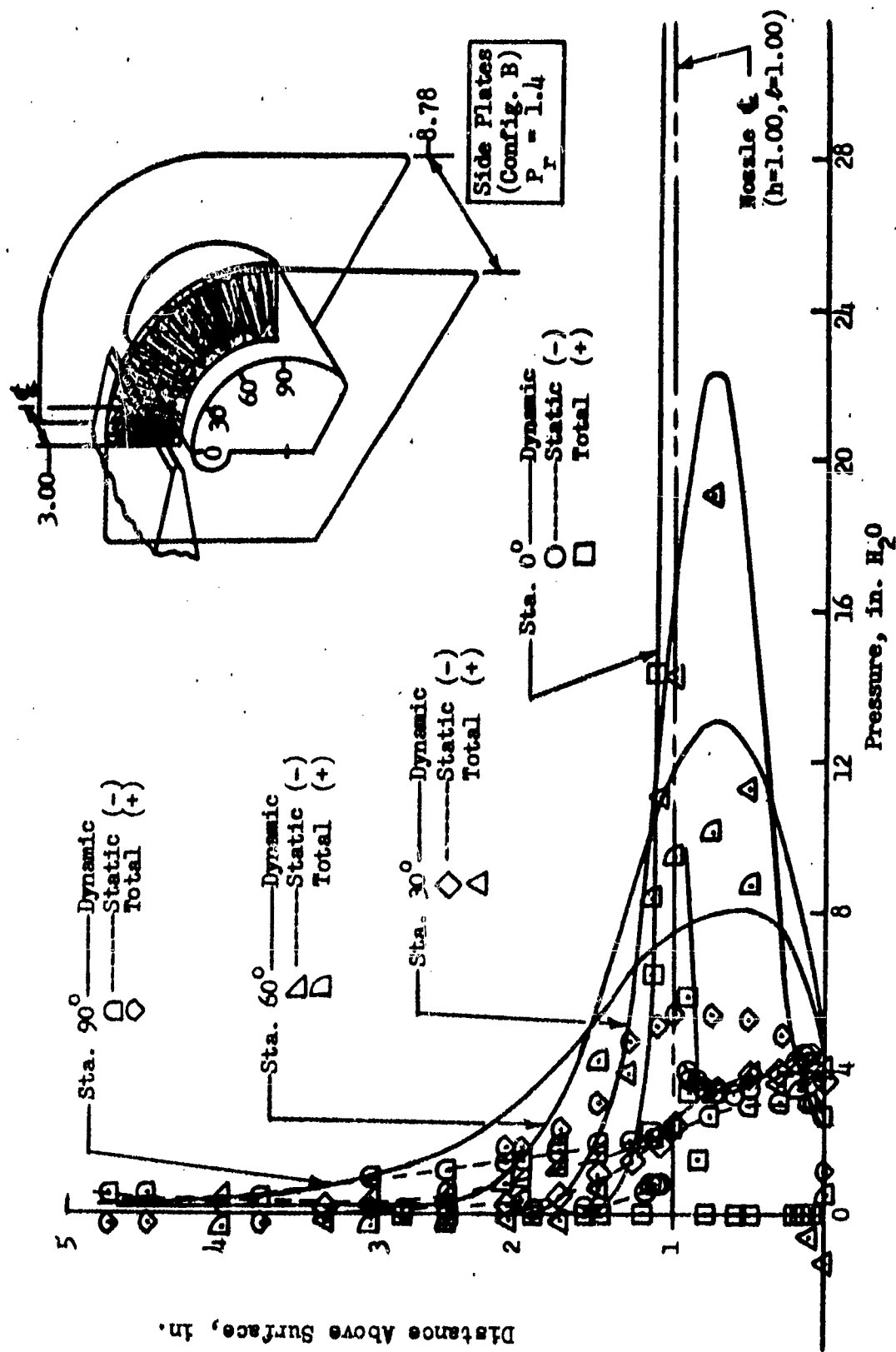


FIGURE 29: PRESSURE PROFILE AROUND DEFLECTION SURFACE

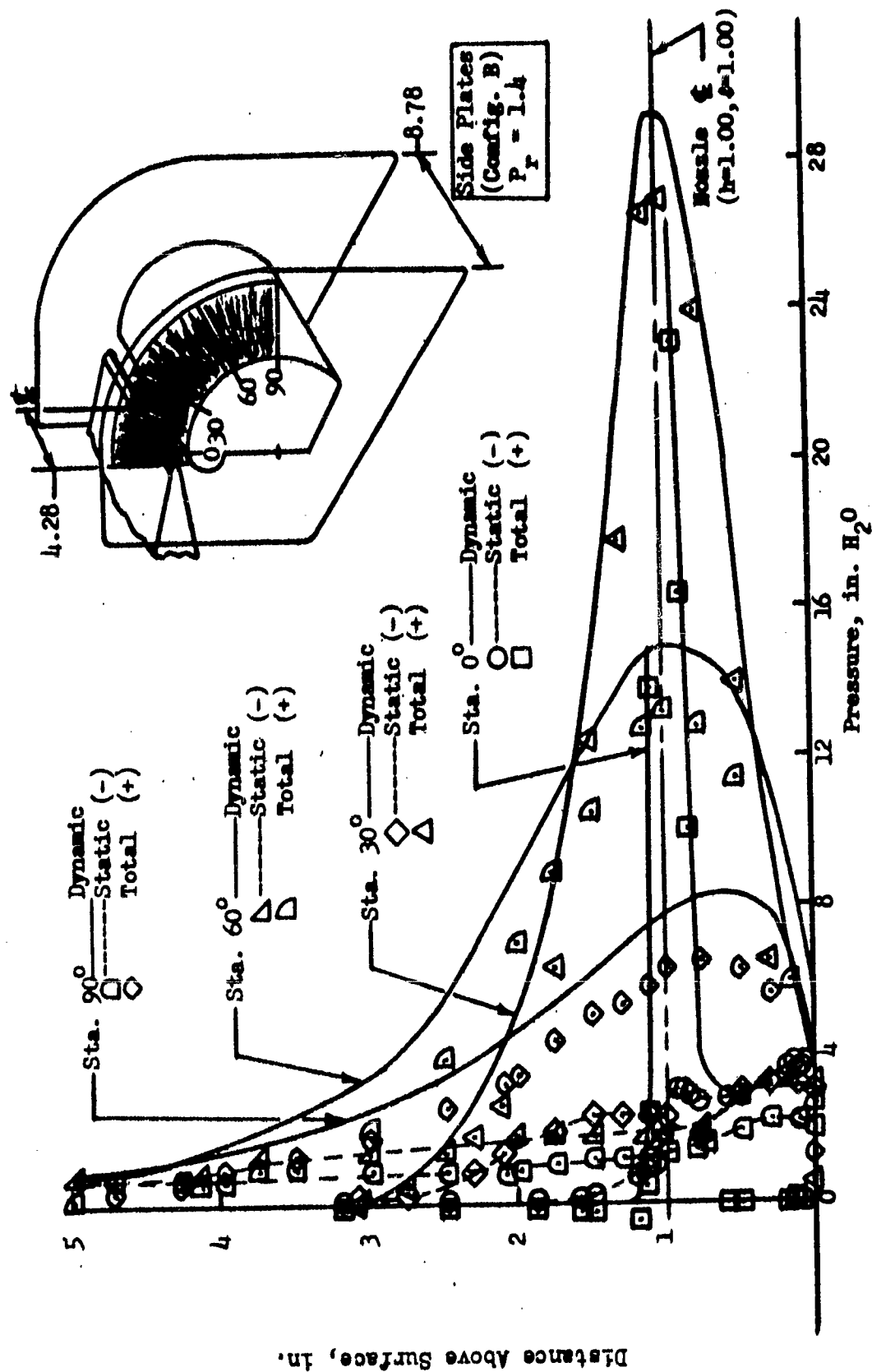


FIGURE 30: PRESSURE PROFILE AROUND DEFLECTION SURFACE

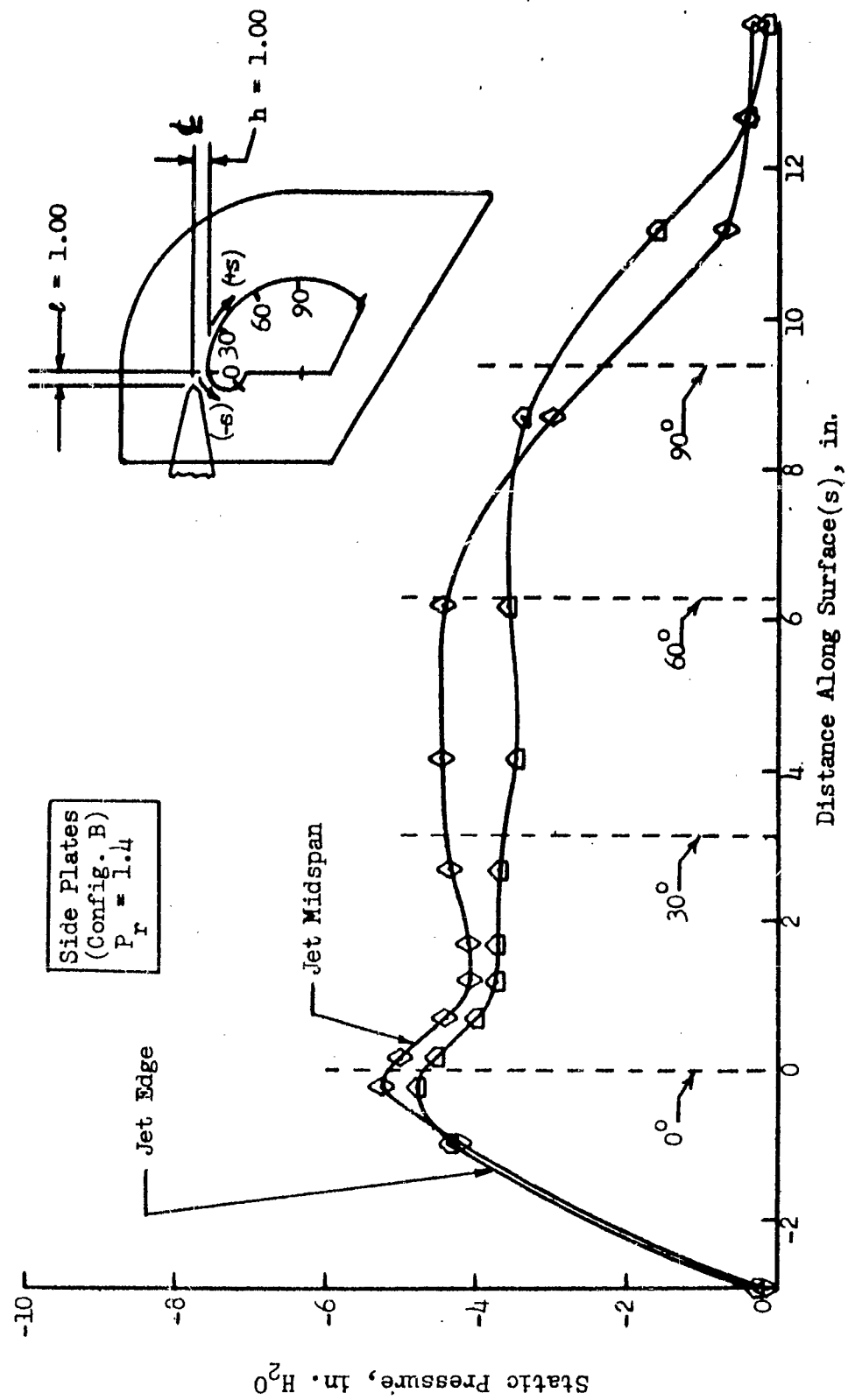


FIGURE 31: SURFACE STATIC PRESSURE DISTRIBUTION

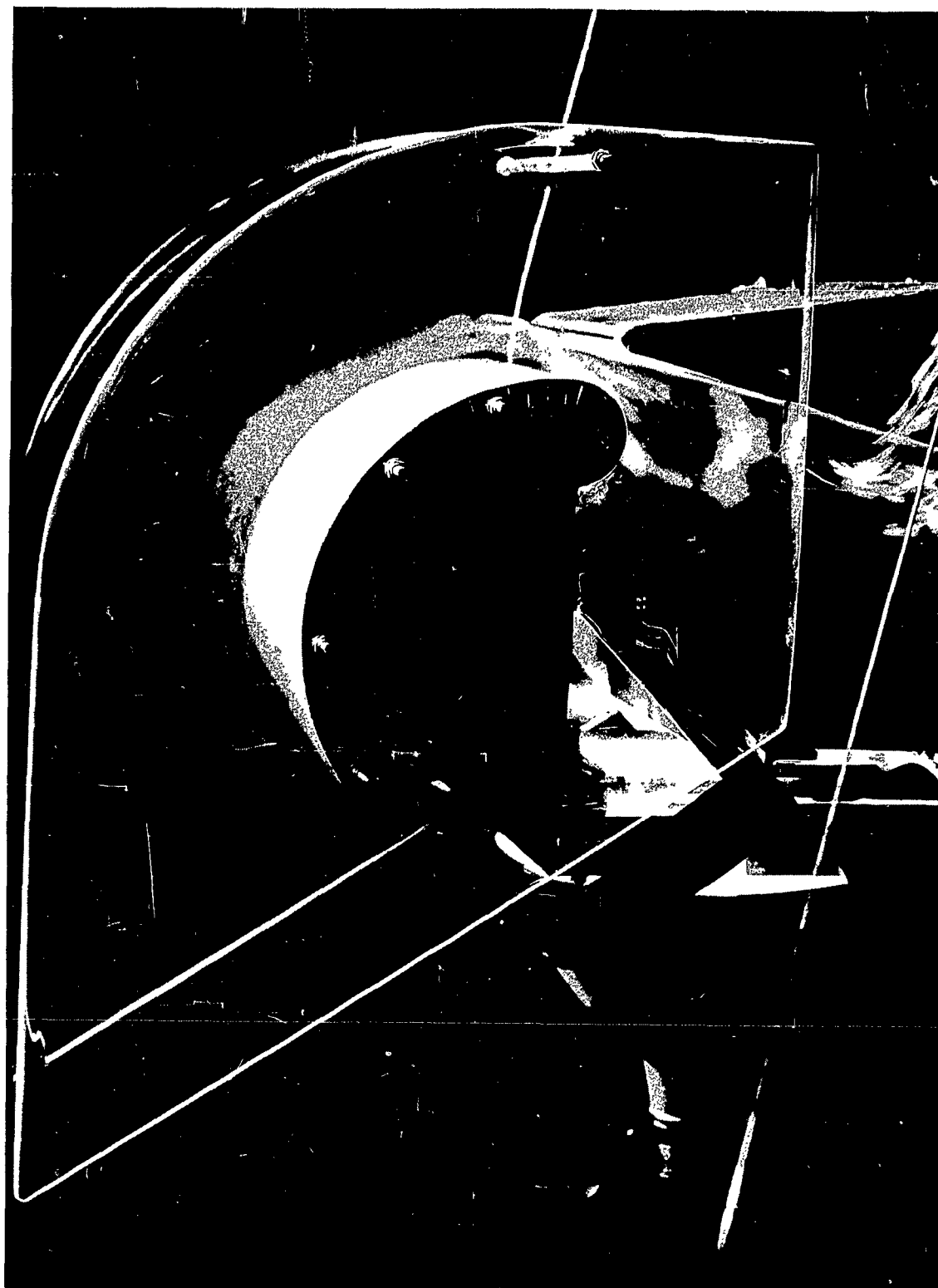


FIGURE 32: FLOW VISUALIZATION OF ENTRAINMENT FROM SIDE OF NOZZLE
(CONFIGURATION B) $h = 1.00$, $l = 1.00$, $P_r = 1.4$

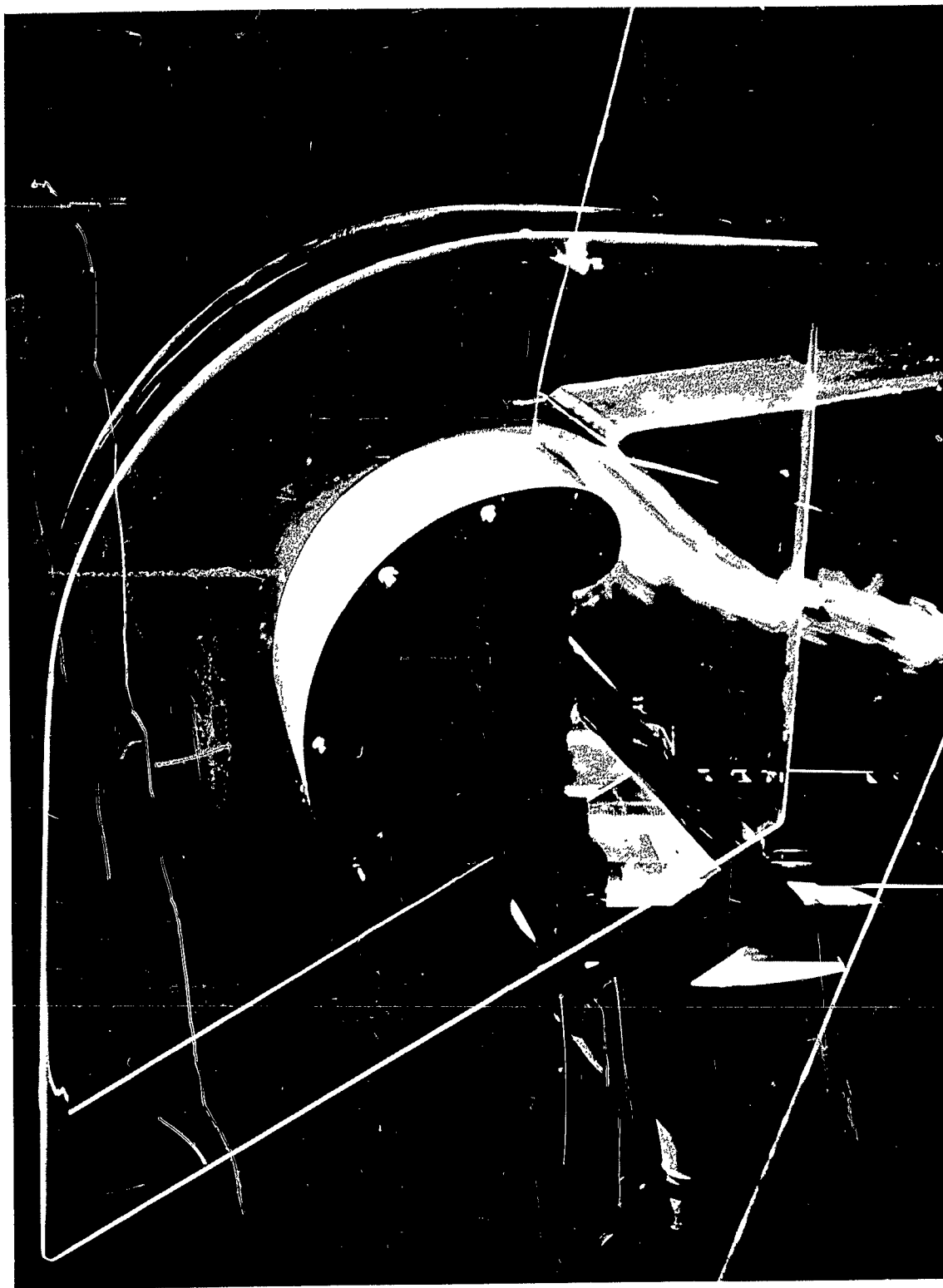


FIGURE 33: FLOW VISUALIZATION BETWEEN JET SHEET AND DEFLECTION SURFACE AT CENTER SPAN (CONFIGURATION B) $h = 1.00$, $l = 1.00$, $P_r = 1.4$



FIGURE 34: FLOW VISUALIZATION OF EXTERNALLY ENTRAINED AIR AT CENTER SPAN
(CONFIGURATION B) $h = 1.00$, $l = 1.00$, $P_r = 1.4$

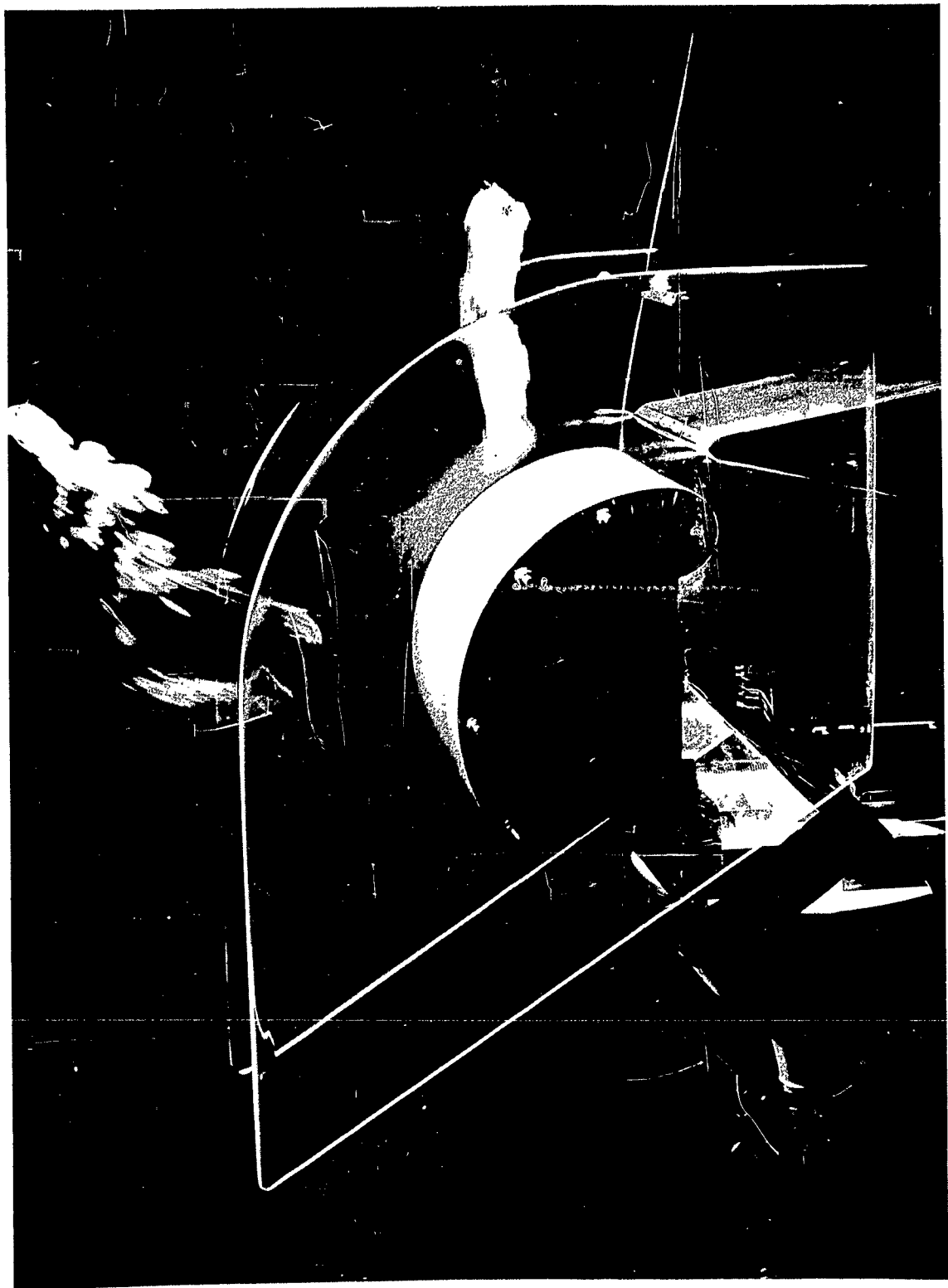


FIGURE 35: FLOW VISUALIZATION OF EXTERNALLY ENTRAINED AIR AT CENTER SPAN
(CONFIGURATION B) $h = 1.00$, $l = 1.00$, $P_r = 1.4$

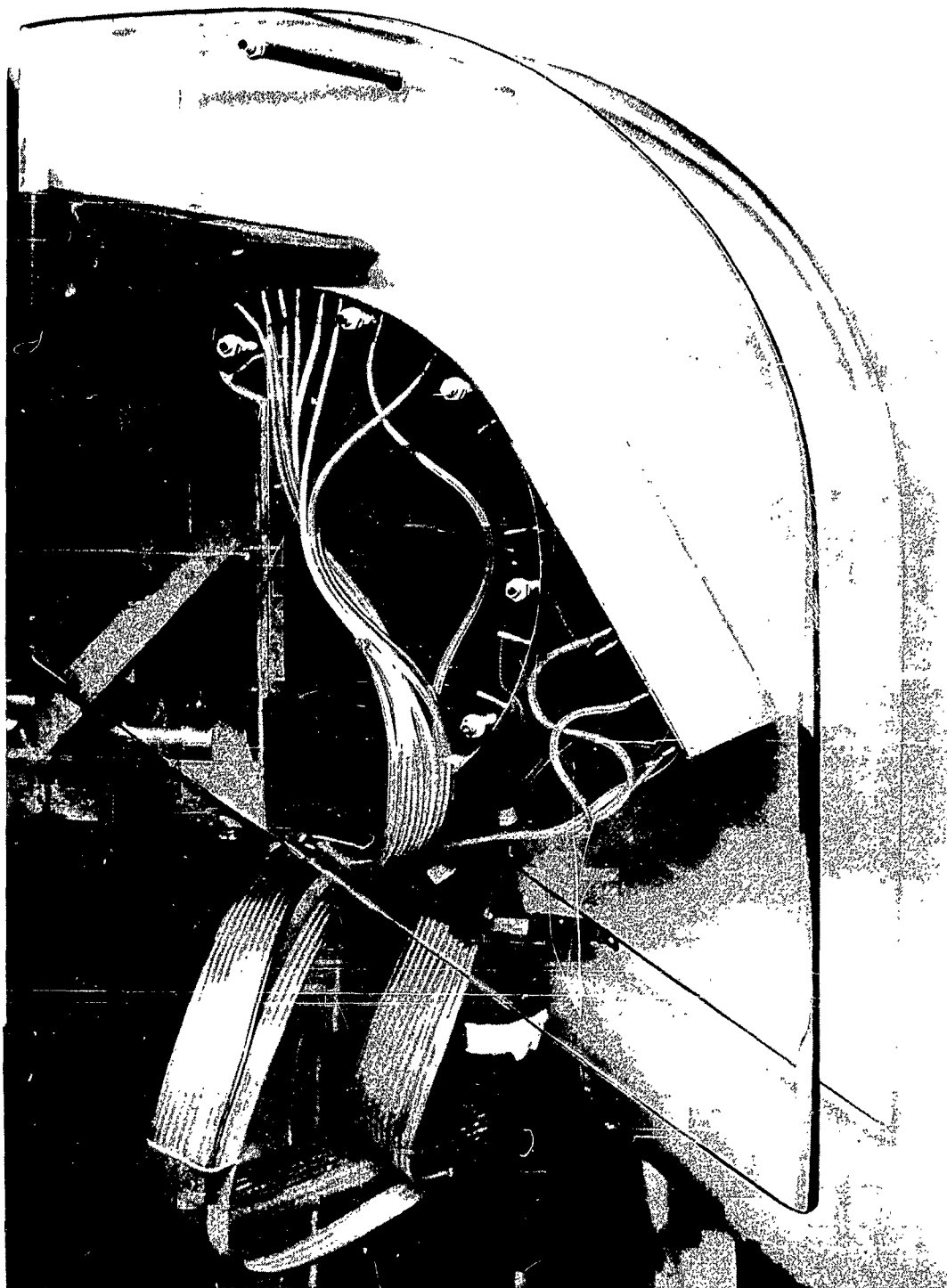


FIGURE 36: CONFIGURATION C INSTALLED ON TEST STAND

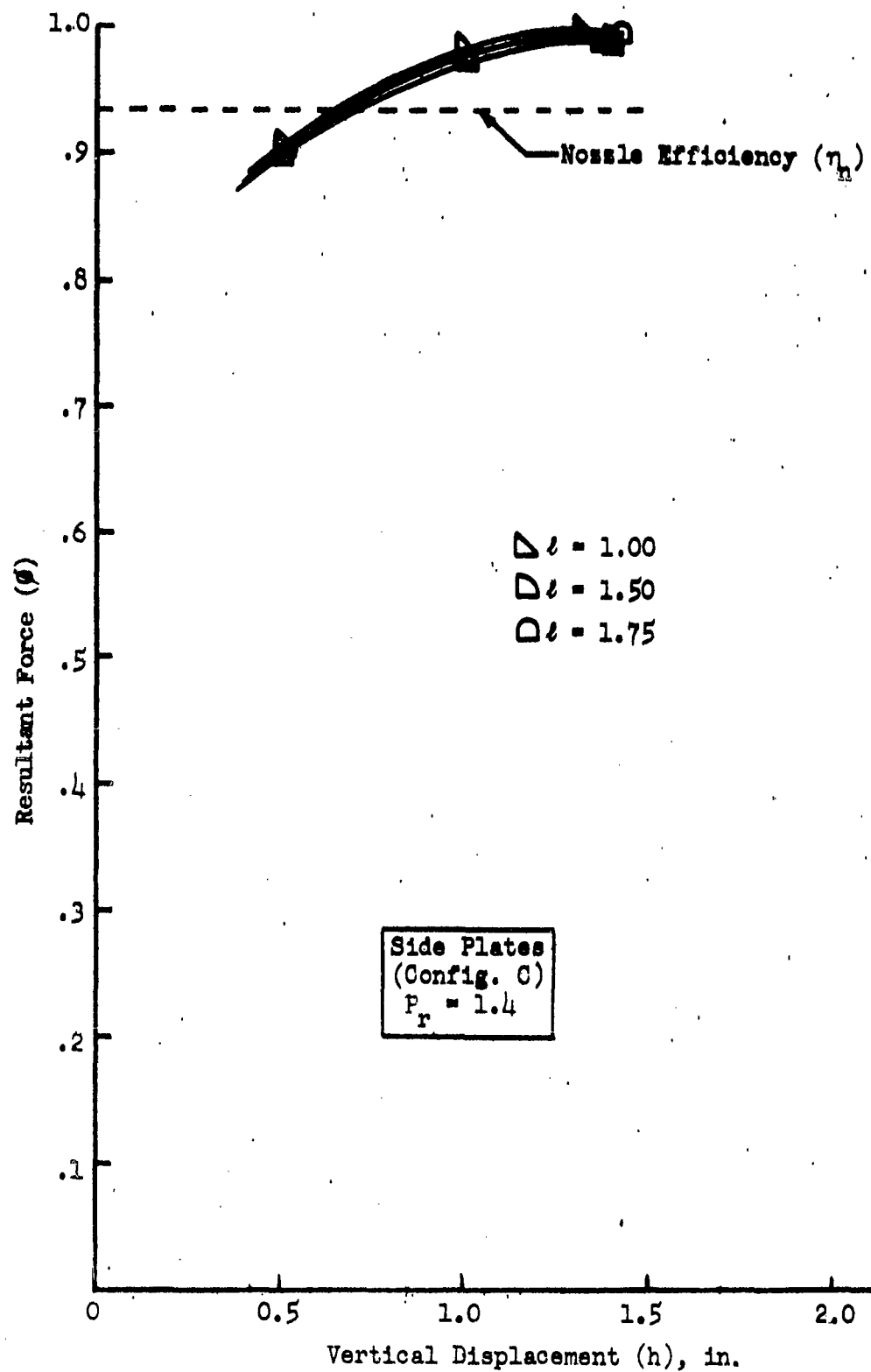


FIGURE 37: EFFECT OF VERTICAL DISPLACEMENT ON RESULTANT FORCE

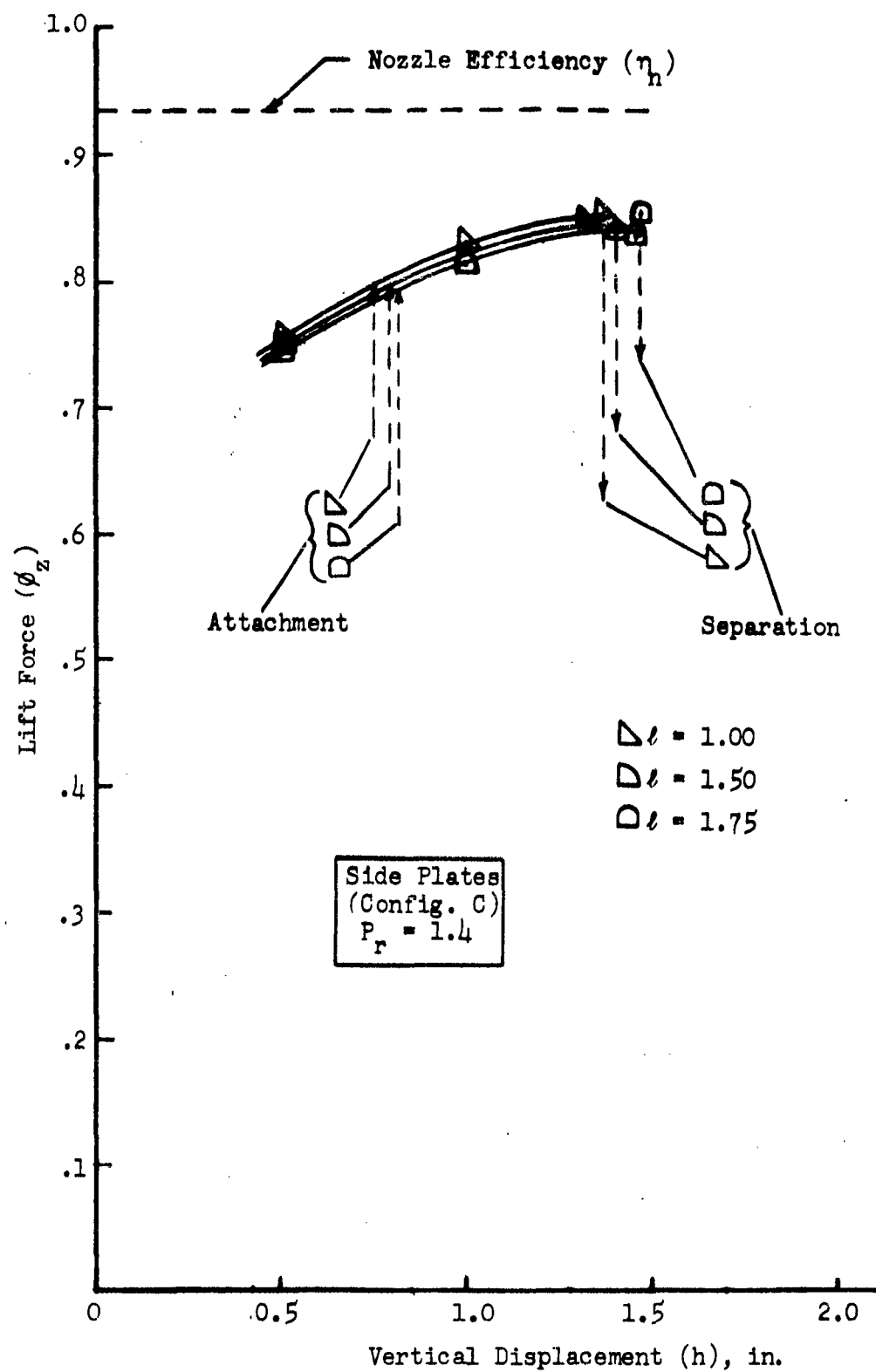


FIGURE 38: EFFECT OF VERTICAL DISPLACEMENT ON LIFT FORCE

CONFIGURATION C PERFORMANCE DATA

P_r	h	l	γ
1.4	.50	1.00	56.0
1.4	1.00	1.00	57.4
1.4	1.32	1.00	57.87
1.4	1.37	1.00	59.3
1.4	.50	1.50	55.75
1.4	1.00	1.50	56.75
1.4	1.40	1.50	58.02
1.4	.50	1.75	55.75
1.4	1.00	1.75	56.9
1.4	1.45	1.75	57.82
1.4	1.47	1.75	58.55

FIGURE 39: EFFECT OF VERTICAL DISPLACEMENT ON DEFLECTION ANGLE
(CONFIGURATION C)

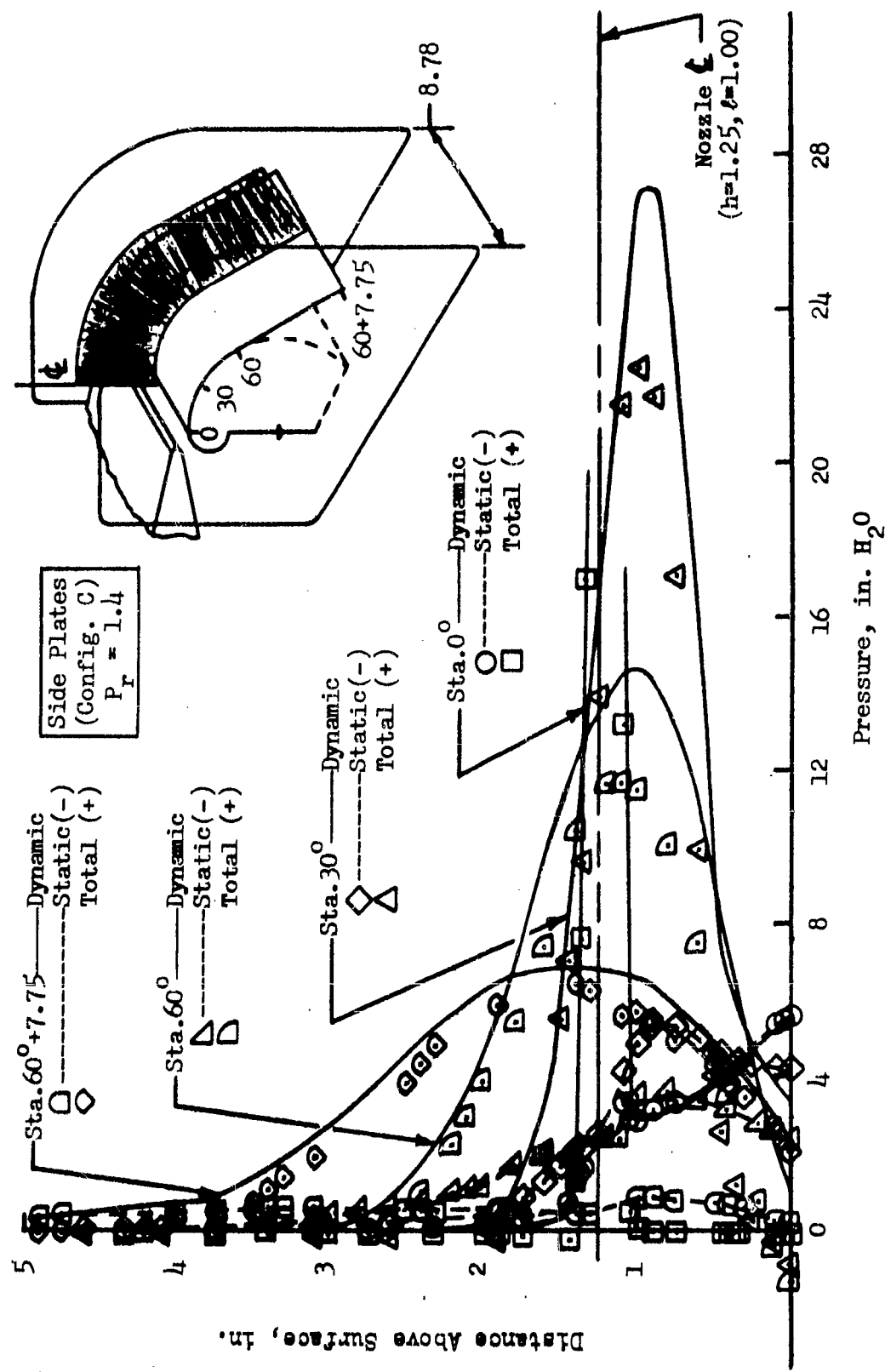


FIGURE 40: PRESSURE PROFILE AROUND DEFLECTION SURFACE

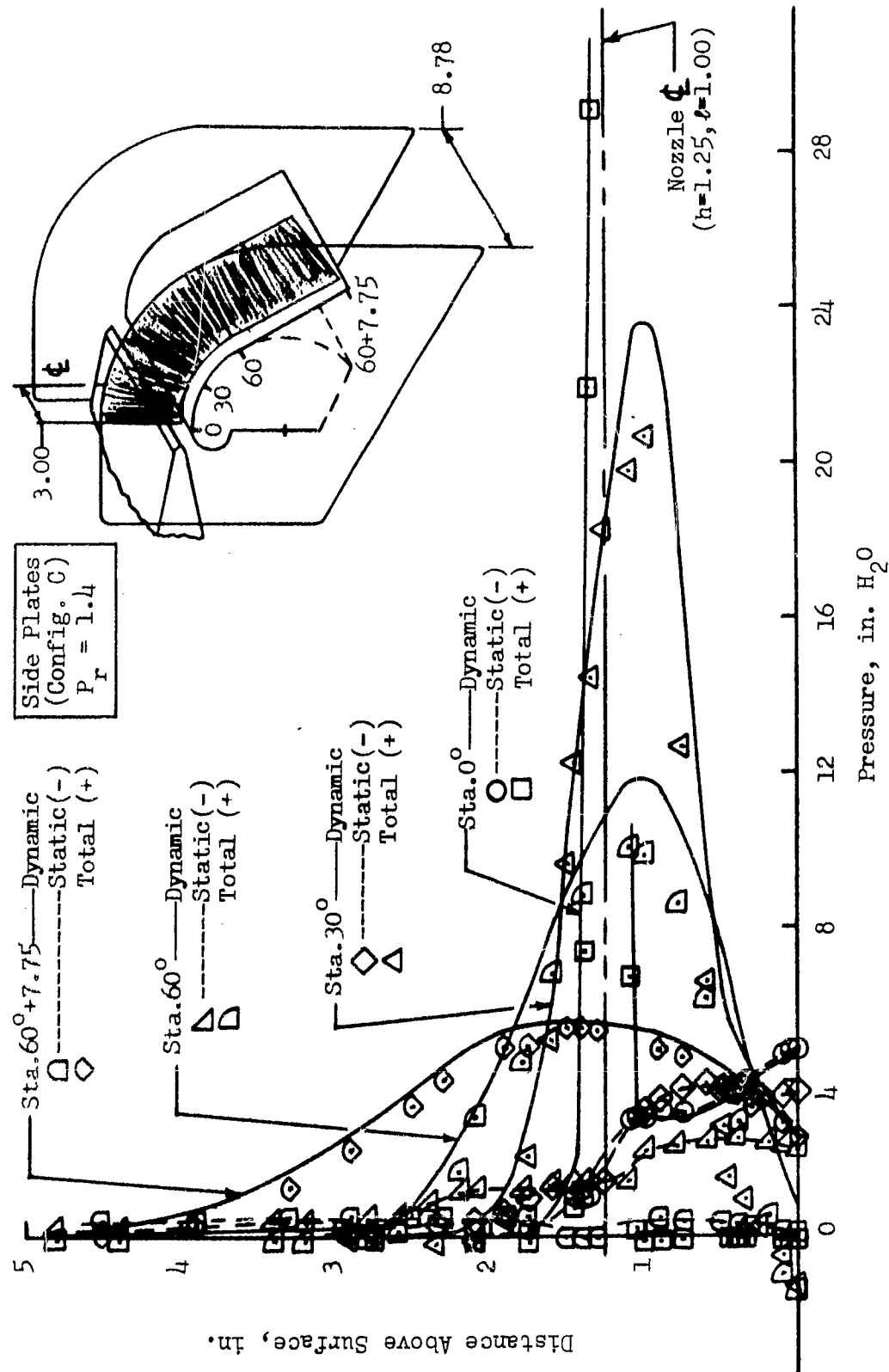


FIGURE 41: PRESSURE PROFILE AROUND DEFLECTION SURFACE

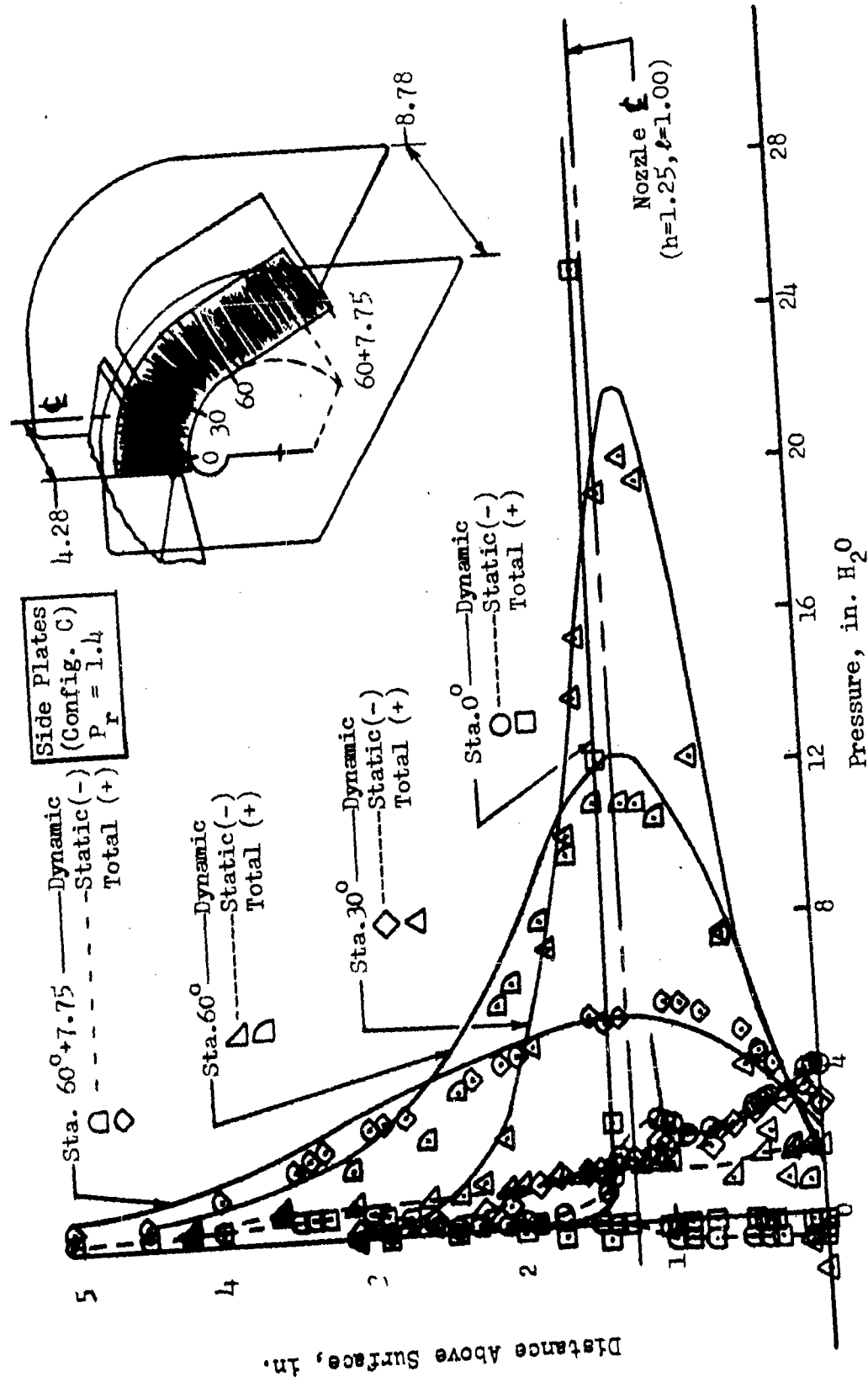


FIGURE 42: PRESSURE PROFILE AROUND DEFLECTION SURFACE

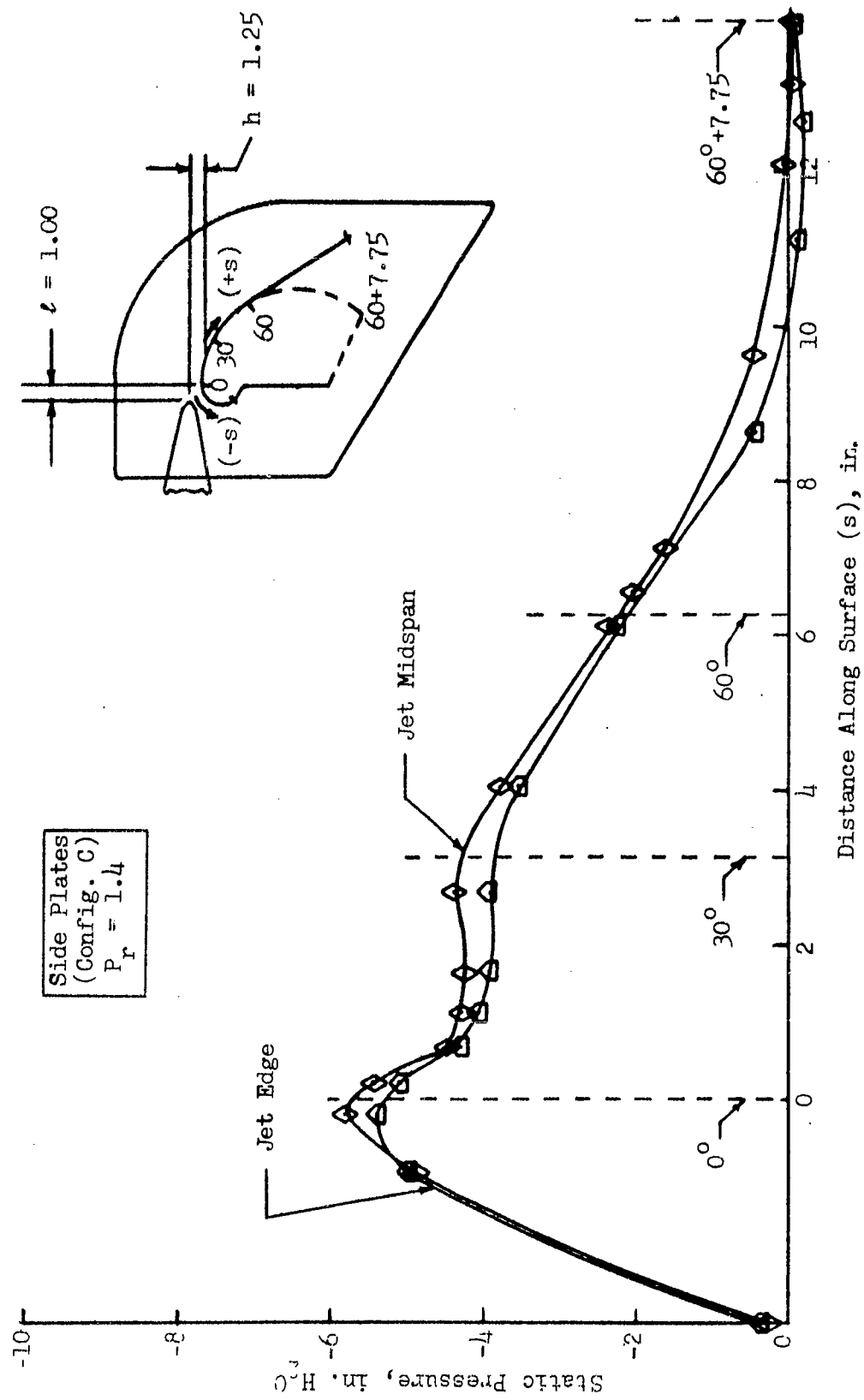


FIGURE 43: SURFACE STATIC PRESSURE DISTRIBUTION

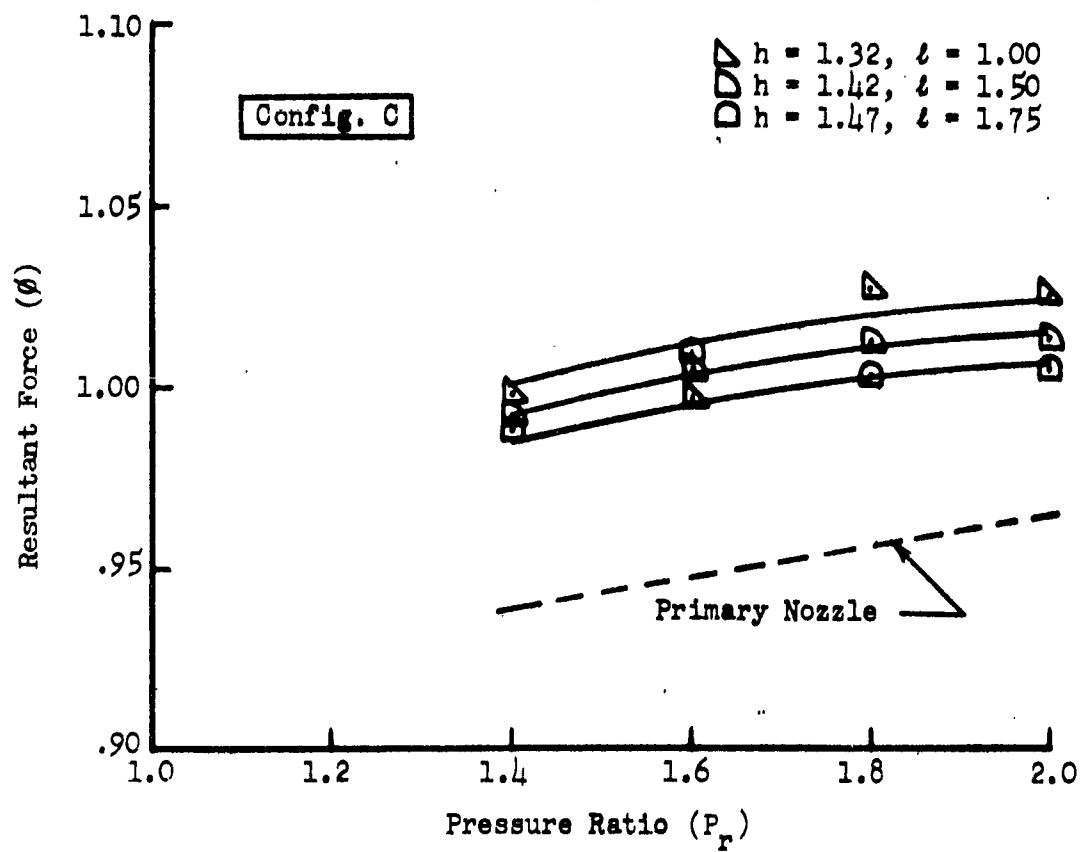


FIGURE 44: EFFECT OF PRESSURE RATIO ON RESULTANT FORCE

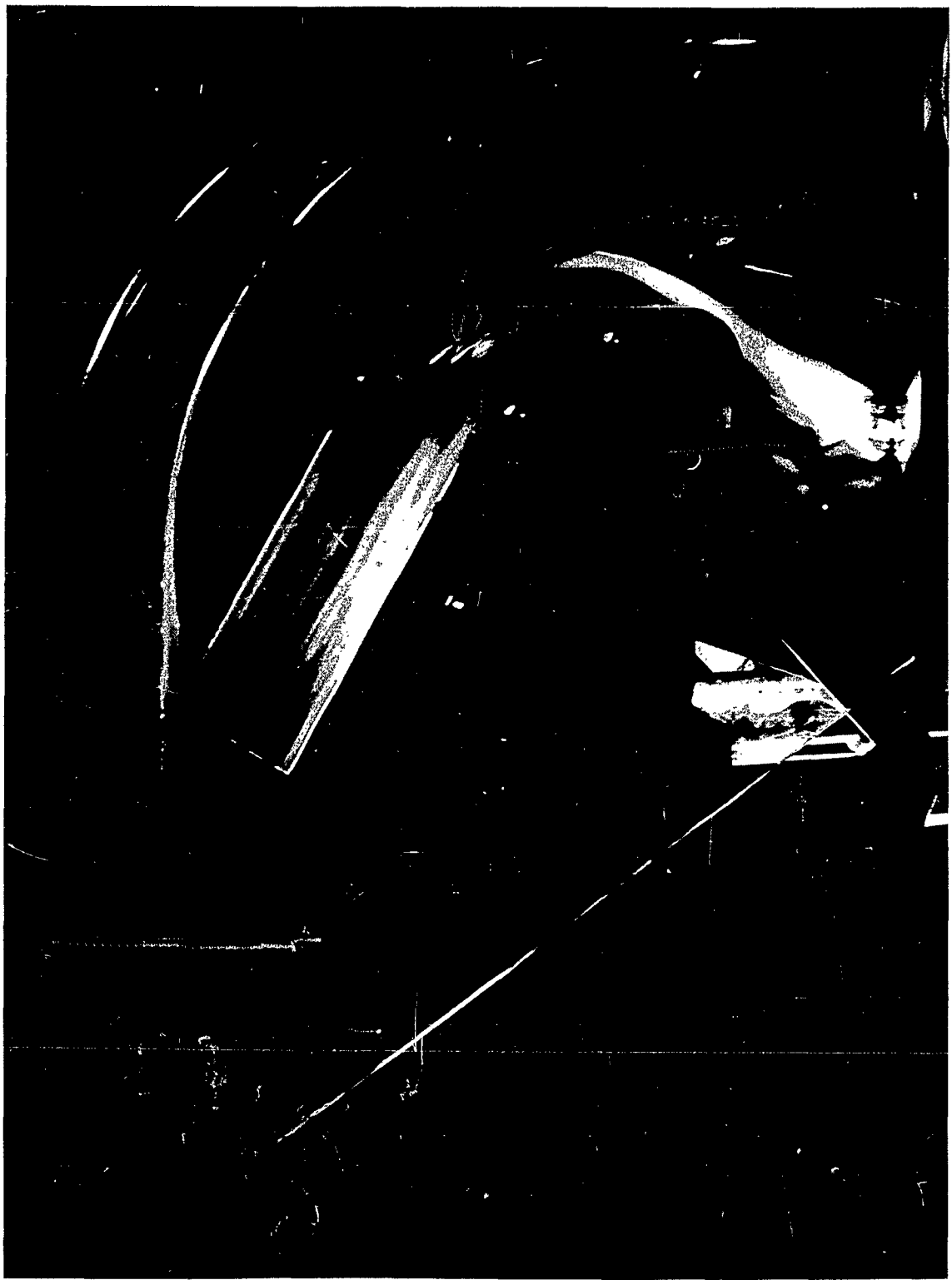


FIGURE 45: FLOW VISUALIZATION BETWEEN JET SHEET AND DEFLECTION SURFACE AT CENTER SPAN (CONFIGURATION C) $h = 1.25$, $l = 1.00$, $P_r = 1.4$

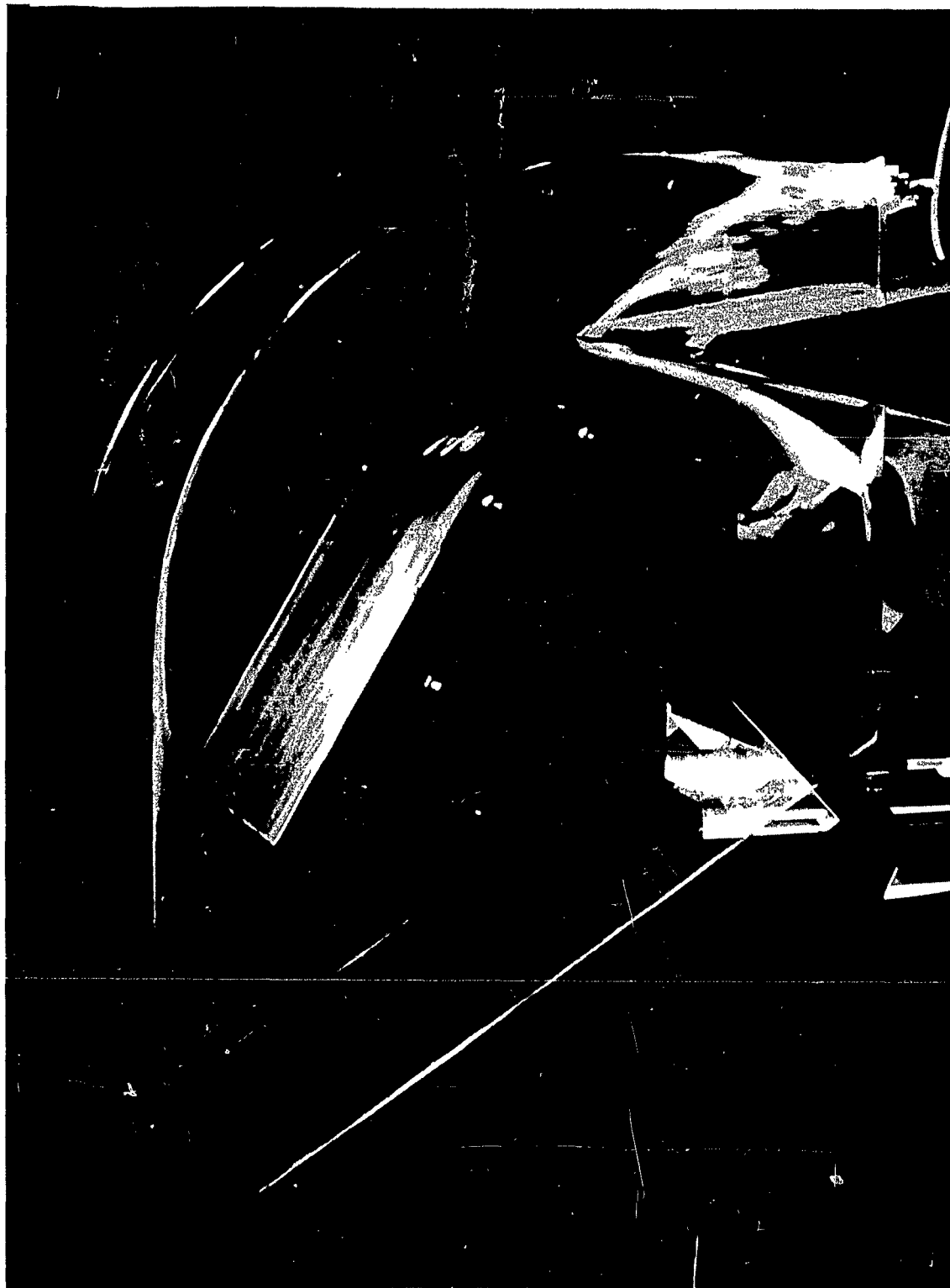


FIGURE 46: FLOW VISUALIZATION OF ENTRAINMENT AT CENTER SPAN
(CONFIGURATION C) $h = 1.25$, $l = 1.00$, $P_r = 1.4$



FIGURE 47: FLOW VISUALIZATION OF ENTRAINED AIR AT CENTER SPAN
(CONFIGURATION C) $h = 1.25$, $l = 1.00$, $P_r = 1.4$

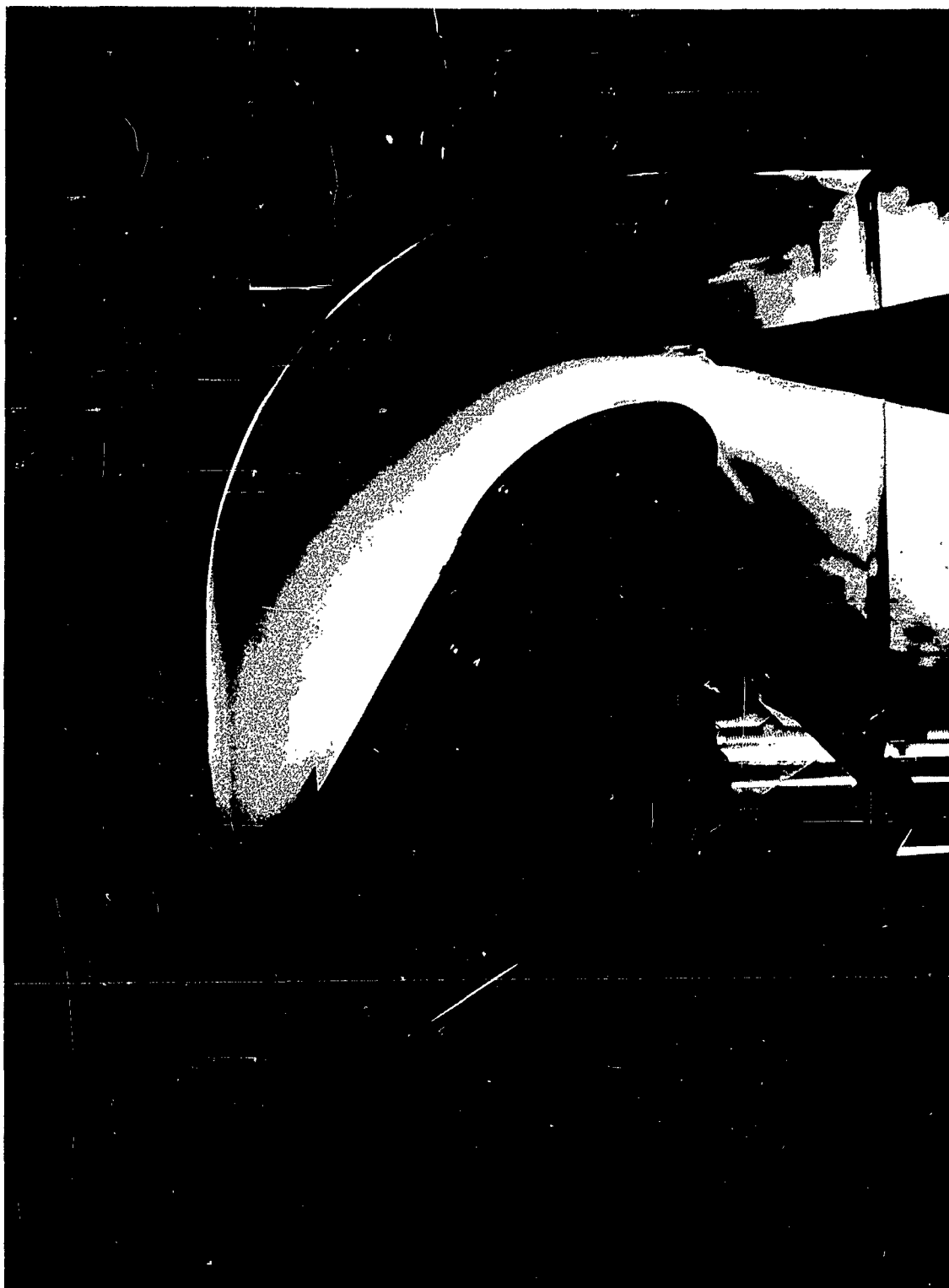


FIGURE 48: FLOW VISUALIZATION OF SECONDARY AIR SHOWN WITH SMOKE GENERATOR
(CONFIGURATION C) $h = 1.25$, $l = 1.00$, $P_r = 1.4$



FIGURE 49: SIDE PLATE-JET BOUNDARY LAYER TRACE (CONFIGURATION B)
 $h = 1.00$, $l = .75$, $P_r = 1.4$



FIGURE 50: SIDE PLATE-JET BOUNDARY LAYER TRACE
(CONFIGURATION C) $h = .80$, $l = .5$, $P_r = 1.4$

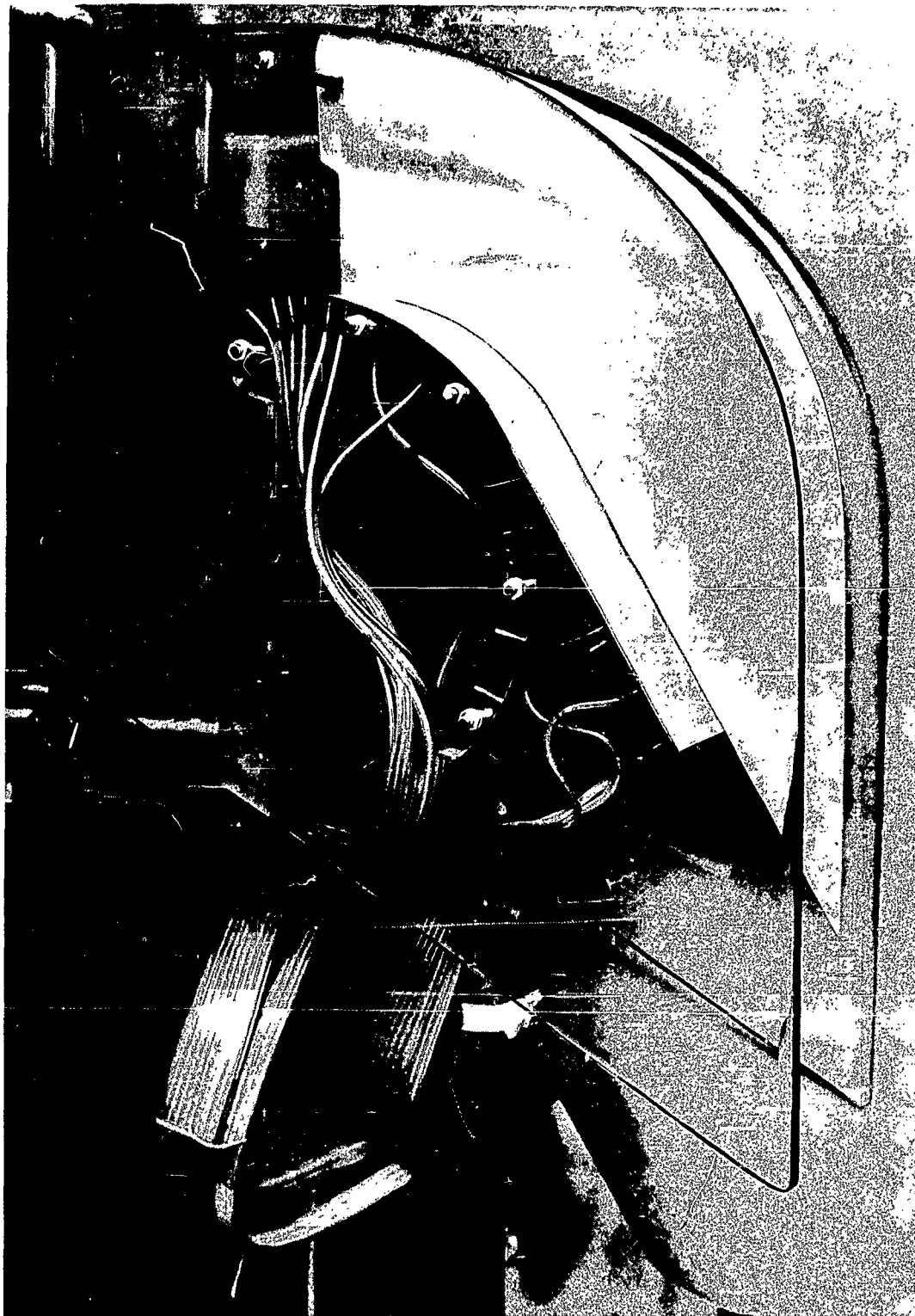


FIGURE 51: CONFIGURATION C WITH SPLITTER

APPENDIX II

MATHEMATICAL ANALYSIS

POTENTIAL FLOW ANALYSIS

THICK JET ANALYSIS

POTENTIAL ANALYSIS

The following solution is patterned after that suggested by Yen and Bursik (ref. 4). The consultation of Prof. Irmgard Flugge-Lotz in devising the analog solution is gratefully acknowledged.

The flow model analyzed is shown in the Z plane (Figure 52); stream I is the primary jet, and stream II is the ambient flow. Streams I and II are considered isoeenergetic with the free streamlines A-B, C-D, and F-G at ambient pressure. The separating streamline E-M-H has continuous pressure across it and velocity direction along it. The flow is partially defined in the hodograph plan ($\zeta = u-iv$, Figure 53) where the free, constant velocity streamlines map as constant radius arcs, the terminals of which are defined by the known velocity directions. The magnitude and direction of the velocity along the streamlines B-X-C, E'-M'-H', and E''-M''-H'' are unknown. However, the conditions imposed upon the dividing streamlines (E-M-H) permit them to be related as follows:

$$P_I = \text{const} = p_{G_\infty} + \frac{\rho v_{G_\infty}^2}{2} = p_G + \frac{\rho v_G^2}{2} = p_F + \frac{\rho v_F^2}{2} \quad (1)$$

$$= p_{H''_\infty} + \frac{\rho v_{H''_\infty}^2}{2} = p_{H''} + \frac{\rho v_{H''}^2}{2}, \text{ etc.}$$

$$P_{II} = \text{const} = p_{A_\infty} + \frac{\rho v_{A_\infty}^2}{2} = p_A + \frac{\rho v_A^2}{2}, \text{ etc.} \quad (2)$$

$$= p_{H'_\infty} + \frac{\rho v_{H'_\infty}^2}{2} = p_{H'} + \frac{\rho v_{H'}^2}{2}, \text{ etc.}$$

As previously stated for pressure continuity,

$$p_{H''} = p_{H'}, \text{ etc.} \quad (3)$$

$$p_A = p_G.$$

Combining (1), (2), and (3),

$$P_I - \frac{\rho v_{H''}^2}{2} = P_{II} - \frac{\rho v_{H'}^2}{2}$$

or

$$\frac{2}{\rho} (P_I - P_{II}) = (v_{H''}^2 - v_{H'}^2) = \text{constant} \quad (4)$$

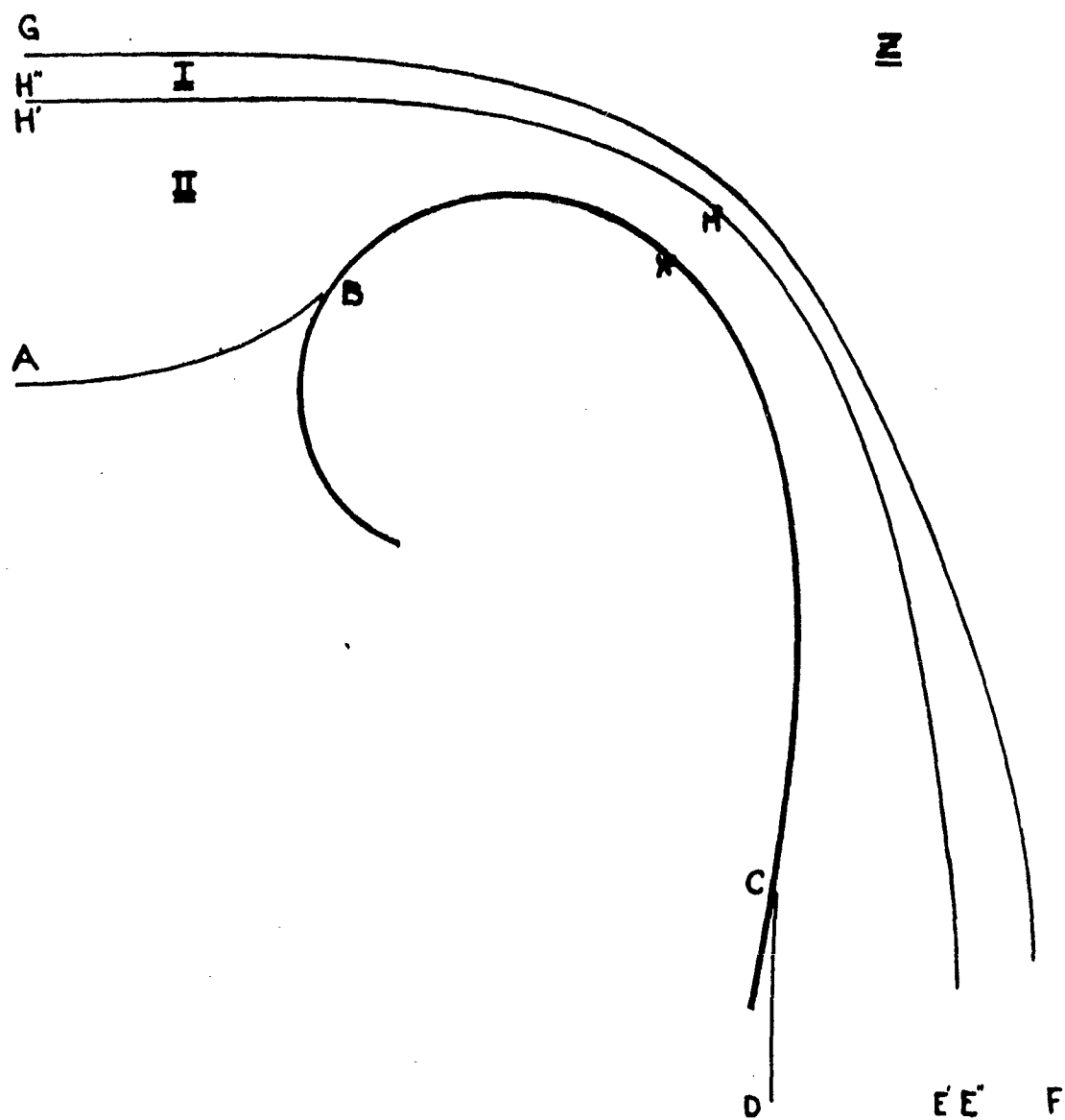


FIGURE 52: MATHEMATICAL MODEL IN PHYSICAL PLANE

and

$$\begin{aligned}
 \frac{2}{\rho} (P_I - P_{II}) &= (v_G^2 - v_A^2) = \text{constant} \\
 &= v_A^2 \left(\frac{v_G}{v_A} \right)^2 - 1 \\
 &= v_A^2 [\sigma^2 - 1]
 \end{aligned} \tag{5}$$

where: $\sigma = \frac{v_G}{v_A}$, the velocity ratio between the jet and ambient streams.

Combining (4) and (5),

$$v_{H''}^2 - v_{H'}^2 = (\sigma^2 - 1)v_A^2$$

Normalizing to v_A , the following relation is obtained relating the streamlines of velocity discontinuity:

$$\left. \frac{v_{H''}^2}{v_A^2} - \frac{v_{H'}^2}{v_A^2} = \sigma^2 - 1 \right|_{\text{at } \theta_{H''} = \theta_{H'}} \tag{6}$$

To simplify the determination of the flow net, and to improve its accuracy, the system is mapped into the logarithmic hodograph plane, Ω (figure 53),

where $\Omega = \tau - i\theta$

$$\tau = \ln \frac{V}{v_A}$$

θ = velocity direction.

The location of points A, B, C, D, E, and G in the Ω plane is obvious. The shape of B-X-C, E'M'H', and E''M''H'' is not obvious. The shape of B-X-C and E'M'H' or E''M''H'' may be arbitrarily chosen (E'M'H' and E''M''H'' are dependent through expression (6)). Having chosen E'M'H' or its dependent, the other is computed from (6). Two methods of analog solution are possible at this point. The flow net can be solved to satisfy the chosen B-X-C, i.e., alter E-M-H to suit; or more simply, B-X-C may be altered to satisfy the chosen E-M-H. B-X-C is known to be correct in the Ω plane when E'M'H' and E''M''H'' map congruently back into the physical plane (Z). The transformation back into the Z plane is achieved by numerical integration of the flow net. The flow nets are

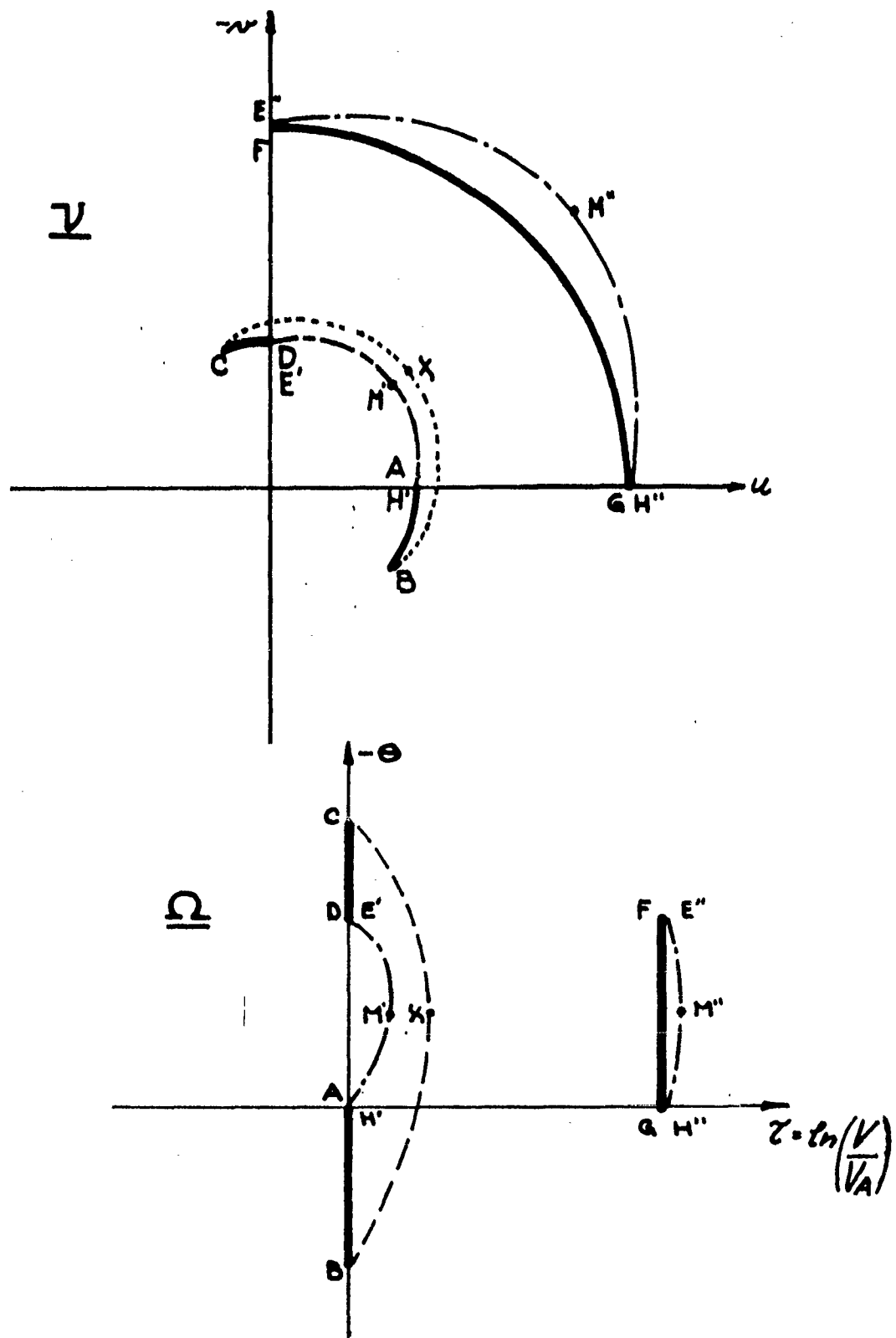


FIGURE 53: MATHEMATICAL MODEL IN HODOGRAPH PLANE

determined for the closed figures ABXCDM' and FGM'' separately, with potential applied across A and D, and F and G.

The numerical integration is obtained as follows:

$$\frac{V}{V_A} = \frac{u-iv}{V_A} = \frac{1}{V_A} \frac{dW}{dZ} = \frac{V}{V_A} e^{-i\theta}$$

$$\Omega = \ln \frac{1}{V_A} \frac{dW}{dZ} = \ln \frac{V}{V_A} - i\theta = \tau - i\theta$$

$$\frac{1}{V_A} \frac{dW}{dZ} = e^{\Omega}$$

$$\int dZ = \frac{1}{V_A} \int \frac{dW}{e^{\Omega}}$$

Along a streamline, the stream function, Ψ , is constant and

since

$$W = \phi + i\Psi$$

$$dW = d\phi$$

or

$$Z - Z_1 = \frac{1}{V_A} \int_1 \frac{d\phi}{e^{\Omega}}$$

Now

$$e^{\Omega} = e^{\tau - i\theta} = \frac{e^{\tau}}{e^{i\theta}} = \frac{e^{\tau}}{\cos\theta + i \sin\theta}$$

$$Z - Z_1 = \frac{1}{V_A} \int_1 \frac{(\cos\theta + i \sin\theta) d\phi}{e^{\tau}}$$

separating into real and imaginary parts

$$Z - Z_1 = \frac{1}{V_A} \int_1 e^{-\tau} \cos\theta + i \int_1 e^{-\tau} \sin\theta d\phi$$

and the flow can be mapped back into Z plane, and E'-M'-H' and E''-M''-H'' compared. If they are congruent, the solution is complete; if not, A-B-X-C-D is altered in the Ω plane and a second trial is made. Once a solution is obtained, the complete flow field may be mapped into the Z

plane to permit study of the transition from parallel to vortex flow. The solution will also permit prediction of the deflection surface pressures.

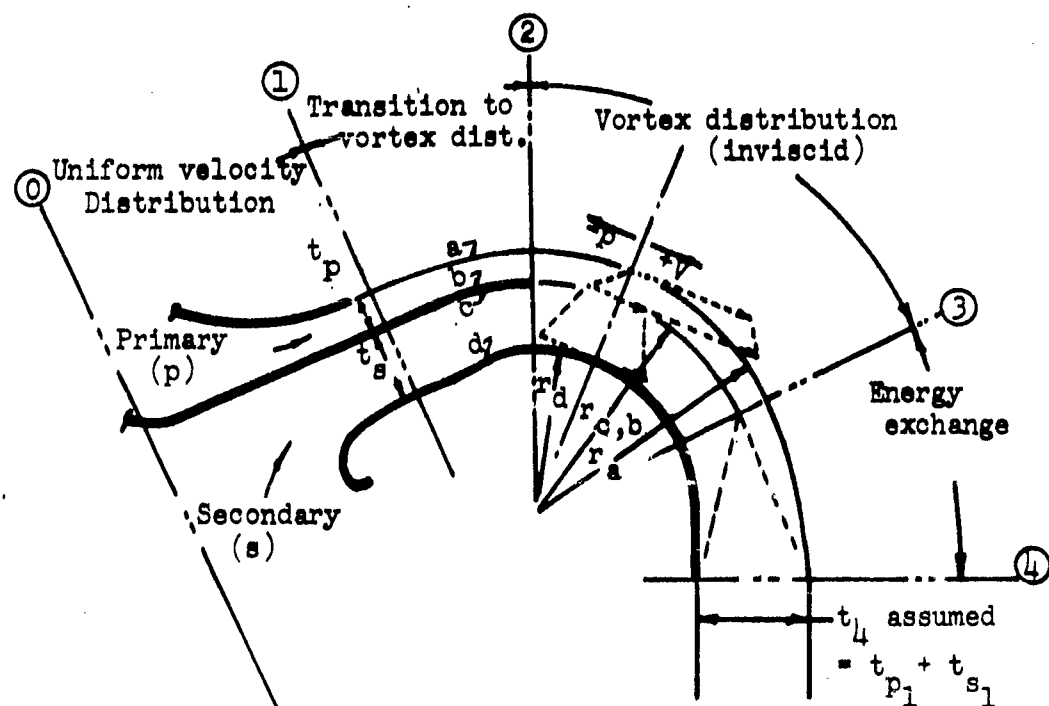
THICK JET ANALYSIS OF THE VENTILATED CLINGING FLOW PHENOMENON

By E. R. Sargent

The following analysis of the ventilated clinging flow phenomenon is based on several broad assumptions and is intended only to serve as a preliminary tool in: (1) determining the relative significance of the controlling variables, and (2) establishing the upper limits of performance. In general, the analysis visualizes stream conditions with fully developed, inviscid vortex flow, followed by a zone where energy exchange takes place at an efficiency sufficient to maintain steady state conditions.

The simplified flow model and the symbols used are shown in Figure 54. The analysis is based on the following principal assumptions:

1. The velocity distribution at station 1 is uniform for both primary and secondary streams.
2. Between stations 2 and 3 the flow has a fully developed vortex velocity distribution ($V_r = \text{const}$).
3. Mixing or energy transfer takes place between stations 3 and 4 with an efficiency of η .
4. The flow is ejected at station 4 at ambient pressure with a uniform velocity through a total gap equal to $t_{p_1} + t_{s_1}$.
5. The static pressure of the primary stream at station 1 is uniform and equal to ambient.
6. The static pressure at the inner (b) and outer (c) streamlines of the primary and secondary flow respectively between stations 2 and 3 is equal ($P_{2_b} = P_{2_c}$).
7. The static pressure of the secondary stream at station 1 is uniform and equal to outer streamline (c) pressure at stations 2 to 3.
8. The flows are incompressible, inviscid, and at a uniform temperature.
9. The only flow mixed with primary flow is that induced between curved plate and the primary jet.



A	Area	
C	Constant of integration	
E	Energy	
F	Force	
g	Gravitational acceleration	
m	Mass flow rate	
p	Static pressure	
P	Total pressure	
r	Radius	
t	Thickness of stream	
V	Velocity	
η	Efficiency	
ρ	Density	
		Subscripts
		a } streamlines as noted
		b } in figure
		c }
		d }
		c Centrifugal
		p Primary
		s Secondary
		Δp Pressure differential

FIGURE 54: MATHEMATICAL MODEL - THICK JET ANALYSIS

DERIVATION

Assumption 4 and the continuity relation applied between station 1 and 4 give:

$$m_s + m_p = m_4 \quad (1)$$

or

$$\rho V_{s1} t_{s1} + \rho V_{p1} t_{p1} = \rho V_4 t_4 = \rho V_4 (t_{p1} + t_{s1}) \quad (2)$$

The reduction in energy of the primary stream caused by the energy exchange process between stations 3 and 4 is:

$$\begin{aligned} E_{p3} - E_{p4} &= E_{p0} - E_{p4} = E_{p1} - E_{p4} = \frac{1}{2} m_p (v_{p1}^2 - v_4^2) \\ &= \frac{1}{2} \rho t_{p1} V_{p1} (v_{p1}^2 - v_4^2) \end{aligned} \quad (3)$$

since

$p_{p1} = p_{p4}$ = ambient pressure and no losses occur between station 0 and 3 by assumption 8.

Likewise, the gain in energy of the secondary stream is:

$$E_{s4} - E_{s0} = \frac{1}{2} m_s v_4^2 = \frac{1}{2} \rho t_{s1} V_{s1} v_4^2 \quad (4)$$

since

$E_{s0} = 0$, (static condition).

Let the efficiency of energy transfer be η ; therefore,

$$(E_{p1} - E_{p4}) \eta = E_{s4} - E_{s0} \quad (5)$$

or

$$\frac{1}{2} m_p (v_{p1}^2 - v_4^2) \eta = \frac{1}{2} m_s v_4^2 \quad (6)$$

or also

$$\frac{1}{2} \rho t_{p1} V_{p1} (v_{p1}^2 - v_4^2) \eta = \frac{1}{2} \rho t_{s1} V_{s1} v_4^2 \quad (7)$$

The thrust augmentation ratio is defined as:

$$\phi = \frac{F_4}{F_{p1}} = \frac{m_4 v_4}{m_{p1} v_{p1}} = \left(\frac{m_p + m_s}{m_p} \right) \left(\frac{v_4}{v_{p1}} \right) \quad (8)$$

and from equation (6):

$$\frac{m_s}{m_p} = \eta \left[\left(\frac{v_{p1}}{v_{p4}} \right) - 1 \right] \quad (9)$$

therefore,

$$\phi = (1-\eta) \frac{v_4}{v_{p1}} + \frac{v_{p1}}{v_4} \eta. \quad (10)$$

An expression for the velocity ratio in terms of stream thickness ratio and efficiency can be obtained by combining the continuity equation (2) and energy equation (7);

$$\left(\frac{t_{s1}}{t_{p1}} + 1 \right) \cdot \left(\frac{v_4}{v_{p1}} \right)^3 - (1-\eta) \left(\frac{v_4}{v_{p1}} \right)^2 - \eta = 0 \quad (11)$$

therefore,

$$\phi = f \left(\frac{t_{s1}}{t_{p1}}, \eta \right). \quad (12)$$

This equation is independent of the curvature of the streams.

However, for a given value of $\frac{t_{s1}}{t_{p1}}$ and η , there is only one curved path

that a fully developed inviscid vortex flow can take, when its inner side is bounded by a surface of constant radius and its outer side free, and at ambient pressure. The boundary radii of the primary and secondary flow streamlines can be evaluated in the following way. The fact that a stream with a uniform energy or total pressure distribution will establish a free vortex distribution ($Vr = \text{const.}$), when flowing through a constant radius channel, is basic (see reference 8), and can be derived as follows:

The centrifugal force acting on an elemental fluid volume of area, dA ,

and thickness, dr , flowing on a curved path of radius, r at velocity, V , is:

$$dF_c = \rho dA \frac{V^2}{r} dr. \quad (13)$$

For a constant stream total pressure distribution, the pressure force is obtained from the Bernoulli equation,

$$P = p + \frac{1}{2} \rho V^2 \quad (14)$$

or

$$\frac{dP}{dr} = 0 = \frac{dp}{dr} + \rho V \frac{dV}{dr}. \quad (15)$$

$$\text{The pressure force, } dF_{\Delta p} = dp dA = -\rho V dA dr \quad (16)$$

For steady state conditions,

$$dF_{\Delta p} = dF_c \quad (17)$$

or from 13 and 16,

$$-\rho V dA dV = \rho dA \frac{V^2}{r} dr \quad (18)$$

or

$$-\frac{dV}{V} = \frac{dr}{r} \quad (19)$$

integrating

$$-\int \frac{dV}{V} = \int \frac{dr}{r} \quad (20)$$

$$-(\ln V + C_v) = \ln r + C_r \quad (21)$$

or

$$Vr = \text{const.} \quad (22)$$

The radius of curvature of the streams at station 2 can be related to the flow condition at station 1 by noting that at station 2, the pressure of the inner primary jet streamline is equal to pressure of the

outer secondary flow streamline. The inviscid flow assumption 8 permits:

$$P_p = p_{p_1} + \frac{1}{2} \rho v_{p_1}^2 = p_{a_2} + \frac{1}{2} \rho v_{a_2}^2 = p_{b_2} + \frac{1}{2} \rho v_{b_2}^2 \quad (23)$$

and also,

$$P_s = 0 = p_{s_1} + \frac{1}{2} \rho v_{s_1}^2 = p_{c_2} + \frac{1}{2} \rho v_{c_2}^2. \quad (24)$$

But,

$$p_{b_2} = p_{c_2}$$

and

$$p_{p_1} = 0 \text{ (ambient pressure)}$$

therefore,

$$\frac{1}{2} \rho (v_{p_1}^2 - v_{b_2}^2) = - \frac{1}{2} \rho v_{c_2}^2. \quad (25)$$

From equation (22)

$$r_{a_2} v_{a_2} = r_{b_2} v_{b_2} \text{ or } v_{b_2} = \frac{r_{a_2}}{r_{b_2}} v_{a_2} \quad (26)$$

since by assumption 5, $p_{p_1} = 0 = p_{a_2}$, from equation (23) $v_{p_1} = v_{a_2}$,

therefore,

$$v_{b_2} = \frac{r_{a_2}}{r_{b_2}} v_{p_1}. \quad (27)$$

By substituting equation (27) in equation (25)

$$v_{p_1}^2 - v_{p_1}^2 \left(\frac{r_{a_2}}{r_{b_2}} \right)^2 = - v_{c_2}^2, \quad (28)$$

but by assumption 1, $V_{c2} = V_{s1}$; therefore

$$V_{s1} = V_{p1} \sqrt{\left(\frac{r_a}{r_b}\right)^2 - 1} \quad (29)$$

(Note that $r_{a2} = r_a$ and $r_{b2} = r_b$)

By substituting equation (29) in equation (2), it can be shown that

$$\frac{V_{t1}}{V_{p1}} = \frac{\frac{t_{p1}}{t_{s1}} + \sqrt{\left(\frac{r_a}{r_b}\right)^2 - 1}}{1 + \frac{t_{p1}}{t_{s1}}} \quad (30)$$

Equation (30) can be substituted in equation (11) and an expression obtained that shows

$$\frac{r_a}{r_b} = f\left(\frac{t_{s1}}{t_{p1}}, \eta\right) \quad (31)$$

The radius of the curved plate, r_d , can be determined from considerations of continuity of flow between stations 1 and 2.

For continuity of the primary stream between stations 1 and 2:

$$V_{p1} t_{p1} = \int_{r_b}^{r_a} V_{p2} dr_{p2} \quad (32)$$

From equation (22):

$$V_{p2} r_{p2} = V_{a2} r_{a2} = \text{const.} \quad (33)$$

or

$$V_{p2} = \frac{r_{a2}}{r_{p2}} V_{a2} = \frac{r_{a2}}{r_{p2}} V_{p1} \quad (34)$$

since ambient pressure exists in the primary flow at station 1 and along its outer streamline, a.

By noting that: $r_{a_2} = r_a = r_{a_3}$, $r_{b_2} = r_b = r_{b_3}$, and $r_{p_2} = r = r_{p_3}$, and by the substitution of equation (34) into equation (32):

$$V_{p_1} t_{p_1} = V_{p_1} r_a \int_{r_b}^{r_a} \frac{dr}{r} = V_{p_1} r_a \left[\ln r_a - \ln r_b \right] \quad (35)$$

or

$$t_{p_1} = r_a \ln \frac{r_a}{r_b} \quad (36)$$

Likewise, it can be shown:

$$t_{s_1} = r_b \ln \frac{r_b}{r_d}, \quad (37)$$

since by assumption 7 the pressure of the secondary stream at station 1 is equal to its outer streamline pressure at station 2, thus making

$$V_{s_1} = V_c.$$

Therefore,

$$\frac{t_{s_1}}{t_{p_1}} = \frac{r_b}{r_a} \frac{\ln \frac{r_b}{r_d}}{\ln \frac{r_a}{r_b}} \quad (38)$$

The substitution of equation (31) in equation (38) shows that:

$$\frac{r_d}{r_b} = f \left(\frac{t_{s_1}}{t_{p_1}}, \eta \right) \quad (39)$$

Several parameters can be used to relate the mathematical model to the physical configuration. If the geometry of a test configuration tends to establish condition of flow as assumed at station 1, then the parameter

t_{s1}/t_{p1} should be used. In this case it can be shown that for a given value of t_{s1}/t_{p1} and η there is a specific value of r_d/t_{p1} .

From equation (27):

$$\frac{r_d}{t_{p1}} = \frac{r_d}{r_a \ln \frac{r_a}{r_b}} = \frac{1}{\frac{r_a}{r_b} \frac{r_b}{r_d} \ln \frac{r_a}{r_b}}. \quad (40)$$

Substitution of equations (31) and (39) in (40) shows that:

$$\frac{r_d}{t_{p1}} = f \left(\frac{t_{s1}}{t_{p1}}, \eta \right). \quad (41)$$

If the conditions at station 2 are more typical of test hardware, a similar relation can be found as follows:

$$\frac{t_{s2}}{t_{p2}} = \frac{r_b - r_d}{r_a - r_b} = \frac{1 - \frac{r_d}{r_b}}{\frac{r_a}{r_b} - 1} = f \left(\frac{t_{s1}}{t_{p1}}, \eta \right)$$

and also,

$$\frac{r_d}{r_{p2}} = \frac{r_d}{r_a - r_b} = \frac{1}{\frac{r_b}{p_d} \left(\frac{r_a}{r_b} - 1 \right)} = f \left(\frac{t_{s1}}{t_{p1}}, \eta \right).$$

The analytical performance of the ventilated clinging flow device is shown in terms of these parameters in Figure 55.

The analysis assumes an arbitrary energy efficiency; however, normal inelastic mixing occurs with an unavoidable loss in energy. The curves show that the efficiency cannot be below a certain minimum to achieve an increase in thrust. Assumption 4 is essentially the condition for a constant area mixing chamber ejector. The momentum equation can be applied to the mixing zone and related to the energy equation to determine an upper limit of the energy transfer efficiency. This information would be of little value, however, without including further refinements, such as the effects of the ambient air mixing at the outer surface of

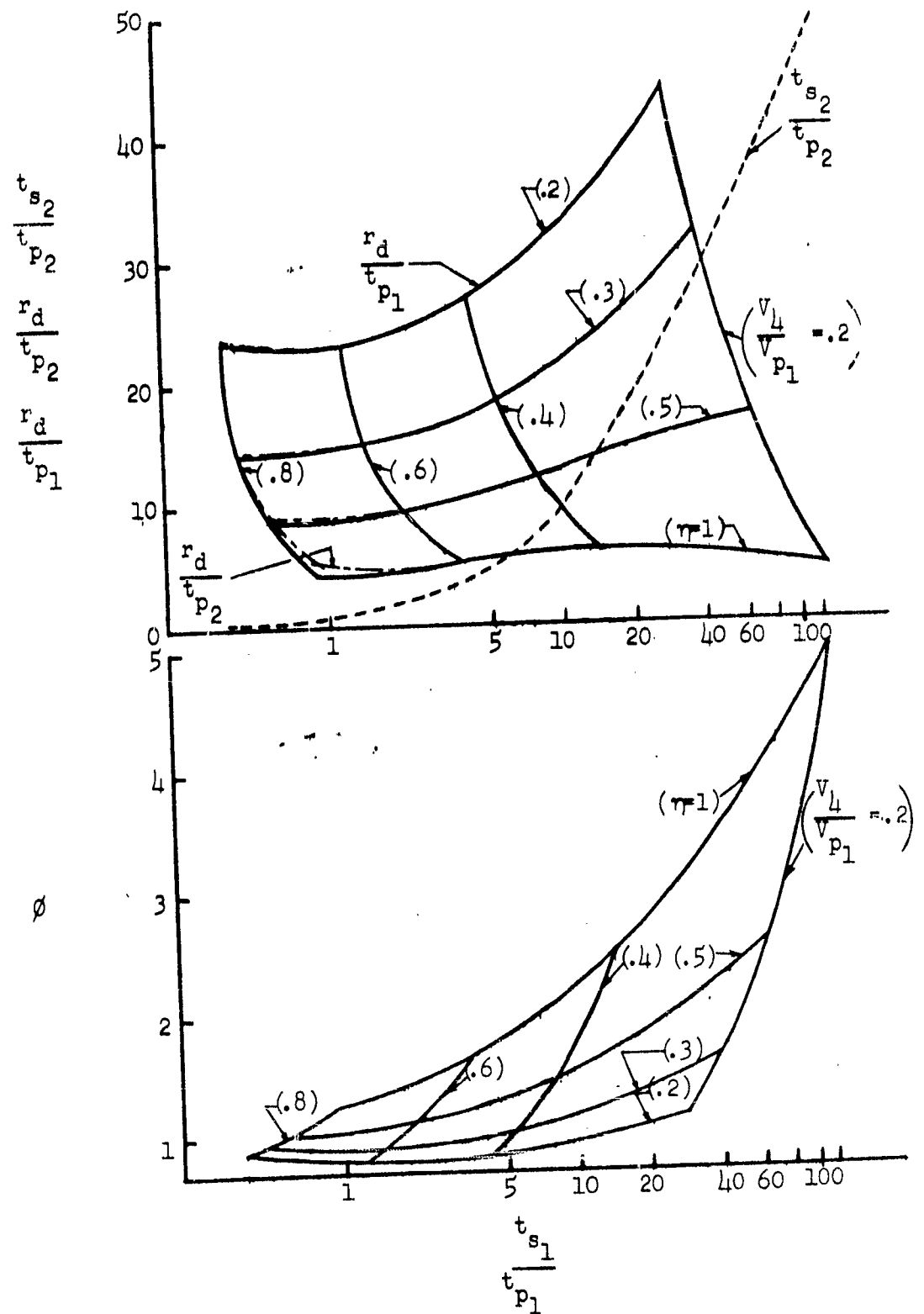


FIGURE 55: PERFORMANCE ENVELOPE - THICK JET ANALYSIS

the clinging stream, the velocity profile of the wake, and the conformity of the flow with the assumed circular path which has centers coincident with the deflection surface. The significance of this later situation, particularly in the vicinity of the primary nozzle outlet, is indicated by a comparison of test results with the analysis. The test conditions of Configuration C giving maximum augmentation are:

$$\frac{t_{s1}}{t_{p1}} \approx \frac{t_{s2}}{t_{p2}} \approx \frac{1.4}{.085} = 16.5, \quad \frac{r_d}{t_{p1}} \approx \frac{r_d}{t_{p2}} \approx \frac{6.02}{.085} = 70.8$$

Referring to the plot of ϕ vs. $\frac{t_{s1}}{t_{p1}}$ in the lower portion of Figure 55,

it is seen that for a value ϕ greater than 1.0 at $\frac{t_{s1}}{t_{p1}} = 16.5$, η must be

larger than .2. However, the curves in the upper portion of the figure

show a value of $\frac{r_d}{r_{p1}}$ less than 40, which is incompatible with tested con-

figurations. This discrepancy can be explained if the curvature of the primary flow immediately downstream of the nozzle outlet was greater (shorter radius) than assumed in the theory. Figure 40 actually indicates that initially the primary jet wake draws toward the surface and then moves outward at greater downstream distances. Also, Figure 43 indicates a higher suction immediately downstream of the nozzle which would be caused by a greater flow curvature in this area. It may very well be that for optimum performance, the deflection surface should have a greater initial curvature with a gradual transition to an essentially flat surface.

APPENDIX III

TEST FACILITY, EXPERIMENTAL PROCEDURES, AND DATA REDUCTION

I. FACILITY

The air supply system consists of two Allison V1710 supercharger compressors operating in series, each driven by a 150 HP Ford industrial engine. The discharge of the compressors is ducted to the gimbaled 4-inch-diameter rigid supply duct. The flexible joint and gimbal system are installed in the supply duct approximately 14 feet upstream of the nozzle vertical centerline. This gimbal system minimizes extraneous forces and permits angular freedom, whereby force measurements are made by restraining the duct movements with Toledo pendulum-type scales.

II. PROCEDURES

A. FORCE MEASUREMENT

A system check at the beginning of the program established a small correction based on nozzle total pressure (P_j) for Bourdon tube effect for both the vertical and horizontal force measurements. Leakage rate was established at this time and eliminated. The horizontal and vertical force measuring apparatus was calibrated prior to each new series of tests (model changes) by dead weight loading to insure that the continued use of established calibration factors was valid; i.e., to insure that no changes occurred in the system which would invalidate established thrust and lift calibrations.

B. FLOW MEASUREMENT

The primary flow metering system was designed to meet ASME requirements and incorporates a standard sharp-edged orifice in the supply duct approximately 20 feet upstream of the nozzle. Pressure measurements are made with mercury manometers. Temperatures were sensed by chromel vs. alumel thermocouples and measured with a Rubicon potentiometer.

C. FLOW VISUALIZATION

1. The majority of the flow visualization studies and subsequent photographs shown in this report were conducted using a fabric tuft saturated in titanium tetrachloride. This provided adequate smoke for distinguishing flow streamlines of entrained air and some of the mixing action taking place along the deflection surface.

2. A second smoke source, which became available late in the program, was the type 1963 Fogmaker which produces a vaporized oil fog. This unit is produced by the Mole-Richardson Co. of Hollywood, California. This source provided the excellent picture of the jet mixing action in Figure 48. Further experimentation with this device should result in developing a technique readily adaptable to studies of this nature with highly successful results. It is by far the best source of smoke found by the writers for this type of work.

D. BOUNDARY LAYER TRACE

The boundary layer traces in Figures 7, 49, and 50 were obtained by coating the surface with a mixture of carbon black and kerosene prior to operating the model.

E. PRESSURE SURVEYS

The surface and wake pressure surveys were obtained with the use of a multitube water manometer. The rake used in the tests is shown in

Figure 24. The construction details are shown in Figure 56. The pressure rake consists of seven groups of five each static and total pressure probes. Groups 1 and 7 are outside the jet span, 5.97 inches from the jet centerline (left and right, respectively); and in the case of Configurations B and C, these groups are outside the side plates. Groups 2 and 6 are located immediately inside the jet edge, 4.28 inches from jet centerline. Groups 3 and 5 are located 3 inches on either side of the jet centerline, and group 4 is located on the centerline.

Discrepancies, between deflection surface tap pressures and the "near the surface" pressures obtained in the wake survey, are due to local interference effects when rake-to-surface distance approaches zero. Therefore, the rake was removed from the system for measurement of the static surface pressures to eliminate the interference effects in those readings.

F. TESTS

Two basic types of tests were conducted, and slightly different data were taken in each type. One type was to obtain performance data, i.e., vertical (lift) and horizontal (thrust or drag) measurements, as a function of the geometrical variables, h , ℓ , and surface configurations. The data obtained from this type of test determined the values of h and ℓ for the second type of test, which was primarily the wake and surface pressure survey. The data measurements taken in these tests were:

1. Vertical and horizontal scale readings
2. Total pressure at the nozzle manifold, P_j
3. Temperature 2 feet upstream of the nozzle vertical centerline, T_j
4. Flow rate (inlet pressure, differential pressure, and temperature in flow section), \dot{w}
5. Dimensions describing position of deflection surface with respect to nozzle exit planes, h and ℓ
6. Rake position (position around surface in degrees and distance from bottom probe to surface, viz. 30° -- 0.10)
7. Barometric pressure
8. Manometer panel recordings by photographs.

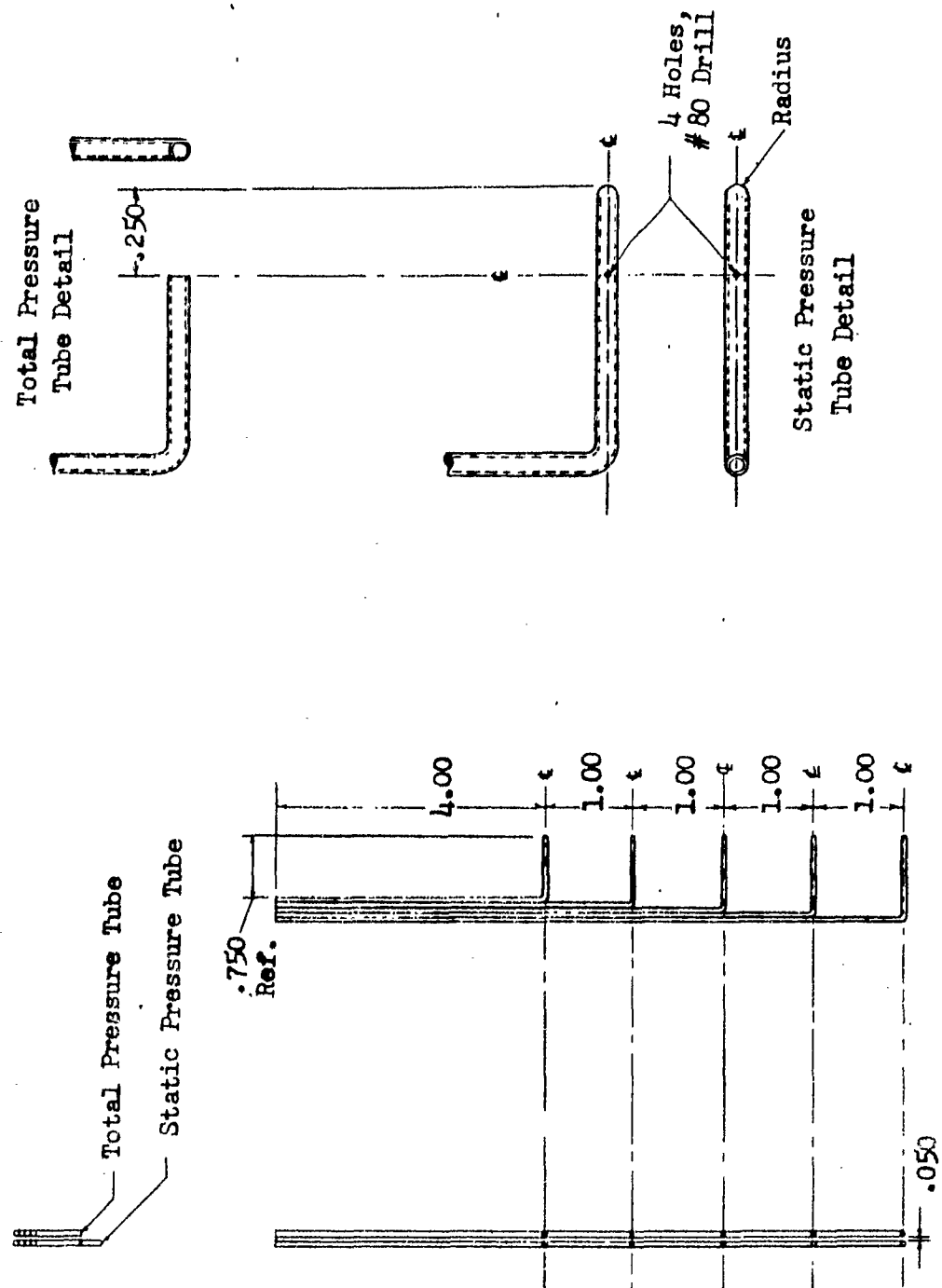


FIGURE 5: RAKE DETAIL, WAKE PRESSURE SURVEY

III. DATA REDUCTION

A. NORMALIZED FORCES, ϕ and ϕ_z

The forces are normalized in a manner to reflect thrust augmentation or the lack of it. Thrust augmentation is defined as the ratio of the total measured thrust divided by the ideal thrust produced by the isentropic expansion of the measured primary flow from the supplied total pressure (P_j) to ambient pressure. Expressed in equation form, it is as follows:

$$\phi = \frac{F_r}{\frac{\dot{w}_m V_{theo}}{g}}, \quad \phi_z = \frac{F_z}{\frac{\dot{w}_m V_{theo}}{g}}$$

where

$$V_{theo} = \left\{ 2 g J C_p T_j \left[1 - \frac{P_o}{P_j} \frac{k-1}{k} \right] \right\}^{1/2} \quad (\text{pressures are in absolute units}).$$

$\Delta s = 0$

To simplify data reduction, let

$$\theta = \frac{T_j}{T_{osl}},$$

where

$$T_{osl} = 520^\circ R$$

By multiplying and dividing the right hand side of the velocity expression by T_{osl} and substituting:

$$V_{theo} = \sqrt{\theta} \left\{ 2 g J C_p T_{osl} \left[1 - \frac{P_o}{P_j} \frac{k-1}{k} \right] \right\}^{1/2},$$

which, when appropriate gas properties are used for the gas temperature involved, reduces to:

$$V_{theo} = f \left(\frac{P_o}{P_j}, \theta \right).$$

Air properties at a $300^\circ F$ ($C_p = .24$, $k = 1.4$) and a pressure ratio

$$\frac{P_o}{P_j} \text{ of } \frac{1}{1.4}, \text{ gives:}$$

$$\frac{V_{\text{theo}}}{g} = 23.5 \sqrt{\theta},$$

or for data reduction purposes, the expression

$$\phi = \frac{F_r}{23.5 \dot{w} \sqrt{\theta}} \quad \text{and} \quad \phi_z = \frac{F_z}{23.5 \dot{w} \sqrt{\theta}}.$$

B. RESULTANT FORCE

The resultant force and its direction are determined as follows:

$$(1) \quad F_r = \sqrt{F_z^2 + F_x^2}$$

$$(2) \quad \gamma = \arctan \frac{F_z}{F_x}$$

DISTRIBUTION

Army War College	1
Aviation Test Office, Edwards AFB	1
U. S. Army Polar Research and Development Center	1
Deputy Chief of Staff for Logistics, D/A	2
The Research Analysis Corporation	1
Army Research Office, Durham	1
Office of Chief of R&D, D/A	2
Naval Air Test Center	2
Army Research Office, OCRD	1
Deputy Chief of Staff for Military Operations, D/A	1
U. S. Army Engineer Research & Development Laboratories	2
U. S. Army Tank-Automotive Center	2
The Ordnance Board	1
U. S. Army Combat Developments Command Transportation Agency	1
U. S. Army Aviation and Surface Materiel Command	3
U. S. Army Transportation Research Command	66
U. S. Army Transportation School	4
U. S. Army Airborne, Electronics and Special Warfare Board	1
U. S. Army Research & Development Group (Europe)	2
Chief of Naval Operations	1
Bureau of Naval Weapons	2
Bureau of Supplies and Accounts, N/D	1
U. S. Naval Supply Research and Development Facility	1
U. S. Naval Postgraduate School	1
Bureau of Ships, D/N	1
U. S. Naval Ordnance Test Station	1
David Taylor Model Basin	1
Marine Corps Landing Force Development Center	1
Marine Corps Educational Center	1
U. S. Army Standardization Group, Canada	1
British Army Staff, British Embassy	4
U. S. Army Standardization Group, U. K.	1
NASA-LRC, Langley Station	2
Ames Research Center, NASA	2
Lewis Research Center, NASA	1
NASA Representative, Scientific and Technical Information Facility	1

U. S. Government Printing Office	1
Defense Documentation Center	10
U. S. Army Medical Research & Development Command	1
Human Resources Research Office	2
U. S. Strike Command	1
U. S. Army Mobility Command	3
U. S. Army Materiel Command	6
Human Engineering Laboratory	1
Office of the Assistant Secretary of Defense for R&E	1
U. S. Maritime Administration	1

<p>Hiller Aircraft Co. Div. of ELTRA Corporation, Palo Alto, California INVESTIGATION OF VENTILATED CLINGING FLOW PHENOMENON. Report ARD-311 M. F. Gates and L. A. Burdick TRECOT Technical Report 63-38, August 1963, 94 pp. Contract DA 44-177-TC-848. Task 1D021701A04812 Unclassified report</p>	<p>1. V/STOL 2. Jet Flap 3. Clinging Flow</p>	<p>1. V/STOL 2. Jet Flap 3. Clinging Flow</p>
<p>This phenomenon is the result of a jet sheet following a curved surface located close to, but separated from, the jet by an induced stream of ambient air.</p>	<p>(over)</p>	<p>(over)</p>
<p>Hiller Aircraft Co. Div. of ELTRA Corporation, Palo Alto, California INVESTIGATION OF VENTILATED CLINGING FLOW PHENOMENON. Report ARD-311 M. F. Gates and L. A. Burdick TRECOT Technical Report 63-38, August 1963, 94 pp. Contract DA 44-177-TC-848. Task 1D021701A04812 Unclassified report</p>	<p>1. V/STOL 2. Jet Flap 3. Clinging Flow</p>	<p>1. V/STOL 2. Jet Flap 3. Clinging Flow</p>
<p>This phenomenon is the result of a jet sheet following a curved surface located close to, but separated from, the jet by an induced stream of ambient air.</p>	<p>(over)</p>	<p>(over)</p>

Analytical and experimental investigations were conducted. A thick jet analysis of the phenomenon was derived that assesses the thrust augmentation possibilities of the concept. The experimental investigation documented the resulting performance and flow field. The experimental data presented indicates a thrust augmentation of 6% based on the primary jet thrust while deflecting the jet 58° from its original direction.

Analytical and experimental investigations were conducted. A thick jet analysis of the phenomenon was derived that assesses the thrust augmentation possibilities of the concept. The experimental investigation documented the resulting performance and flow field. The experimental data presented indicates a thrust augmentation of 6% based on the primary jet thrust while deflecting the jet 58° from its original direction.

Analytical and experimental investigations were conducted. A thick jet analysis of the phenomenon was derived that assesses the thrust augmentation possibilities of the concept. The experimental investigation documented the resulting performance and flow field. The experimental data presented indicates a thrust augmentation of 6% based on the primary jet thrust while deflecting the jet 58° from its original direction.

Analytical and experimental investigations were conducted. A thick jet analysis of the phenomenon was derived that assesses the thrust augmentation possibilities of the concept. The experimental investigation documented the resulting performance and flow field. The experimental data presented indicates a thrust augmentation of 6% based on the primary jet thrust while deflecting the jet 58° from its original direction.